THESIS FOR THE DEGREE OF DOCTOR OF PHILOSOPHY

Compartmental Models Of Lipoprotein Kinetics

Martin Adiels

Department of Mathematics
CHALMERS UNIVERSITY OF TECHNOLOGY
GÖTEBORG UNIVERSITY
Göteborg, Sweden 2004

Compartmental Models Of Lipoprotein Kinetics
Martin Adiels
ISBN 91-7291-540-4

Doktorsavhandlingar vid Chalmers tekniska högskola
Ny serie nr 2222
ISSN 0346-718X

Department of Mathematics
Chalmers University of Technology and Göteborg University
S-412 96 Göteborg
Sweden
Telephone +46 (0)31 7721000

Abstract

This thesis considers multi compartmental models of lipoprotein kinetics. Lipoproteins are the carriers of lipids such as triglycerides and cholesterol in the blood plasma. They also play a central role in the development of cardiovascular diseases. Obesity and diabetes mellitus type2 (DM2) are associated with a disturbed lipid metabolism and are associated with an increased risk for cardiovascular diseases.
To investigate the lipoprotein metabolism we have constructed a combined multi compartmental model that simultaneously models both the transport of the particles and the transport of their triglyceride content. From the combined model we can estimate production-, transfer- and clearance rates of both the number of particles and the amount of triglycerides. By the estimated fluxes and pools we can predict the average size of lipoproteins newly synthesised in the liver.

Experimental data consists of tracer/tracee data from a control group (n=17) and a group of DM2 patients (n=10). From these data we investigate the differences in the basal lipoprotein metabolism.
We propose a time-dependent model that can be used to investigate non-steady state behavior, e.g. immediate responses to drugs and food intake. We examine the response to insulin in a few subjects.

We also discuss a stochastic model that gives a more close description of the life cycle of a lipoprotein particle. Such models could more easily model the close interactions of different lipoprotein species and structural changes in the lipoprotein composition.

In the first two chapters we briefly describe the lipoprotein metabolism and the background for multi compartmental modelling and we discuss the problem of identifying unknown parameters in the model from measured data. In the next chapter we discuss the experimental data. Chapter four describes the combined multi compartmental model which is the main result in this thesis. In the next chapter we discuss potential limitations of the compartmental model and presents the stochastic model. The sixth chapter gives a short description of a parameter-free analysis of the experimental data. In chapter seven we describe the implementation of the model in the program SAAMII and discuss the impact of some assumptions and constraints of the model. We also summarise the two papers that are appended to this thesis. These papers are on a more medical perspective and the results are only discussed briefly. In the last chapter we discuss some extensions of the model.

This work was carried out in a collaboration between the School of Mathematical Sciences, Chalmers University of Technology and The Wallenberg Laboratory at the Sahlgrenska Academy, Göteborg University. There has also been a very close collaboration with the Division of Cardiology, Helsinki University Central Hospital, Finland and the Department of Pathological Biochemistry, Glasgow Royal Infirmary, UK.

The major part of this thesis is the construction of the mathematical model of lipoprotein kinetics. Appended to this thesis are two medical papers, with the implementation of the model.

Paper I
Martin Adiels, Chris Packard, Muriel J. Caslake, Philip Stewart, Aino Soro, Jukka Westerbacka, Bernt Wennberg, Sven-Olof Olofsson, Marja-Riitta Taskinen, and Jan Borén.
A new combined multicompartmental model for apolipoprotein B100 and triglyceride metabolism in VLDL subfractions.
In Press.

Paper II
Martin Adiels, Jan Borén, Muriel J. Caslake, Philip Stewart, Aino Soro, Jukka Westerbacka, Bernt Wennberg, Sven-Olof Olofsson, Chris Packard, and Marja-Riitta Taskinen.
Overproduction of VLDL1 Driven by Insulin Resistance Is a Dominant Feature of Diabetic Dyslipidemia.
Submitted.

The thesis

This work was carried out in a collaboration between the School of Mathematical Sciences, Chalmers University of Technology and The Wallenberg Laboratory at the Sahlgrenska Academy, Göteborg University. There has also been a close collaboration with the Division of Cardiology, Helsinki University Central Hospital, Finland and the Department of Pathological Biochemistry, Glasgow Royal Infirmary, UK.
The first part of the thesis was the final result of the five semester ECMI program. ECMI stands for the European Consortium for Mathematics in Industry and is a collaboration between universities in Europe for a programme in applied mathematics. The first two semesters of the program consists of core courses and the next two semesters are individual courses focusing on the upcoming project. The last semester is devoted to a mathematical project which in many cases originate from the industry.
This work was funded by NTM, Chalmers University of Technology, Stochastic Centre, and the Wallenberg Laboratory.

Acknowledgements

First of all I would like to thank my supervisor, professor Bernt Wennberg, for his support during these five years and for his help with finalising this manuscript.

My medical supervisors, professors Jan Borén and Marja-Riitta Taskinen, has not only supported me financially but also been been very encouraging and helpful whenever I have had questions about lipoproteins.

The group in Glasgow, professor Chris Packard and Dr. Muriel Caslake, has helped me with the modelling, which I am very thankful for.

I am very thankful for being invited into the field of lipoproteins and diabetes and I am grateful to everyone involved in this project.

The first years of my work was done as part of the ECMI programme, and I would like to thank the programme leaders and my first year supervisor Peter Kumlin and also Bo Johansson for introducing me to ECMI.
I wish to thank all my fellow ECMI colleagues, Robert, Johan I, Tobias and the Eriks, to name a few. A special thank to ECMI99 Greger, Sara, Henrik and Erik.

Last but not least I wish to thank my friends and family who always has supported me.

List of Abbreviations

apoB	Apolipoprotein B-100
apoB-100	Apolipoprotein B-100
apoB-48	Apolipoprotein B-48
CE	Cholesterol Ester
Chyl	Chylomicrons
CETP	Cholesterol Ester Transfer Protein
DM2	Diabetes Mellitus type-2
ER	Endoplasmic Reticulum
FC	Free Cholesterol
FCR	Fractional Catabolic Rate
FTR	Fractional Transfer Rate
FDCR	Fractional Direct Catabolic Rate
HDL	High Density Lipoproteins
HTGL	Hepatic Triglyceride Lipase
IDL	Intermediate Density Lipoproteins
LDL	Low Density Lipoproteins
PL	Phosphor Lipids
TG	Triglyceride
VLDL	Very Low Density Lipoproteins

Table 1: List of common abbreviations

Triglyceride An ester formed by glycerol and three fatty acids.
Phospholipids A lipid containing one or more phosphate groups. Phospholipids are soluble in both water and lipids.
Lipase An enzyme that catalyses the hydrolysis of triglyceride.
Hydrolysis Reaction where water is added to produce two or more products.
Endocytosis Uptake of extracellular material through the plasma membrane.
Adipose tissue A type of connective tissue that consists of stored cellular fat.
Endoplasmic reticulum A membrane network in the cytoplasm of cells. The ER is involved in synthesis, modification and transport of cellular material.
In Vivo An experiment within a living organism.
In Vitro An experiment in an artificial environment, outside a living organism.

Introduction

Compartmental modelling is a way to construct and describe some special system of equations. A compartment corresponds to an amount of materia with homogenous kinetics, and the compartmental model is the equations that describes the fluxes of material between the compartments, the removal of material and the external input of material into the system. We briefly summarise the theory of compartmental modelling and discuss; requirements on the model for the solution to be non-oscillating, implementations of delays or lags in the system and methods for determining if the unknown parameters are identifiable from experiments. The main result in this thesis is a combined multi compartmental model for the lipoprotein metabolism. The model, which describes the both lipoprotein and triglyceride (TG) metabolism, is adapted to data from isotopic labelling experiments.

A problem with isotopic labelling, is that labelled atoms can be replaced by non-labelled atoms. We describe a technique to deal with loss of labelled tracer without loss of tracee. In this case, the tracers are stable isotopes where hydrogen atoms are replaced by deuterium to form heavier molecules. It turns out that in the process where the tracer is incorporated into the lipoproteins some of the deuterium atoms were replaced by hydrogen atoms. The partially labelled molecules gave some problems in the analysis of the enrichments. We investigated the impact of this on the results and the estimated parameters.

The thesis deals mainly with the use of compartmental modelling in lipoprotein metabolism, but we also describe a stochastic model where each particle is modelled independently. Each particle is followed from the formation of the particle, though the delipidation chain until it is catabolised or removed. The circulation times between successive events (an event can be loss of TG, gain of an apoC molecule etc.) are first considered to be exponentially distributed, and we show that this leads to solutions identical to the solution to the compartmental formulation. However, the stochastic formulation allows for great flexibility if the holding times is not exponentially distributed. The stochastic simulation also gives a better description of the life cycle of a particle.

The project has been a collaboration between the bio-mathematics group at the School of Mathematical Sciences, Chalmers University of Technology and the Wallenberg Laboratory at the Sahlgrenska Academy, Göteborg University. There has also been a very close collaboration with the Division of Cardiology, Helsinki University Central Hospital, Finland and the Department of Pathological Biochemistry, Glasgow Royal Infirmary, UK.

Lipoproteins
The transport of lipids and cholesterol in the human body takes place in the blood system and is carried out by lipoproteins. Lipoproteins are spherical particles with a core of triglycerides (TG) and cholesterol ester (CE). Surrounding the core, which is non-polar, there is a monolayer of phospholipids (PL). The non-polar tail of the PL is pointing inwards, facing the core, and the polar head is pointing outwards. This configuration allows the otherwise hydrophobic lipids to be transported in the plasma. There is also some free cholesterol (FC) in the shell that stabilises the surface. On the surface of the particles different proteins are attached. These proteins can act as anchors, binding the particle to the cell wall, activating or inactivating different enzymes that remove TG, PL or add CE to the particle.
Depending on the composition of TG, CE, PL, FC and protein, the mass, diameter and density of particles vary widely. The combination of proteins and the particle density are used to define classes and subclasses of particles.

We focus on lipoproteins called Very Low Density Lipoproteins (VLDL), but both the experimental and modelling techniques are readily applicable to intermediate- and low density lipoproteins (IDL and LDL) as well. The VLDL are rich in TG and are synthesised in the liver. After the lipoproteins are released into the plasma, they start to loose TG to skeletal muscles and adipose tissue. As the TG content decreases the density increases. Particles of intermediate density are called Intermediate Density Lipoproteins (IDL) and ultimately, as most of the TG is lost, the particles becomes Low Density Lipoproteins (LDL). The liver produces mostly VLDL, but studies with tracer/tracee experiments and kinetic models suggests that the liver can synthesise and secrete both IDL and LDL sized particles. The density span of VLDL is often subdivided into two groups, $VLDL_1$ and $VLDL_2$.
Recent studies show that different kinds of LDL may originate form different types of VLDL, i.e. particles secreted as large, TG rich, $VLDL_1$ particles ends up as smaller and denser LDL. The smaller, less TG rich, $VLDL_2$ end up as normal LDL. The clearance rate of the small, dense LDL is much slower than for ordinary LDL. The small, dense LDL are more atherogenic and is associated with an increased risk of cardiovascular disease (CVD).
High levels of plasma TG is often due to a relatively high concentration of $VLDL_1$. Obesity and insulin resistance are correlated with high plasma TG levels and increased risk for CVD.

The two main areas that we wish to investigate are

1. The difference between lipoprotein kinetics in healthy controls and diabetes mellitus type-2 (DM2) subjects. We wish to know what mechanisms are responsible for the increased $VLDL_1$ pool in subjects with DM2. Is it an increased production, a decreased clearance rate, a combination or other factors? What can be said about the composition and size of the particles in the two groups of subjects?

2. The effects of insulin on lipoprotein metabolism. Insulin is a very important hormone which acts in several different ways. It lowers the levels of both glucose and free fatty acids (FFA) in the plasma, but it also (directly or indirectly) affects the synthesis of lipoproteins and most likely it affects lipoprotein lipase (LPL) activity. DM2 is associated with a low response to insulin. How does this affect the lipoprotein kinetics in subjects with DM2, and how is the lipoprotein metabolism changed when the insulin level is increased?

Data
To investigate these questions we have experimental data from both healthy control subjects as well as data from DM2 subjects. This project is a collaboration with Professor Marja-Riitta Taskinen at the Division of Cardiology, Helsinki University Central Hospital, Finland and Professor Chris Packard at the Department of Pathological Biochemistry, Royal Infirmary, University Hospital, Glasgow, Scotland. All data were collected in Helsinki and the analyses of the samples was performed both in Helsinki and in Glasgow.

In this thesis we study the kinetics by tracer/tracee experiments. The particles are labelled by stable isotopes and the enrichment is measured using Gas Chromatography/Mass Spectrometry (GC/MS). The total amount of material is also measured. From these data the fluxes of material can be estimated.
The experimental data consists of data from healthy control subjects (n=17) and DM2 patients. Each subject have measurements of enrichments and pool sizes of $VLDL_1$ and $VLDL_2$. Two studies are performed; A basal study, which is in a fasting steady-state, and a clamp study, where a constant insulin infusion is given.
In the studies two labels are simultaneously injected. These label both the particle itself, more precisely the single protein called apolipoprotein B-100, which is attached to all $VLDL_1$ and $VLDL_2$ particles, and the TG content.
The two tracers used are leucine and glycerol. In the liver the leucine is incorporated into a protein called apolipoprotein B, which is a protein that is attached to all $VLDL_1$, $VLDL_2$, IDL and LDL particles. The fraction of labelled particles can be estimated by measuring the enrichment of labelled leucine. The glycerol tracer is incorporated into TG and the fraction of labelled TG can be estimated by measuring the enrichment of labelled glycerol.

In the basal study the subjects are fasting before and during the turnover. With this setup the $VLDL_1$ and $VLDL_2$ pools are in equilibrium and are almost constant during the study. In the clamp study, a constant insulin injection is started 30 minutes before the tracers are injected. Intravenous glucose is given to keep the plasma glucose levels constant.

The Model
To investigate the kinetics, a combined multi compartmental model was developed. The model consists of several sub-models which describe the kinetics of the tracers before they are incorporated into the lipoprotein particles. Some of these sub-models could be replaced by forcing functions or by other sub-models if other tracers are used or if the experimental setup is modified.
In the lipoprotein model, each compartment corresponds to a collection of lipoprotein particles with a fixed size, defined by the amount of triglycerides per particle. The model consists of the equations describing the fluxes of material (particles and triglycerides) between compartments. The rate of change of material in a compartment is the difference of the fractional transfer from all other compartments and the fractional transfer from the compartment. In this application the fractional transfer coefficients are considered to be independent of the compartmental masses, and are regarded as constant or time dependent.

The derived model combines two models for the two different tracers to give a more detailed description of the kinetics, compared to models with one tracer. The ideas behind the combination of the models could readily be applied to experiments with more than two

tracers. It also allows for other tracers to be used. The model includes $VLDL_1$ and $VLDL_2$, but can be extended to include IDL and LDL as well. We investigate identifiability of the models and how use of population averages for some transfer coefficients impacts the results.

Outline of the Thesis

This thesis contains a main part where the modelling is described in detail. The model has been applied to experimental data of 17 healthy control subjects, the results of this study is presented in paper I. The results were consistent with earlier studies of apoB and TG kinetics. The combined model revealed a close relation between TG and apoB productions and between TG and apoB pool sizes. For the subjects participating in this study, the production was the main determinant of the pool size.

In paper II we present the results of the application of the model to the 17 control subjects compared to 10 DM2 subjects. Our results show that the overproduction of VLDL particles in diabetes mellitus type 2 is explained by enhanced secretion of $VLDL_1$ apoB and TG. Direct production of $VLDL_2$ apoB and TG was not influenced by diabetes per se. The production rates of $VLDL_1$ TG and apoB were closely related, as were the pool sizes of $VLDL_1$ TG and apoB. $VLDL_1$ and $VLDL_2$ composition did not differ in subjects with DM2 and controls, and the TG to apoB ratio of newly synthesised particles was very similar in the two groups

Results

To summarise this introduction we present the major results:

- We have developed a combined multi compartmental model that simultaneously models the particle and TG transfer between different density ranges. The model is locally identifiable and has no cycles (which guarantees non-oscillating solutions). Briefly, the model is constructed of two multi compartmental systems that describe the particle and TG transports. The fractional transfer rates of the two models are related to form a combined model.

- The model has been applied to both healthy control subjects and diabetes mellitus type-2 (DM2) subjects. The main results are; significantly increased $VLDL_1$ production in DM2 subjects. Comparable production of $VLDL_2$ and fractional transfer rates. The increased $VLDL_1$ production leads to increased $VLDL_1$ pools and therefore also to an increased absolute transfer from $VLDL_1$ to $VLDL_2$, which accounts for an increased $VLDL_2$ pool.

- We discuss the impact of removal of labels from the tracer and propose a stochastic model of the life cycle of lipoprotein particles. The data is not sufficient to justify a stochastic model that is more complex than the compartmental model. However, with more detailed data of the structural changes of the composition of the core and the surface of the lipoprotein during their metabolism more complex models has to be considered.

Contents

Chapter 1

Lipoproteins and Lipoprotein Metabolism

In this chapter we give a brief introduction to lipoproteins and lipoprotein kinetics. A more detailed description can be found in text books as [43].
Lipoproteins are the transporters of triglyceride (TG) and cholesterol ester (CE) in the blood system. They carry lipids from the intestine and the liver to skeletal muscles, adipose tissue and also back to the liver. As TG and CE molecules are non-polar they are hydrophobic. The lipoproteins are almost spherical particles with a core of TG and CE. Surrounding the core there is a monolayer of phospholipid (PL) and free cholesterol (FC). The fatty acid tail of the PL is non-polar and points inwards, meeting the non-polar core lipids. The phosphor group is polar and points outwards from the shell, making the particle mix well with water. The FC stabilises the shell, much like one layer of a membrane.
Different proteins are attached to the surface. These proteins, called apolipoproteins, interact with enzymes in the plasma and the arterial walls and regulates the metabolism of the particle. There exist several variants of lipoproteins all sharing the structure described above but with different kinetic behavior and different tasks. There are three main categories of lipoproteins. They are structurally different as they carry different apolipoproteins, but they also differ in their density.

ApoB-100 carrying lipoproteins The apoB-100 carrying lipoproteins all carry exactly one molecule of apolipoprotein B-100 (apoB-100 or just apoB). This molecule cannot be removed or replaced but is unique for each particle. The apoB carrying lipoproteins are divided into different groups, depending on their density. The largest, and most TG rich, particles have the lowest density and are called Very Low Density Lipoproteins (VLDL), intermediate sized particles are called Intermediate Density Lipoproteins (IDL) and the particles with the relatively highest density are the Low Density Lipoproteins (LDL). The VLDL, IDL and LDL are the same particles but at different stages in their metabolism. For instance, when a VLDL lose TG it forms a IDL. These particles are synthesised in and secreted from the liver and their main task is to transport lipids and cholesterol to skeletal muscles and adipose tissue.

Chylomicrons Particles similar to the VLDL are formed in the intestine. These particles are called chylomicrons and instead of apoB-100, these particles are equipped with an apolipoprotein called apolipoprotein B-48 (apoB-48). The apoB-48 molecule is identical

to the first 48% of the amino acids of an apoB-100 molecule. The chylomicrons are mostly present in the postprandial state.

HDL Apart from the apoB carrying lipoproteins, the liver also produces High Density Lipoproteins (HDL). The HDL transport cholesterol back to the liver.

Besides apoB and apoB-48, several other apolipoproteins are present on the surface of the lipoproteins. The apolipoproteins may catalyse or inhibit hydrolysis of TG or catalyse transfer of CE to the particle. These apolipoproteins can be transferred between different species of particles. The concentration of apolipoproteins on the surface of the lipoproteins depends on the time the particle has circulated the plasma, the composition of the particle and also on the size. For instance newly secreted particles are low in apoC but these are added from HDL. In only a few minutes after synthesis the particle is fully equipped with apoC and is ready to deliver TG. Most of the surface of LDL is covered by the apoB molecule, leaving almost no room for other apolipoproteins.

	Chyl	VLDL	IDL	LDL	HDL
density g/ml	<0.95	0.95-1.006	1.006-1.019	1.019-1.063	1.063-1.21
density S_f		20-400	12-20	0-12	
diameter nm	80-100	30-80	25-30	20-25	8-13
TG content %	90-95	50-65	25-40	4-6	7
CE %	2-4	8-14	20-35	34-35	10-20
FC %	1	4-7	7-11	6-15	5
PL %	2-6	12-16	16-24	22-26	25
protein %	1-2	5-10	12-16	22-26	45
major proteins	A-I (31)	C (40-50)	B-100 (60-80)	B-100 (>95)	A-I (65)
(% of total	C (32)	B-100(30-40)	C (10-20)	C (<1)	A-II (10-23)
protein)	E (10)	E (10-15)	E (10-15)	E (<1)	C (5-15)
	B-48 (5-8)				E (1-3)

Table 1.1: The different lipoproteins and their typical compositions. CE, cholesterol ester; FC, free cholesterol; PL, phospholipid. Adapted from [45].

In table 1.1 (adapted from [45]) the basic characteristics of the different lipoproteins are summarised. To differentiate between the different groups of lipoproteins, separation based on density is the most widely used method. Experimentally the subdivision is performed by consecutive ultracentrifugation. The discrimination is based on the Svedberg flotation index, S_f. The flotation index is a measure of the rotational velocity needed to make a particle float in a solution. A particle of mass M in a centrifuge is subjected to a centrifugal force $F_C = M\omega^2 r$, a buoyancy force $F_B = M\omega^2 r\rho_s/\rho_p$ and a frictional force $F_f = fv$, where ω is the angular velocity of the rotor, r is the distance of the particle to the rotor centrum, ρ_s is the density of the solvent, ρ_p is the density of the particle, f is the frictional coefficient and v the velocity of the particle. The Svedberg flotation index is defined as $S = v/(\omega^2 r) = M(1 - \rho_s/\rho_p)/f$. VLDL ranges from S_f 400 to 20. To get a better discrimination between particles, the VLDL fraction is further subdivided into subgroups VLDL_1 (S_f 400 to 60) and VLDL_2 (S_f 60 to 20).

1.1 Secretion

VLDL particles are synthesised in the liver. The precise mechanism of the lipoprotein assembly is not entirely known but evidence shows that it consists of two steps. First, two different VLDL-precursors, apoB containing particles and lipid droplets, are formed [1], [8]. The apoB containing particles are formed during the translation of the protein and in the following translocation to the lumen of the endoplasmic reticulum (ER). The mechanisms by which the other VLDL-precursor (the lipid droplets) is formed and how these two precursors are fused (the second step) are not known.
A small fraction of the lipoprotein particles are secreted from the liver into the IDL and LDL subfractions. In humans the apoB-48 carrying lipoproteins, the chylomicrons, are synthesised in the intestine.

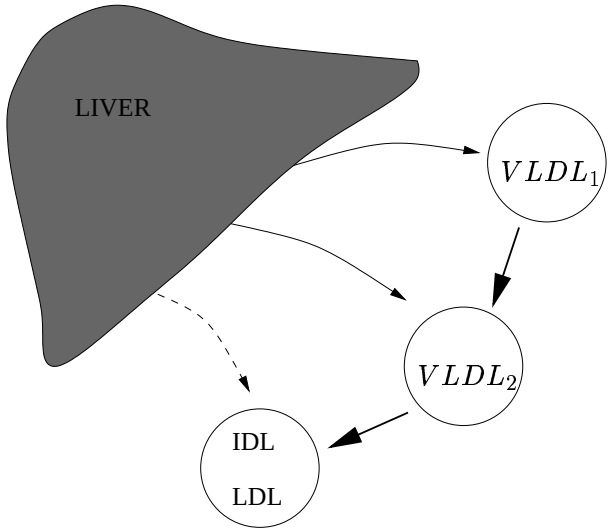

Figure 1.1: Most of the apoB containing lipoproteins are secreted in the $VLDL_1$ and $VLDL_2$ subfractions. Some apoB is secreted as IDL and LDL.

1.2 Plasma Kinetics

Circulating VLDL particles contain exactly one apoB molecule but also apolipoprotein C and E (apoC and apoE). The VLDL particles are secreted carrying only apoB, and apoC is added from reservoirs in HDL. After approximately 5 minutes a particle is fully equipped with apoC and is ready to deliver fatty acids to peripheral tissues. This delay allows for the particles to be well distributed in the plasma before the hydrolysation begins.
VLDL particles lose their TG content as the apoC activates the lipoprotein lipase (LPL) in the capillaries of the peripheral tissues. The apoB molecule is believed to bind to a specific proteoglycan on the cell wall and the neighboring LPL is activated by the apoC. LPL hydrolyses the 1 and 3 ester linkage of the TG to form 2-monoacylglycerol and un-esterified fatty acids. The turnover rate of LPL is approximately 10 molecules per second. One LPL complex acting on an average sized VLDL of $1.5 \cdot 10^5$ TG molecules would reduce the number of molecules by 50% in roughly 2 hours. The true time for such reduction is several-fold

less, suggesting that several LPL simultaneously act on a VLDL molecule. For the larger Chylomicrons (approximately $3 \cdot 10^5$ TG molecules) a 50% reduction from a LPL would take 3 hours whereas the measured $t_{1/2}$ is 10 -15 minutes. It has also been shown that the rate of hydrolysis of chylomicrons increases with the number of apoC per particle, also indicating that several LPL can act simultaneously on a single particle [43].
The particle is not fully hydrolysed in one step, but is probably dislocated from the arterial wall and re-associated several times.
As the *hydrolysis* continues, the density increases and when the density reaches the 1.006-1.019 g/ml range it is defined as an IDL particle. IDL is a substrate for cholesterol ester transfer protein (CETP). The CETP catalyses the exchange of TG for CE between apoB carrying lipoproteins and HDL. $30 - 50\%$ of the IDL is catabolised by *endocytosis* as the apoB and apoE allow the particles to bind to the LDL-receptor, primarily in the liver. The larger VLDL particles are not substrate for this, most likely because of the larger size. The rest of the IDL undergo further hydrolysation under the action of hepatic triglyceride lipase (HTGL or HL) and loose their apoC and apoE to HDL and produce a cholesterol-rich LDL particle. Figure 1.2 shows a schematic view of lipoprotein metabolism.
The LDL are rich in cholesterol and are commonly known as *bad cholesterol* (i.e. atherogenic lipoproteins). The HDL is the *good cholesterol*. The LDL particles can be further classified, in terms of their density, into LDL I, II and III. These can be found in two pools LDL-α and LDL-β, which arise from different sources. Particles secreted into $VLDL_1$ becomes an LDL-β particle and the LDL-α particles arise from particles secreted into the $VLDL_2$, IDL and LDL subfractions, as shown in figure 1.3. The LDL particles contain no or very little apoC and apoE.

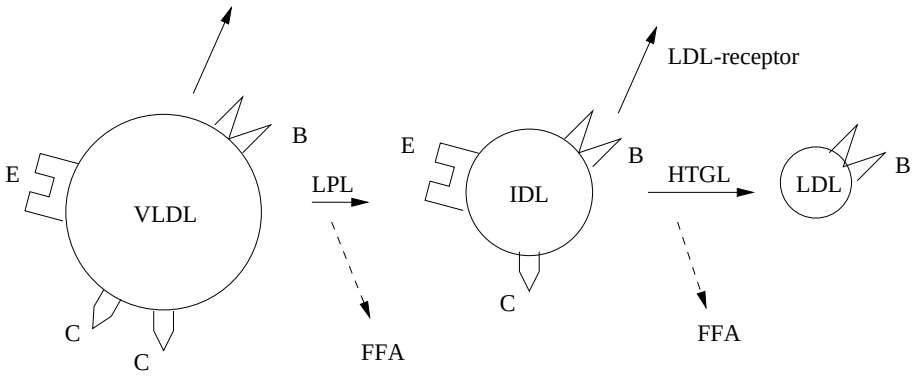

Figure 1.2: Schematic view of lipoprotein metabolism

1.3 General Model of Lipoprotein Metabolism

The metabolism of VLDL particles is mainly governed by hydrolysis by LPL. To some extent direct removal of particles by LDL or VLDL receptors might occur. $VLDL_2$ might be substrate for cholesterol ester transfer protein (CETP). The CETP removes TG in exchange for CE, hence the absolute amount of CE can increase during a particles lifetime. A consequence of this is that the amount of TG in a particle could be changed without changing the density of the particle.

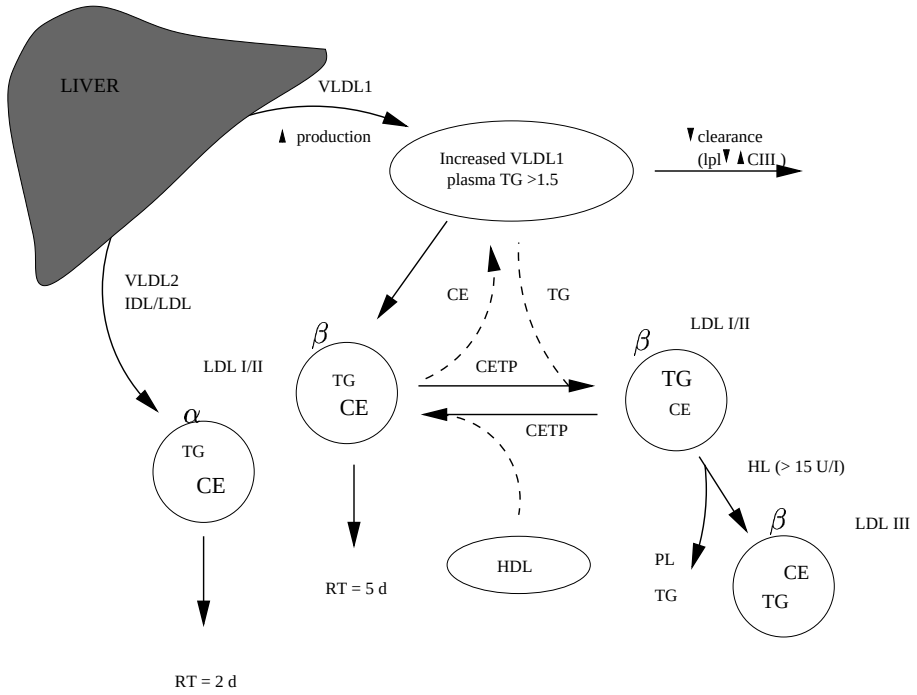

Figure 1.3: Kinetic evidence suggests that the two metabolically distinct pools in LDL (α and β) arise from different sources. Pool α is the major species detected in subjects with low to normal plasma triglyceride (TG) levels. LDL with the kinetic properties of pool β result from delipidation of $VLDL_1$. The two LDL species have substantially different residence times (RT) in the circulation. LDL-III generation is favored when the plasma triglyceride level is $>$ 1.5 mmol/l. As plasma triglyceride levels rise, $VLDL_1$ accumulate because of overproduction or defective removal. The action of HL removes lipid from the LDL-II to form LDL-III. CE, cholesterol ester; CETP, cholesterol ester transfer protein; PL, phospholipids.

The activity of LPL has been shown to depend on the apoC (apoCII and apoCIII), apoE, the composition of surface components and the TG to apoB ratio. There is also a competition for LPL enzymes between VLDL and chylomicrons, which is apparent at least after a meal (postprandial) [7].
Traditionally, the definition of the different subclasses is based on the density of the particles, as in table 1.1. Within the S_f ranges of $VLDL_1$ and $VLDL_2$ the composition, and the diameters, may vary widely. This complicates both the practical and theoretical analysis.
For a particle, let tg be the amount of TG, ce the amount of CE, pl the amount of PL, fc the amount of FC and na the amount of non-apoB proteins. Let $x = (tg, ce, pl, fc, na)$. Now x can be represented by a point in $\mathbb{R}^{5+}$. Let $S(x)$ be the S_f index of a particle of composition x, let $d(x)$ the diameter of the particle and let $D(x)$ be the density.
Let $\rho = (\rho_{tg}, \rho_{ce}, \rho_{pl}, \rho_{fc}, \rho_{na})^t$ be the vector of densities of the components in the composition vector x and let v be the corresponding vector of specific volume i.e. $v_i = 1/\rho_i$. The density values used is 0.915 for TG; 0.9579 for CE; 1.033 for FC; 1.031 for PL; for proteins a density of 1.288 g/ml was used, as calculated in [37].

The theoretical diameter can be calculated in different ways.
1) Given the composition of a particle, the apparent volume of a particle is given by

$$V(x) = x^T v = \pi d^3/6,$$

or

$$d(x) = \sqrt[3]{6x^T v/\pi}.$$

2) The phospholipid and free cholesterol shell has been measured to be approximately 21 nm. Given the amount of PL and FC in a particle the volume of the spherical shell can be calculated and from this the diameter of the particle can be calculated.
3) Analogously the diameter of the lipid core can be calculated from the TG and CE content.

The density of the particle can be calculated from the particle mass divided by the volume calculated from the above diameter. According to [24] the flotation index can be calculated as $S_f = d^2(\rho_s - \rho_p)/1.847$, where ρ_s is the density of the solution and ρ_p is the density of the particle.
With different combinations of the core and surface components, particles with identical S_f value but with different composition and diameter can exist. Furthermore within the $VLDL_1$ and $VLDL_2$ S_f span, a wide range of compositions and diameters are possible. In fact, data from several studies ([37], [25], [17], [23]) show that the ranges of densities vs diameter may overlap. For instance in [37] particles in S_f 20-100 (D) had a mean diameter of 35 (range 24-45), in S_f 100-175 (C) the mean diameter was 46 (35-62) and in S_f 175-400 (B) the mean was 61 (41-97). Hence the largest particles in of maximal S_f 100 can be larger than the smallest particles of minimal S_f 175. Data from this and other studies ([25], [17], [23]) are presented in figure 1.3. Consequently, using the method of Svedberg (i.e. ultracentrifugation) to separate particles gives overlapping spectra of densities and diameters.
To summarise, the newly secreted lipoprotein first circulates in the plasma until it is equipped will apoC and apoE. It then circulates in the plasma until it connects to LPL, which starts to hydrolyse the TG. The number of LPL acting (and hence the speed of hydrolysation) depends on several different factors, many of which are not known or at present date not possible to justify or test experimentally. Even known factors, such as apolipoprotein composition, are not fully investigated. A few hypothesis are:

- The exposed area of the shell, i.e. the area where the LPL can act. Parts of the surface can be blocked by apolipoproteins. For example the surface of the LDL particles are mostly covered by the apoB molecule.
- The apolipoproteins on the surface can both catalyse (apoCII is known to catalyse LPL) and inhibit the LPL.
- It is possible that the composition of the shell, i.e. content of free cholesterol and phospholipids, plays a role in the affinity for LPL.
- As the TG molecules that are closest to surface are removed the relative concentration of CE near the surface is increased. This will give a lack of substrate that could slow down the hydrolysation.

In all, the speed of hydrolysation might depend on the composition (which includes diameter) and on the material that has already been removed (which might alter the composition of the surface and the of the core close to the surface).

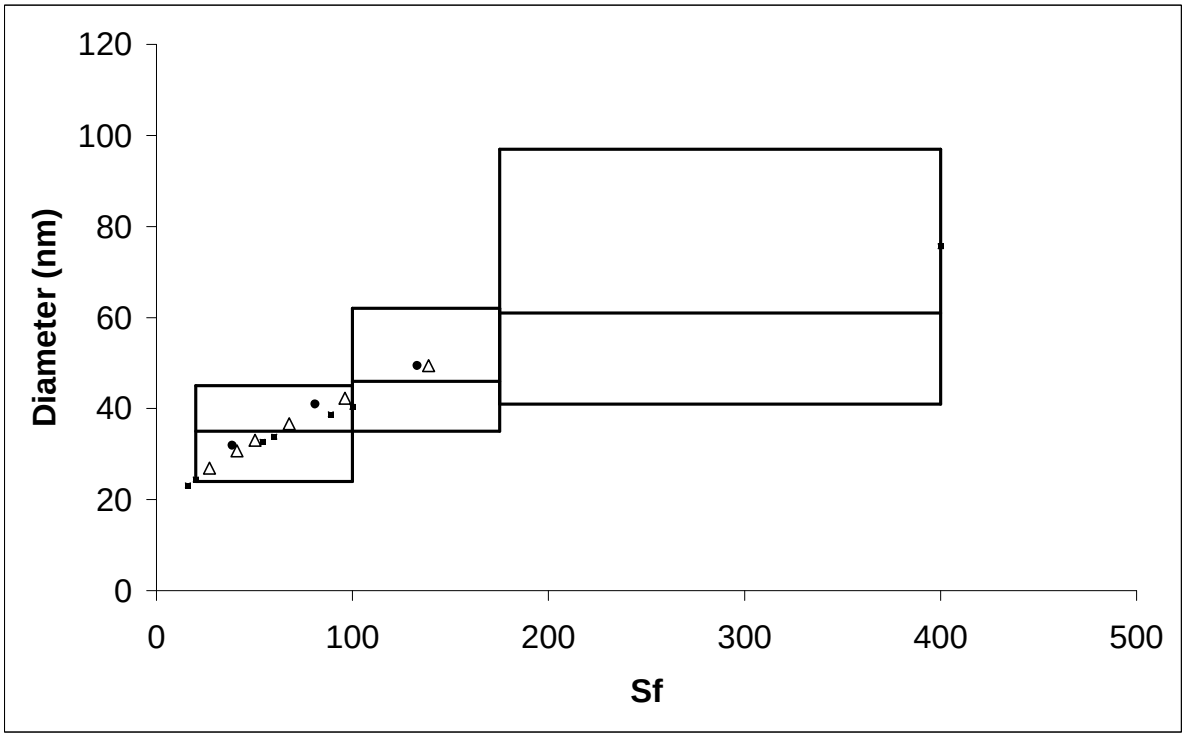

Figure 1.4: Data from [37] shows the relation between S_f index (x-axis) and diameter (y-axis). Three subdivisions of VLDL were used S_f 175-400 (B), S_f 100-175 (C) and S_f 20-100 (D). In (B) the mean diameter was 61 (range 41-97), in (C) 46 (35-62) and in (D) 35 (24-45). These numbers are presented as boxes with the mean as horizontal lines. One clearly sees that the overlap of diameters between the three fractions. Black boxes (■) represents data from [25], white triangles (△) are data from [17] and black circles (•) from [23]. In these studies different techniques were used to determine the diameter but it is obvious that the range of diameters within different subfractions of VLDL overlap.

Chapter 2

Multi Compartmental Modelling

Ordinary and Partial Differential Equations (ODE and PDE) are widely used to describe experiments in physics, chemistry and biology. For instance a simple model for the number of VLDL, IDL and LDL particles could be described by a system of four ordinary differential equations.
The mass of apoB corresponds to the number of particles and if the number of particles is large we can formulate the equations in terms of apoB mass instead of the number of particles. Let $b(t)$ be the apoB mass in the liver, and $v(t)$, $i(t)$ and $l(t)$ the apoB mass in VLDL, IDL and LDL respectively. The input of new apoB into the liver is $u(t)$. The transfer rates of apoB between liver and VLDL, VLDL and IDL and IDL and LDL are denoted $T_{v,b}$, $T_{i,v}$ and $T_{l,i}$. There may also be losses by direct catabolism of particles; denote these by C_α where $\alpha = b, v, i, j$. The equations describing the change of mass are

$$\begin{aligned}
\frac{db}{dt} &= u(t) - T_{v,b}(b,v,t) - C_b(b,t), \\
\frac{dv}{dt} &= T_{v,b}(b,v,t) - T_{i,v}(v,i,t) - C_v(v,t), \\
\frac{di}{dt} &= T_{i,v}(v,i,t) - T_{l,i}(i,l,t) - C_i(i,t), \\
\frac{dl}{dt} &= T_{l,i}(i,l,t) - C_l(l,t).
\end{aligned}$$

A way to obtain these equations is *multi compartmental modelling*. Multi compartmental modelling is commonly used in biochemistry and [36] is recommended for further reading. For a more mathematical description [3] or chapter 8 in [40] gives a good introduction. The following definitions can be found in [3] or [40].

Definition 1 (Compartment). A compartment is a well-mixed and kinetically homogeneous amount of material. A multi compartmental system is a finite set of compartments that interact by exchanging material. A multi compartment model is the set of mathematical equations describing the fluxes of material.

A compartment does not necessary correspond to a physical volume. In a chemical reaction with substance A and B, $A + B \rightleftharpoons AB$ one compartment may represent free mass of A and one compartment the mass of A bound to AB.

Definition 2 (Fractional transfer coefficient). The fraction of material transferred from compartment i to compartment j per time unit is called the fractional transfer coefficient and

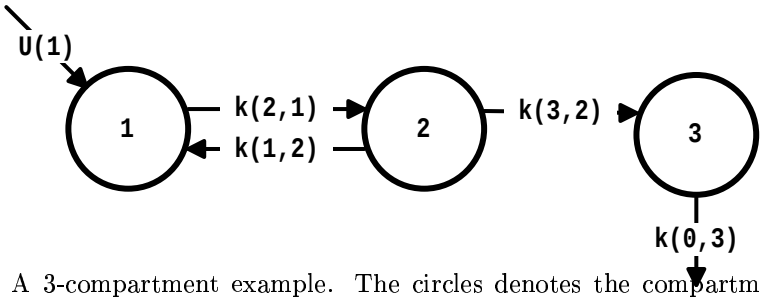

Figure 2.1: A 3-compartment example. The circles denotes the compartments and the arrows denotes the flux of material.

is denoted $k(j,i)$ or $k_{j,i}$. The flux from compartment i to compartment j is denoted $FLUX(j,i) = k(j,i)\ Q_i$, where Q_i is the mass in compartment i.

A compartmental model is often described graphically by circles or boxes (compartments) and arrows (fluxes) connecting the circles, as in figure 2.1. Throughout this thesis Q_i or q_i are used for the amount of material in a compartment i. Loss from a compartment i (not to other compartments) is described as a flux to the environment (or a compartment 0), and the corresponding fractional transfer coefficient is $k_{0,i}$. External input of material to compartment i is denoted $U_i(t)$. The equation for the rate of change of material in a compartment i in an n compartment system is

$$\frac{dQ_i(t)}{dt} = \sum_{\substack{j=1 \\ j\neq i}}^{n} k_{i,j}(\mathbf{Q},t)Q_j - \sum_{\substack{j=0 \\ j\neq i}}^{n} k_{j,i}(\mathbf{Q},t)Q_i + U_i(t). \tag{2.1}$$

Defining $k_{i,i} = -\sum_{\substack{j=0 \\ j\neq i}}^{n} k_{j,i}(\mathbf{Q},t)$, equation (2.1) becomes

$$\frac{dQ_i(t)}{dt} = \sum_{j=1}^{n} k_{i,j}(\mathbf{Q},t)Q_j + U_i(t). \tag{2.2}$$

The resulting system can be formulated as

$$\frac{d\mathbf{Q}(t)}{dt} = \mathbf{K}(\mathbf{Q},t)\mathbf{Q}(t) + \mathbf{U}(t). \tag{2.3}$$

Definition 3 (Linear multi compartmental models). A multi compartmental model of n compartments is linear if all $k_{j,i}$ are constants or depend on time only.

For linear models (which are the most common) it is often useful to write the input $\mathbf{U}(t)$ as $\mathbf{BV}(t)$, where $\mathbf{B}$ is an n by m matrix and $\mathbf{V} \in \mathbb{R}_+^m$. The reason is that the input to one compartment may be a linear combination of more than one input. An input may go to more than one compartment in an unknown proportion, but in most cases the matrix $\mathbf{B}$ consists of 0s and 1s. $\mathbf{B}$ is called the *input distribution matrix*.

Definition 4 (Steady-state). A multi compartmental model $\frac{d\mathbf{Q}(t)}{dt} = \mathbf{K}(\mathbf{Q},t)\mathbf{Q}(t) + \mathbf{U}(t)$ is in steady-state if the input $\mathbf{U}$ and $\mathbf{K}$ are independent of time, and the change of masses is 0.

The resulting equation in a steady-state model is

$$-\mathbf{U} = \mathbf{KQ}. \tag{2.4}$$

When modelling an experiment, sampling of data corresponds to measuring the masses in the corresponding compartments. In the model one or more compartments correspond to each set of measured data. The function that is sampled is $\mathbf{S}(t) = \mathbf{C}\mathbf{Q}(t)$. If the samples are taken at m places $\mathbf{S} \in \mathbb{R}^m$ and $\mathbf{C}$ is an m by n matrix. A more general definition can be made with the definition of an output.

Definition 5 (Output). An output is a linear combination of compartments connected to a recording device. The function $S(t) = \mathbf{c}^T\mathbf{Q}(t)$ is used to describe an output, $\mathbf{c}$ is a vector of size n. If there are m outputs these are numbered $S_i(t) = \mathbf{c}_i^T\mathbf{Q}(t),\ i = 1, \ldots, m$.

Note. *If all outputs are sampled at the same time points then* $\mathbf{C} = [\mathbf{c}_1 \cdots \mathbf{c}_m]^T$.

The equations are

$$\begin{aligned} \frac{d\mathbf{Q}(t)}{dt} &= \mathbf{K}(\mathbf{Q}, t)\mathbf{Q}(t) + \mathbf{B}\mathbf{V}(t) \\ S_i(t) &= \mathbf{c}_i^T\mathbf{Q}(t),\ i = 1, \ldots, m \end{aligned} \tag{2.5}$$

Both the formulation in equation (2.3) and the formulation (2.5) are used to describe the system, depending on the situation.

2.1 Basic Properties

From equation (2.1) and (2.2) some properties of the system (2.3) can be formulated. For the matrix $\mathbf{K}$ the following holds

i) Every diagonal element is non-positive ($k_{i,i} \leq 0$).

ii) Every off diagonal element is non-negative ($k_{i,j} \geq 0,\ j \neq i$).

iii) The column sums are non-positive ($-k_{0,i} \leq 0$).

Definition 6 (Compartmental matrix). A matrix satisfying i)-iii) is called a compartmental matrix.

Definition 7 (Exit). A compartment i having $k_{0,i} > 0$ is called an exit.

Let E denote the set of exits. A (directed) graph of a n by n matrix $\mathbf{A}$ is a set of n nodes, connected by arrows. Two nodes i and j are connected with an arrow from i to j if $\mathbf{A}\ (i, j)\ \neq\ 0$.

Definition 8 (Reachable). A compartment j is reachable from a compartment i if the graph of $\mathbf{K}^T$ contains a path between i and j.

For a compartment i the set of reachable compartments can be defined as $R_i = \{j : i \text{ reaches } j\}$.

Definition 9 (Open). A compartmental system is called open if every compartment can reach an exit, i.e. if the graph of $\mathbf{K}^T$ has a path from each compartment to an exit.

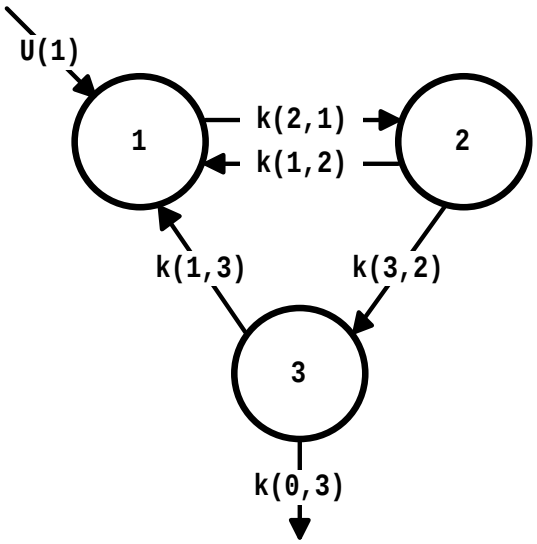

Figure 2.2: An example of a compartmental model with a circuit of length 3. The indices in the circuit are 3,1,2.

The condition for openness can also be formulated as $R_i \bigcap E \neq \emptyset, \forall i = 1, \ldots, n$, where $\emptyset$ denotes the empty set.
Gershgorins theorem states that each eigenvalue of a matrix $\mathbf{B}$ lies in the union of the n disks $|\lambda - b_{i,i}| \leq \sum_{\substack{j=1 \\ j \neq i}}^{n} |b_{i,j}|$. For the matrix $\mathbf{K}$ the centers of the disks are in $k_{i,i} \leq 0$ and the radius is less than or equal to $-k_{i,i}$. Hence, the real part for each eigenvalue λ of $\mathbf{K}$ is non positive ($\Re(\lambda) \leq 0$) and no eigenvalue is purely imaginary.
In an open system with no external input (for $t > 0$) and with an initial amount of material in each compartment, the equation for the change of material is $\frac{d\mathbf{Q}(t)}{dt} = \mathbf{K}\mathbf{Q}(t)$. Clearly $\mathbf{Q}(t) \to 0$ as $t \to \infty$, and the system cannot have a constant particular solution i.e. no eigenvalue of $\mathbf{K}$ is 0. Hence $\Re(\lambda) < 0$ for every eigenvalue λ, and therefore $\mathbf{K}$ is nonsingular.
A *circuit* of a graph is a set of distinct indices $j_1, \ldots\ j_K$ such that $k_{j_1,j_2}, \ldots\ , k_{j_{K-1},j_K}, k_{j_K,j_1} \neq 0$, as in the example in figure 2.2. If λ is an eigenvalue of $\mathbf{K}$ then $\lambda + \alpha$ is an eigenvalue of $\mathbf{M} = \alpha\mathbf{I} + \mathbf{K}$. Moreover if $\mathbf{K}$ is irreducible[1] then $\mathbf{M}$ is irreducible. Theorem 1 in [22] states that if $\mathbf{M}$ is irreducible and non-negative and the longest circuit in the graph of $\mathbf{M}$ has length 2, then all eigenvalues of $\mathbf{M}$ are real.
If $\alpha \in \mathbb{R}$ is chosen such that $\mathbf{M} = \alpha\mathbf{I} + \mathbf{K} \geq 0$, $\mathbf{K}$ is irreducible and the longest circuit of $\mathbf{K}$ are of length 2 then all eigenvalues of $\mathbf{K}$ are real.
Hence, if a compartmental model do not have any circuits longer that 2 the solution will not oscillate. This will be used to investigate the models constructed in section 4.1.3. Oscillations can occur in tracer recycling as discussed in section 2.2.1

[1] A square matrix is reducible it there exist two disjoint (non-empty) sets $i_1, \ldots, i_\eta$ and $j_1, \ldots, j_\mu$ s.t. $a_{i_\alpha, j_\beta} = 0$, for $\alpha = 1, \ldots, \eta$ and $\beta = 1, \ldots, \mu$. A matrix that not is reducible is irreducible.

2.2 Tracer/tracee Experiments

Consider an experiment to study the amount of lipoproteins secreted from the liver per hour. If the lipoproteins are characterised by their density, a particle newly secreted from the liver cannot be distinguished from a particle that has circulated the system for a while. Hence, there is no possibility to measure the actual fluxes of particles. All that can be measured is the number of particles (or the masses) in different density ranges, but that is not enough to describe the kinetics of the particles.

This is a case where tracer/tracee experiments are useful. By introducing markers or labels on some of the particles secreted from the liver, these can be followed by measuring the concentration of labelled particles. The labelled material is called the tracer and the material being studied is called the tracee. Knowledge about the kinetics of the tracee can be gained by studying the kinetics of the tracer.
When choosing the tracer, one must consider several aspects, the most important ones being the following:

i) The biological system should not be able to distinguish between the tracee and the tracer.

ii) In steady-state experiments, the amount of tracer should be small enough not to affect the steady-state.

iii) There should be no exchange of labels between labelled compounds and other compounds, and the natural occurrence of the labels should be negligible or at least under control.

Let $\mathbf{Q}$ be the mass of the tracee and $\mathbf{q}$ the mass of the tracer. The system for the total mass is

$$\frac{d(\mathbf{Q}(t)+\mathbf{q}(t))}{dt} = \mathbf{K}(\mathbf{Q}+\mathbf{q}(t),t)(\mathbf{Q}(t)+\mathbf{q}(t))+\mathbf{U}(t)+\mathbf{u}(t),$$

where $\mathbf{u}(t)$ is the input of tracer. Or, for a single compartment

$$\frac{d(Q_i(t)+q_i(t))}{dt} = \sum_{j=1}^{n} k_{i,j}(\mathbf{Q}+\mathbf{q},t)(Q_j+q_j)+U_i(t)+u_i(t).$$

If the mass of the tracer is assumed to be small compared to the tracee mass, the right hand side can be Taylor expanded in $\mathbf{Q}$, which gives

$$\begin{aligned}&\sum_{j=1}^{n} k_{i,j}(\mathbf{Q},t)Q_j+U_i(t)+\\ &+\sum_{j=1}^{n}(\sum_{l=1}^{n}\frac{\partial k_{i,j}(\mathbf{Q},t)}{\partial Q_l}Q_j+k_{i,j}(\mathbf{Q},t))q_j+\\ &+u_i(t)+O(\|q\|^2).\end{aligned}$$

Subtracting equation (2.2)

$$\begin{aligned}\frac{dq_i(t)}{dt} = &\sum_{j=1}^{n}(\sum_{l=1}^{n}\frac{\partial k_{i,j}(\mathbf{Q},t)}{\partial Q_l}Q_j+k_{i,j}(\mathbf{Q},t))q_j+\\ &+u_i(t)+O(\|q\|^2).\end{aligned}$$

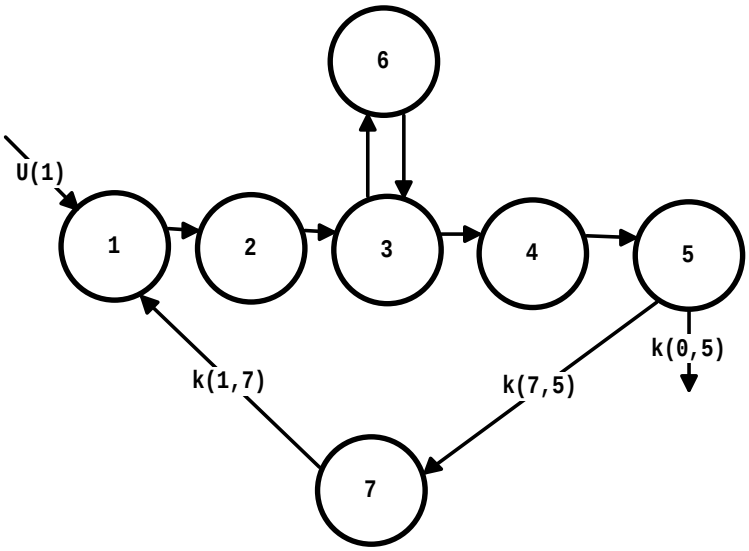

Figure 2.3: The main model consists of compartments 1 to 5. Compartment 6 is a recycling compartment where material is stored before re-entering the system. Material can also be recycled through compartment 7 before it re-enters the system as new material.

If the amount of tracer is small, the quadratic term can be neglected, and the resulting linearised system for $\mathbf{q}$ is

$$\frac{dq_i(t)}{dt} = \sum_{j=1}^{n}(\sum_{l=1}^{n}\frac{\partial k_{i,j}(\mathbf{Q},t)}{\partial Q_l}Q_j + k_{i,j}(\mathbf{Q},t))q_j + u_i(t).$$

In the linear case, the equations are

$$\frac{d(\mathbf{Q}(t)+\mathbf{q}(t))}{dt} = \mathbf{K}(t)(\mathbf{Q}(t)+\mathbf{q}(t)) + \mathbf{U}(t) + \mathbf{u}(t),$$

and subtracting equation (2.3)

$$\frac{d\mathbf{q}(t)}{dt} = \mathbf{K}(t)\mathbf{q}(t) + \mathbf{u}(t). \tag{2.6}$$

2.2.1 Recycling

Recycling of tracer material can occur on different scales. An example is a short *off-line* storage of material, before it re-enters the system. In figure 2.3 compartments 1 to 5 can be considered the main pathway and compartment 6 is a short-term recycling pool. This kind of recycling does not a normally pose problems in the modelling, since it does not introduce cycles in the compartmental model.
On the other hand, recycling of material can occur on a much larger scale. For example the amino acids from an apoB molecule that has been degraded can re enter the liver and be incorporated into a new apoB. In figure 2.3 compartment 7 is a long-term recycling pool.
For the tracee this is usually not a problem, since the amount that is recycled can be incorporated into the external input function. However, for the tracer it is a potential problem. Recycling of labelled material can introduce oscillations as described in section 2.1. The impact of such recycling depend on several things, such as the time scale of the experiment and the magnitude of the recycling.

One way to work around the problem with recycling of tracer material is to introduce a forcing function. If the input compartment is corresponds to a measured enrichment pool then the enrichment in that compartment could be forced to equal the measured enrichment.

2.3 Sampling

In experiments the outputs are sampled. Let m be the number of outputs and N_i the number of time points when the i:th output is sampled, and $t_{i,j}$ the j:th time point, $j = 1, \ldots, N_i$ and $i = 1, \ldots, m$. The outputs are usually ordered so that the tracee outputs are $1, \ldots, m^e$ and the tracer outputs $m^e + 1, \ldots, m$. The samples are denoted $\phi_{i,j}$ and if $\phi_{i,j}$ is a sample of $S_i(t_{i,j})$ we write $\phi_{i,j} \sim S_i(t_{i,j})$. Here $\phi_{i,j} \sim S_i(t_{i,j}) = \mathbf{c}_i^T \mathbf{Q}(t_{i,j})$ for $i = 1, \ldots, m^e$ and $\phi_{i,j} \sim S_i(t_{i,j}) = \frac{\mathbf{c}_i^T \mathbf{q}(t_{i,j})}{\mathbf{c}_i^T \mathbf{Q}(ti,j)}$ for $i = m^e + 1, \ldots, m$.

2.4 Modelling Delays

So far we have only considered regular compartmental systems. However, it is not uncommon that there exist delays (also referred to as lags) in the system, i.e. the transfer of material between two compartments are not instant. In the simple discrete linear case, the delayed system of equations is the modified linear version of system 2.1

$$\frac{dQ_i(t)}{dt} = \sum_{\substack{j=1 \\ j \neq i}}^{n} k_{i,j} Q_j(t - \tau_{i,j}) - \sum_{\substack{j=0 \\ j \neq i}}^{n} k_{j,i} Q_i(t) + U_i(t), \tag{2.7}$$

where $\tau_{i,j}$ is the lag time between the source compartment j and destination compartment i. In the more general case, there can be a distribution of delay times, i.e. the inflow of material to a compartment depends on the mass in the other compartments over a period of time. This would be described by an equation of the form

$$\frac{dQ_i(t)}{dt} = \sum_{\substack{j=1 \\ j \neq i}}^{n} k_{i,j} \int_{-\infty}^{t} Q_j(\tau) h_{i,j}(t - \tau) - \sum_{\substack{j=0 \\ j \neq i}}^{n} k_{j,i} Q_i(t) + U_i(t), \tag{2.8}$$

where $h_{i,j}$ a density function. In the tracer case, there is no material in the system at $t = 0$ and hence the integral in equation (2.8) is from 0 to t. If $h_{i,j} = \delta t$ the equations (2.7) and (2.8) are the same.

2.4.1 Implementing delays

The compartmental system defined by equation (2.8) is not as simple to implement as an linear system without delays. There exist methods of describing delays with linear compartmental subsystems. We here describe the far most common used method, which is the method used in the SAAMII program (Section 2.8).
The delay is modelled as a number (n) of identical compartments, e.g. with the same transfer-coefficients k_D (figure 2.4). The delay time, T_D, is defined to be the time it takes for the first compartment after the delay to reach its maximum amount given an instant input to the delay.

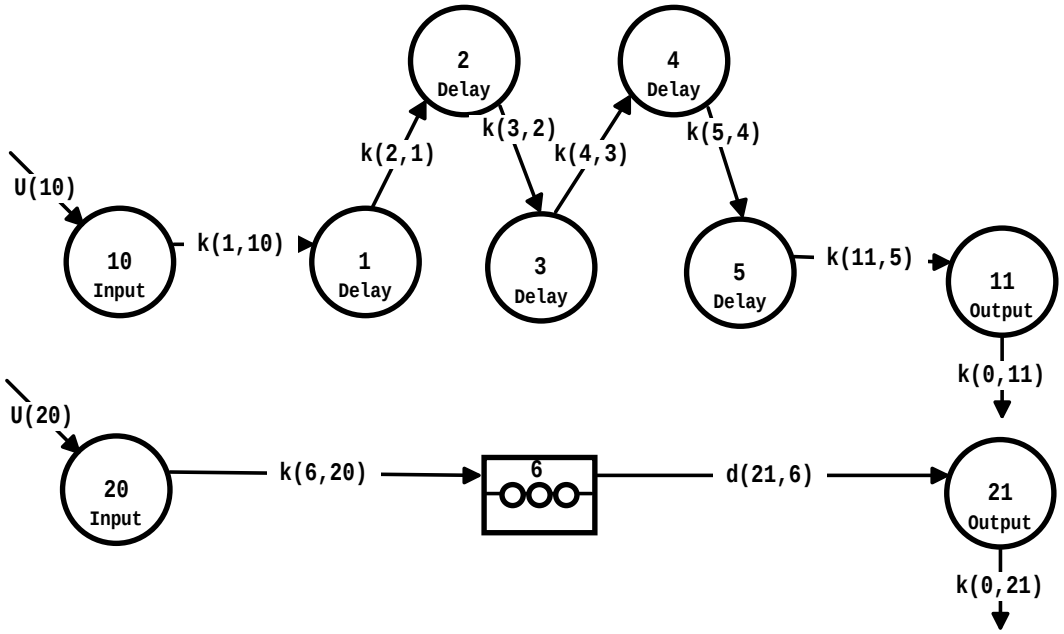

Figure 2.4: Delay as a compartmental system. If the delay time is T, the transfer coefficients $k(2,1)$, $k(3,2)$, $k(4,3)$, $k(5,4$ and $k(11,5)$ are equal to $5/T$. The symbol for compartment 6 is used for delays.

The equations are

$$\frac{d}{dt}\begin{pmatrix} Q_1 \\ Q_2 \\ \vdots \\ Q_n \end{pmatrix} = \begin{pmatrix} -k_D & 0 & 0 & 0 & 0 \\ k_D & -k_D & 0 & 0 & 0 \\ 0 & \ddots & \ddots & \ddots & 0 \\ 0 & \ddots & k_D & -k_D & 0 \\ 0 & 0 & 0 & k_D & -k_D \end{pmatrix} \begin{pmatrix} Q_1 \\ Q_2 \\ \vdots \\ Q_n \end{pmatrix} + \begin{pmatrix} f(t) \\ 0 \\ \vdots \\ 0 \end{pmatrix},$$

or

$$\frac{d\mathbf{Q}(t)}{dt} = \mathbf{K}\mathbf{Q}(t) + \mathbf{U}(t). \tag{2.9}$$

To decide how to choose k_D, fix n and use a instant input

$$\begin{aligned} \mathbf{U} &= \mathbf{0} \\ \mathbf{Q}_0 &= \begin{pmatrix} 1 & 0 & \cdots & 0 \end{pmatrix}^T, \end{aligned} \tag{2.10}$$

The solution to equations (2.9) - (2.10) is

$$\mathbf{Q}(t) = e^{\mathbf{K}t}\mathbf{Q}_0$$

Note that $\mathbf{K} = -k_D\mathbf{I} + k_D\mathbf{N}$, where $\mathbf{N}$ has ones on the first sub-diagonal. Clearly $\mathbf{IN} = \mathbf{NI}$, so

$$\begin{aligned} e^{\mathbf{K}t} &= e^{-k_D t\mathbf{I}} e^{k_D t\mathbf{N}} \\ &= e^{-k_D t}(\mathbf{I} + k_D t\mathbf{N} + \cdots + (k_D t)^{n-1}\frac{\mathbf{N}^{n-1}}{(n-1)!}). \end{aligned}$$

This gives an equation for the mass in the i:th compartment

$$Q_i(t) = e^{-k_D t}\frac{(k_D t)^{i-1}}{(i-1)!}.$$

The maximum is attained when $\dot{\mathbf{Q}} = 0$, i.e.

$$\begin{aligned} 0 = \frac{dQ_i}{dt} &= -k_D e^{-k_D t}\frac{(k_D t)^{i-1}}{(i-1)!} + e^{-k_D t}(i-1)\frac{(k_D t)^{i-2}}{(i-1)!} \\ &= e^{-k_D t}\frac{(k_D t)^{i-2}}{(i-1)!}k_D(-k_D t + (i-1)). \end{aligned}$$

So compartment i in the delay attains its maximum at $t = (i-1)/k_D$, hence the first compartment after the delay attains its maximum at $t = n/k_D$. Therefore it is natural to choose $k_D = n/T_D$.
Inspecting the equations we conclude that the outflow from the delay is $k_D Q_n(t)$ and hence

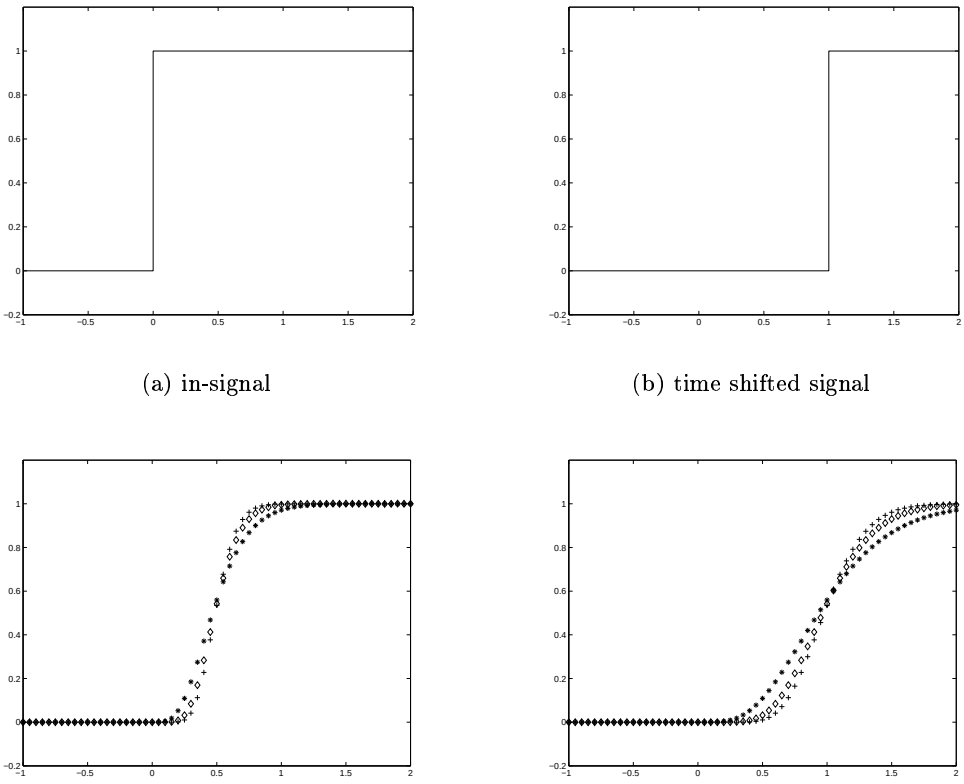

(a) in-signal

(b) time shifted signal

(c) delay-time 0.5 h

(d) delay-time 1 h

Figure 2.5: Delays modelled as in figure 2.4 for $T_D = 0.5$ and $T_D = 1$. Input signal is a constant function. 5 compartments - '$*$', 10 compartments - '$\diamond$' and 15 compartments - '$+$'. Notice that the sharpness of the delay depends on the number of compartments and the desired delay-time.

the density distribution for the delay is

$$h_n(t) = k_D e^{-k_D t} \frac{(k_D t)^{n-1}}{(n-1)!}. \tag{2.11}$$

The number of compartments in the delay controls the shape of the delay curve. With a fixed number of compartments a longer delay time gives a more spread out curve, and consequently with a fixed delay time more compartments will give a steeper curve as in figure 2.5. In fact, if T_D is fixed and $n \to \infty$ then the delay density distribution in equation (2.11) tends to the delta function. A proof of this can be found in [20]. In [20] it is also proved that this linear chain delay is the discrete approximation of the PDE describing the *volume displacement flow*. Furthermore, if the number of compartments tend to infinity then the solution to the linear chain delay converges to the solution to the PDE.

2.5 Solving ODE

The systems that arise are of the form

$$\begin{aligned} \dot{\mathbf{Q}}(t) &= \mathbf{K}(t)\ \mathbf{Q}(t) + \mathbf{U}(t), \\ \mathbf{Q}(0) &= \mathbf{Q}_0. \end{aligned}$$

Here we only give some facts about linear ODE systems. Consider a constant coefficient problem

$$\dot{\mathbf{Q}}(t) = \mathbf{K}\ \mathbf{Q}(t) + \mathbf{U}(t), \tag{2.12}$$

$$\mathbf{Q}(0) = \mathbf{Q}_0. \tag{2.13}$$

The homogeneous system $\dot{\mathbf{Q}}(t) = \mathbf{K}\ \mathbf{Q}(t)$ has the solution $\mathbf{Q}(t) = e^{\mathbf{K}\ t}\mathbf{c}$, for any $\mathbf{c} \in \mathbb{R}^n$. For a (square) matrix $\mathbf{A}$, $e^{\mathbf{A}}$ is defined as

$$e^{\mathbf{A}} = \mathbf{I} + \mathbf{A} + \frac{\mathbf{A}^2}{2!} + \frac{\mathbf{A}^3}{3!} + \cdots .$$

A particular solution to (2.12)-(2.13) is given by

$$\mathbf{Q}(t) = \int_0^t e^{\mathbf{K}(t-s)}\mathbf{U}(s)ds + e^{\mathbf{K}\ t}\mathbf{Q}_0.$$

In the simplest case $\mathbf{U}(t)$ is constant. In most applications the tracer injection is either an instant injection, $\mathbf{u}(t) = \delta(t)$, a constant function $\mathbf{u}(t) = C$ or a combination of these. In the case where U is constant the solution is (if K is nonsingular)

$$\begin{aligned} \mathbf{Q}(t) &= [-e^{\mathbf{K}\ (t-s)}\mathbf{K}^{-1}\ \mathbf{U}]_{s=0}^{s=t} + e^{\mathbf{K}\ t}\mathbf{Q}_0 \\ &= e^{\mathbf{K}\ t}(K^{-1}\mathbf{U} + \mathbf{Q}_0) - \mathbf{K}^{-1}\ \mathbf{U}. \end{aligned}$$

A solution to the linear model, equation (2.6) with $\mathbf{u}(t) = 0$ can be written as

$$\mathbf{q}(t) = c_i \sum_{i=1}^{n} e^{\lambda_i t}\mathbf{v}_i,$$

where c_i are constants, λ_i are eigenvalues of $\mathbf{K}$ and $\mathbf{v}_i$ the corresponding eigenvector. If the eigenvalues have negative real part, then the solution is damped and goes to 0 as t grows. If the eigenvalues are real, then there cannot be any oscillations as discussed in section 2.1.

2.6 Time Dependent Transfer Rates

The transfer rates can very well depend on time. For instance, the transfer rate corresponds to the lipolytic rate which might vary with time due to the insulin infusion in the clamp studies. We define these transfer rates by $k_{i,j}(t) = k^0_{i,j} g_{i,j}(t)$. Where $g_{i,j}(t) = 1$ for $t \leq 0$ and $g_{i,j}(t) > 0$ for $t < T$, where T is the experimental time.
The $g_{i,j}$ model physical/biological reactions which can be considered to be smooth functions of time. However, the data limits the complexity of the functions to be estimated. The distribution of the sampling points as well as the number of data points limits the number of parameters that can be estimated. Initially three classes of functions are considered; piecewise constant, piecewise linear and exponential functions.

2.7 Finding Optimal Parameters

In a general ODE model there are measurements Φ_i of a known function $\mathbf{Y}(t)$ at time points $t = t_i$. The function $\mathbf{Y}(t)$ is a function of the vector of unknown parameters, $\mathbf{p}$, and the solution to the ODE system, $\mathbf{Q}$. The system is

$$(*) \begin{cases} \mathbf{Y}(t) &= \mathbf{G}(\mathbf{Q}, \mathbf{p}, t), \\ \dot{\mathbf{Q}}(t) &= \mathbf{F}(\mathbf{Q}, \mathbf{p}, t), \\ \mathbf{Q}(0) &= \mathbf{0}. \end{cases}$$

Note. $\mathbf{G}$ *can depend on* $\mathbf{p}$ *since an unknown proportion of the compartments might be measured. Initial amounts can be treated as instant injections and* $\mathbf{Q}(0) = \mathbf{0}$.

The problem is to find the collection of parameters $\mathbf{p}$ that solves

$$\min_{\mathbf{p}} \sum_{i=1}^{n} \text{error}(\Phi_i, \mathbf{Y}(\mathbf{p}, t_i)),$$

subject to $(*)$, where $\text{error}(\Phi_i, \mathbf{S}(\mathbf{p}, t_i))$ is a measure of the difference between the calculated and measured value at the i:th time point.

In the linear tracer/tracee compartmental case the samples are as in Section 2.3. The objective function is defined as

$$\text{O}(\mathbf{p}) \quad = \quad \sum_{i=1}^{m} \sum_{j=1}^{N_i} \text{error}(\phi_{i,j}, S_i(\mathbf{p}, t_{i,j})).$$

The minimising problem is to find the $\mathbf{p}$ that achieves

$$\min_{\mathbf{p}} \mathrm{O}(\mathbf{p}),$$

subject to S_i being the solutions to the system

$$(**)\begin{cases} S_i(\mathbf{p}, t_{i,j}) &= \mathbf{c}_i^T \mathbf{Q}(t_{i,j}),\ i = 1, \ldots, m^e, \\ S_i(\mathbf{p}, t_{i,j}) &= \frac{\mathbf{c}_i^T \mathbf{q}(t_{i,j})}{\mathbf{c}_i^T \mathbf{Q}(t_{i,j})},\ i = m^e + 1, \ldots, m, \\ \dot{\mathbf{Q}}(t) &= \mathbf{K}(\mathbf{p}, t)\mathbf{Q} + \mathbf{U}(\mathbf{p}, t), \\ \dot{\mathbf{q}}(t) &= \mathbf{K}(\mathbf{p}, t)\mathbf{q} + \mathbf{u}(\mathbf{p}, t), \\ \mathbf{Q}(0) &= \mathbf{Q}_0(p), \\ \mathbf{q}(0) &= \mathbf{q}_0(p). \end{cases}$$

Note. *In tracer/tracee and isotopic labelling experiments* $\mathbf{q}_0$ *is usually known, but it might be the case that one injection goes into more than one compartment and in an unknown proportion.*

2.7.1 Least squares

The most common choice of error function $\mathrm{error}(\tilde{(x)}, x)$ is the quadratic function, which gives the solution in the least square sense.

$$\mathrm{O}_{\mathrm{LS}}(\mathbf{p}) = \sum_{i=1}^{N} (\Phi_i - \mathbf{Y}(\mathbf{p}, t_i))^2.$$

Assume that $\mathbf{F}(\mathbf{Q}, \mathbf{p}, t)$ is the correct model. Then there exists a parameter vector $\bar{\mathbf{p}}$ such that

$$\Phi_i = \mathbf{Y}(\bar{\mathbf{Q}}, \bar{\mathbf{p}}, t_i),$$

and hence

$$\mathrm{O}_{\mathrm{LS}}(\bar{\mathbf{p}}) = 0,$$

where $\bar{\mathbf{Q}}$ solves

$$\begin{aligned} \dot{\mathbf{Q}}(t) &= \mathbf{F}(\mathbf{Q}, \mathbf{p}, t) \\ \mathbf{Q}(0) &= \mathbf{0}. \end{aligned}$$

The least squares technique is very common in parameter estimation, numerical analysis and optimisation. There is a large literature in least squares techniques and it can be found in almost any book in numerical analysis, statistics, optimisation etc. For the implementation used here, books like [14] and [40] on Regression Analysis or [5] on nonlinear parameter estimation, give the necessary information.
A motivation for the least squares method is that if the errors are independent and identically distributed $\mathrm{N}(0, \sigma^2)$ the least squares estimate coincides with the maximum likelihood estimate. One can also see the least square estimation as the solution that minimises (in the usual norm) the residual, i.e. the least square solution is the projection of the true solution.
An objective function with a simple sum of squares is often unsatisfactory. The size of the measurements may vary, here the tracee/tracer ratios are of order 10^{-3} and pool sizes are up

to 10^2, or some measurements are less reliable than others. A solution to these two drawbacks is to introduce weighted least squares. The weighted least squares problem is here defined as

$$\mathrm{O}_{\mathrm{WLS}}(\mathbf{p}) = \sum_{i=1}^{N} w_i(\Phi_i - \mathbf{Y}(\mathbf{p}, t_i))^2, \tag{2.14}$$

for $w_i > 0$.

In the compartmental model the data is organised in different sets, of different sizes. The weighted least squares formulation is then:

$$\mathrm{O}_{\mathrm{WLS}}(\mathbf{p}) = \sum_{i=1}^{m}\sum_{j=1}^{N_i} w_{i,j}(\phi_{i,j} - S_i(\mathbf{p}, t_{i,j}))^2.$$

Assume that $\mathbf{K}(\mathbf{p}, t)$, $\mathbf{U}(\mathbf{p}, t)$ and $\mathbf{u}(\mathbf{p}, t)$ are the correct model. Then there exists an parameter vector $\bar{\mathbf{p}}$ such that

$$\phi_{i,j} = S_i(\bar{\mathbf{p}}, t_{i,j}),$$

and hence

$$\mathrm{O}_{\mathrm{WLS}}(\bar{\mathbf{p}}) = 0.$$

Here $\bar{\mathbf{p}}$, $\bar{\mathbf{Q}}$ and $\bar{\mathbf{q}}$ satisfies $(**)$.
To guarantee the uniqueness of the solution $\bar{\mathbf{p}}$ the model has to be investigated for identifiability, as described in section 2.9.
So far we assumed that there exists no errors in the measurements. Unfortunately this assumption is not true in most applications, and then the sample is the sum of the true value and an error term $e_{i,j}$. Hence,

$$\phi_{i,j} = S_i(\mathbf{p}, t_{i,j}) + e_{i,j}.$$

Or equivalently,

$$e_{i,j} = \phi_{i,j} - S_i(\mathbf{p}, t_{i,j}).$$

We assume that the expectation $\mathbb{E}(e_{i,j}) = 0$ and that the variance of the error element $e_{i,j}$ is $v_i\sigma_{i,j}$, where v_i is a variance parameter for data set j and $\sigma_{i,j}$ is the standard deviation associated to the sample $\phi_{i,j}$.
In this paper we use the variance of the measurement as weights for the data, i.e. we let $w_{i,j} = 1/(v_i\sigma_{i,j}^2)$ in 2.14.

$$\mathrm{O}_{\mathrm{WLS}}(\mathbf{p}) = \sum_{i=1}^{m}\sum_{j=1}^{N_i}\left(\frac{\phi_{i,j} - S_i(\mathbf{p}, t_{i,j})}{v_i\sigma_{i,j}}\right)^2.$$

If a point is measured with high accuracy, i.e. its variance is small, then that data point will have a large weight in the objective function. The variance parameter v_i and the standard deviation $\sigma_{i,j}$ has to be estimated from the data, from previous experiments or from a priori knowledge about the errors in the analysis of data.
As will be discussed in Section 2.8, in the software used, SAAMII, the objective function also includes a logarithmic term of the weights. It is also possible to include a Baysian term in the objective function. This can be useful if some *a priori* information for some parameters are known from earlier experiments and studies or from analysis of the analytic methods.

2.7.2 Search algorithms

After choosing a starting point $\mathbf{p}_0$ there are several approaches to look for an optimal solution. In general, most search algorithms are based on the following; First a *search direction* is chosen, and then a *step length*. The most common choice is the *steepest descent* search direction; it finds the direction in which the greatest change of the objective function is achieved. The algorithm chooses a new search direction and a new step length in each iteration and repeats until an approximation of the optimum is reached.

2.8 Software

In the work described in this thesis a commercially available program called **SAAMII** (*Simulation, Analysis And Modelling*) is used to create the model and perform the optimisation. SAAMII consists of a numerical and a compartmental module. The compartmental module has a graphical interface where compartments and transfers are drawn on a canvas and the corresponding equations are generated. A system is easily created by drawing compartments on the screen and transfer rates are assign by linking compartments together.
In SAAMII tracer/tracee experiment is then created by making a *system* (tracee) and a tracer experiment. The outputs are created as samples of the compartments and are associated with user data. Delays are modelled as a single component and implemented as described in Section 2.4.

2.8.1 Optimisation in SAAMII

In SAAMII the objective function is a weighted least squares function with the variance as weights. The variance model is

$$\begin{aligned} Var(e_{i,j}) &= V_{i,j}(v_i, \phi_{i,j}, S_i(\mathbf{p}, t_{i,j})) \\ &= v_i \ \sigma_{i,j}, \end{aligned}$$

where v_i is a measure of the set variance i.e of how good the data set are. The objective function also includes a logarithmic term of the weights. Without such a term, the objective function could be arbitrary decreased by choosing parameters that increase the estimated variance. The complete objective function in SAAMII is

$$\mathrm{O}_{\mathrm{SAAM}}(\mathbf{p}) = \frac{1}{M}\sum_{i=1}^{m}\sum_{j=1}^{N_i}\frac{(\phi_{i,j} - S_i(\mathbf{p}, t_{i,j}))^2}{V_{i,j}(v_i, \phi_{i,j}, S_i(\mathbf{p}, t_{i,j}))} + \log(V_{i,j}(v_i, \phi_{i,j}, S_i(\mathbf{p}, t_{i,j}))).$$

Here M is the total number of time sample points. There is also a possibility to use Baysian estimation of one or more parameters. If there are some parameters with a known mean and standard deviation (from earlier studies or population means) these parameters are being treated as an extra data set. The extra term in the objective function is

$$\sum_{k=1}^{N_b}(\frac{p_k - m_k}{\sigma_k})^2 + \log(\sigma_k^2),$$

where p_k are the parameters, m_k their mean values and σ_k the standard deviation. N_b is the number of parameters being estimated with Baysian estimation.

2.8.2 Variance and weights

For the variance model, the eight combinations in table 2.1 are possible.

Variance model	based on data	based on model
Known standard deviation, d	$\sigma_{i,j} = d$	$\sigma_{i,j} = d$
Known fractional standard deviation, f	$\sigma_{i,j} = f\ \phi_{i,j}$	$\sigma_{i,j} = f\ S_i(\mathbf{p}, t_{i,j})$
Known poisson statics, r	$\sigma_{i,j} = \sqrt{r\ \phi_{i,j}}$	$\sigma_{i,j} = \sqrt{r\ S_i(\mathbf{p}, t_{i,j})}$
General formula, A, B, C	$\sigma_{i,j} = \sqrt{A + B\ \phi_{i,j}^C}$	$\sigma_{i,j} = \sqrt{A + B\ S_i(\mathbf{p}, t_{i,j})^C}$

Table 2.1: Variance models used in SAAMII, d, f, r, A, B, C are user supplied parameters.

The v_i component is estimated by

$$\hat{v}_i = \frac{1}{N_i} \sum_{j=1}^{N_i} \frac{(\phi_{i,j} - S_i(\mathbf{p}, t_{i,j}))^2}{V_{i,j}(1, \phi_{i,j}, S_i(\mathbf{p}, t_{i,j}))}.$$

We have used the fractional standard deviation model, as described in sections 2.7 and 3.

More extensive documentation of SAAMII can be found in [47] or at *www.saam.com*.

2.9 Identification

System identification theory deals with question weather the unknown parameters in the model can be determined from the experiment. This is a very complex field of research and the available results are often only relevant in special cases. Structural identifiability was first introduced by Bellman and Åstrom in [4] in 1970.
The following is adapted from [11]. In system identification theory, the concepts of *controllable* and *observable* are very important. A system is controllable if each state variable can be independently influenced from the inputs and observable if each state variable can be reconstructed from the outputs. We use the term *structurally* controllable (observable) if the system is controllable (observable) almost everywhere in the parameter space. Furthermore, a state variable is input (output) connectable if there exists a path (in the graph of K) from an input to the state variable (from the state to en output). A system is input-output connectable if all state variables are input and output connectable.

A linear compartmental system as defined by equation (2.5), in section 2, is

$$\begin{aligned} \frac{d\mathbf{Q}}{dt} &= \mathbf{K}(p)\mathbf{Q}(t) + \mathbf{B}(p)\mathbf{V}(t), \\ \mathbf{S}(t) &= \mathbf{C}(p)\mathbf{Q}(t), \end{aligned} \tag{2.15}$$

where the matrices K, V and C depend on the unknown parameter vector p.

The system is structurally controllable (observable) if the following two conditions hold [12]

1. The system is input (output) connectable,
2. $rank([K\ B]) = n \qquad (rank \begin{bmatrix} K \\ C \end{bmatrix} = n)$.

$[\mathbf{K}\ \mathbf{B}]$ and $\begin{bmatrix}\mathbf{K}\\ \mathbf{C}\end{bmatrix}$ are block matrices composed of $\mathbf{K}$, $\mathbf{B}$ and $\mathbf{C}$.
A necessary condition for structural identifiability is for the system to be input-output connectable.

To show that a system is structurally identifiable is considerable more difficult. For the purpose here we limit ourself to discuss linear compartmental models, assuming delays are implemented as linear chains.
One approach to show structural identification is by introduction of Markov parameters as discussed in [9] and [19]. The test then consists in determining the rank of a large matrix of derivatives.
Other methods are based on the transfer function of the model. Taking the Laplace transform

$$\begin{aligned} s\hat{\mathbf{Q}}(s) &= \mathbf{K}(p)\hat{\mathbf{Q}}(s)\mathbf{B}(p)\hat{\mathbf{V}}(s), \\ \hat{\mathbf{Q}}(s) &= (s\mathbf{I}-\mathbf{K}(p))^{-1}\mathbf{B}(p)\hat{\mathbf{V}}(s), \\ \hat{\mathbf{S}}(s) &= \mathbf{C}(p)(s\mathbf{I}-\mathbf{K}(p))^{-1}\mathbf{B}(p)\hat{\mathbf{V}}(s). \end{aligned}$$

Finally, the transfer function $\mathbf{H}(s,p)$ is defined as

$$\begin{aligned} \mathbf{H}(s,p) &= [\frac{\hat{\mathbf{S}}_i(s)}{\hat{\mathbf{V}}_j(s)}] = [\mathbf{H}_{ij}(s,p)] \\ &= \mathbf{C}(p)(s\mathbf{I}-\mathbf{K}(p))^{-1}\mathbf{B}(p). \end{aligned} \tag{2.16}$$

The measured outputs can be written as

$$S_j(t) = \sum_{i=0}^{n} A_{i,j}(p)e^{\lambda_{i,j}(p)t},$$

where $A_{i,j}$ and λ_i can be estimated from data, for instance by using least squares optimisation.
The Laplace transform of $\mathbf{S}(t)$ is

$$\begin{aligned} \hat{S}_j(s) &= \sum_{i=0}^{n} \frac{A_{i,j}(p)}{s-\lambda_i} \\ &= \frac{\sum_{i=0}^{n-1}\beta_{i,j}s^i}{\sum_{i=0}^{n}\alpha_{i,j}s^i}. \end{aligned} \tag{2.17}$$

Some special compartmental systems, e.g. closed and almost closed catenary and mamillary systems, have been showed to be identifiable ([4], [10]). This was done by investigating the transfer functions, i.e. comparing the coefficients in the two equations (2.16) and (2.17). The input function is often chosen to be the dirac delta function.
However, for more complex models, comparing the coefficients is often a difficult task. The coefficients α_{ij} and β_{ij} are functions of the parameters in the model. Even for small models the number of terms can be large, and the number of variables in the terms can be large. In [9] a method based on the rank of the matrix of the derivatives of the α_{ij}'s and β_{ij}'s with respect to the unknown parameters is described.
In [2] Audoly et. al. presented a computer algebra algorithm for structurally identification. It uses computer algebra to solve the system formed by comparing equations (2.16) and (2.17). Here we give a brief description of the algorithm. The algorithm uses *cycles* and *paths* rather than the unknown parameters. A path is a set of consecutive edges in the graph and a cycle is a path that starts and ends the same compartment. In the algorithm a path (cycles) are

expressed as the polynomial of transfer coefficients of the edges of the path (cycle). Briefly, the algorithm does the following steps.

1. Express the α_{ij}'s and β_{ij}'s as polynomials in paths and cycles by comparison of coefficients in equation (2.16).
2. Assign a numerical value to the right hand side by randomly assigning a numerical value to all unknown parameters. The parameters should fulfill the equation (2.15).
3. Use the Buchberger algorithm to find a Gröbner basis for the set of polynomials in cycles and paths.
4. Replace the cycles and paths by their expression in the unknown parameters and apply the Buchberger algorithm again.

If the model is identifiable then the basis is in triangular form. The introduction of the cycles and paths reduces the complexity of the system. If there are no cycles in the model this step is un-necessary. Other methods, using other techniques to solve the system of polynomials exist.

Yet another approach is based on local algebraic observability. Sedoglavic [41] presented a probabilistic algorithm based on algebraic observability. The algorithm finds the observable and non-observable variables of a system in polynomial time. This method does not require the system to be linear.
Above we defined a state to be observable if it could be reconstructed from the output. The unknown parameters in the compartmental model are the transfer coefficient and unknown parameters in the input-distribution matrix B and output matrix C. These unknown parameters can be considered as variables with zero derivative. Hence if the following system is observable, the parameters are identifiable.

$$\begin{aligned} \frac{d\mathbf{p}}{dt} &= \mathbf{0}, \\ \frac{d\mathbf{Q}}{dt} &= \mathbf{K}(p)\mathbf{Q}(t) + \mathbf{B}(p)\mathbf{V}(t), \\ \mathbf{S}(t) &= \mathbf{C}(p)\mathbf{Q}(t) \end{aligned}$$

We will not describe the algorithm here but refer to [41].

Both the methods by Sedoglavic and Audoly are suitable for the kind of models that we study in this thesis, and we have used them to verify that our models in fact are identifiable. Note, however, that in the case of time dependent transfer coefficients fall outside the frame unless the time dependence is parameterised with a finite number of parameters.

Chapter 3

The Experimental Setup

A central role in the analysis lies in detecting differences in the lipid metabolism between healthy control subjects and patients with diabetes mellitus type-2 (DM2). The data consists of seventeen healthy controls and ten DM2 subjects.

The available data consists of composition measurements of $VLDL_1$ and $VLDL_2$. This data consists of concentrations of TG, CE, FC, PL, total protein and apoB protein. These concentrations are measured at 0, 4 and 8 hours in the basal study and at -0.5, 0, 4 and 8 hours for the clamp study. In the modelling we use the TG and apoB concentrations converted into absolute masses. The fasting study is in the fasting state, the subjects are fasting for 8 hours prior and during the study. This gives an approximate steady-state. In the clamped study, insulin is given at -0.5 hours and the tracers are given at 0 hours. To compensate for the insulin, which lowers the plasma glucose levels, glucose in given during the study.
There are also measurements of the enrichment of the tracers leucine - corresponding to apoB and glycerol - corresponding to TG.
All experiments and analysis of samples (not including enrichments) were carried out at the Division of Cardiology, Helsinki University Central Hospital, Finland. The enrichments were analysed at the Department of Pathological Biochemistry, Glasgow Royal Infirmary, Scotland. The study was initiated before our collaboration was started and the outline of the experiment was therefore already decided. For the sake of completeness, we give a detailed description of the experiment appendix A. Here we give rather detailed description of the analysis of the enrichments.

3.1 Tracer/tracee Experiments

The pool sizes alone cannot be used to determine the synthesis and catabolic rates of $VLDL_1$ and $VLDL_2$ particles. It is therefore necessary to introduce tracers. Tracers are particles behaving exactly as the particles whose kinetics we wish to investigate (the tracee). A small amount of tracer is introduced and then the concentration of the tracer relative the tracee is measured. If the tracer is introduced as an instant injection (bolus injection) the enrichment curves (the tracer/tracee ratios) corresponds to the impulse response of the system.
The choice of tracee's here are the apoB and the TG. Since each lipoprotein particle has exactly one apoB molecule, the mass of apoB corresponds to the number of particles. The apoB molecule is a very long protein-chain of about 500 kD (kilo dalton) and over 4500 amino

acid residues, consisting of about 12% leucine.
Labelled leucine ($^2H_3$-Leucine) was injected into the plasma by which it is distributed to various places including the liver where it is used in the synthesis of proteins. The labelled leucine will appear in all proteins containing leucine, among these the apoB molecule.
When labelling the TG there are two possibilities, either to label the fatty acids or to label the glycerol. The choice was to label the glycerol backbone of the TG molecule by (1,1,2,3,3 ^2H)-glycerol. The labelled glycerol is incorporated into the TG in the esterification of the fatty acids in the liver.

3.2 Methods

3.2.1 Turnover Protocol

All subjects were admitted at 7:30 a.m. to the metabolic ward of the Helsinki University Central Hospital after a 12-h overnight fast. A saline infusion was started. Thirty minutes later, leucine (5,5,5-D^3), 7 mg/kg body weight (bw), and glycerol (1,1,2,3,3-D^5), 500 mg, were injected as a bolus in a vain in one arm. Samples were obtained from a vain in the other arm. For measurement of free $^2H_3$-leucine concentration in plasma, blood samples were taken before the tracer injection and at 2, 4, 6, 8, 10, 12, 15, 20, 30, and 45 min and 1, 2, 3, 4, 6, and 8 h. For measurement of $^2H_3$-leucine and $^2H_5$-glycerol in $VLDL_1$ and $VLDL_2$, blood samples were taken before the injection of tracers and at 15, 30, 45, 60, 75, 90, 120, and 150 min and 3, 4, 5, 6, 7, and 8 h. In some subjects, additional samples were taken at 8 minutes. The particle composition and apoB mass of the $VLDL_1$ and $VLDL_2$ fractions were determined 30 min before and 0, 4, and 8 h after the injection. The subjects continued to fast until 5 p.m., when the last blood sample was taken.

3.2.2 Analysis

A detailed description of the isolation and analysis of lipoproteins is given in appendix A. Here we give a brief description of the analysis.
$VLDL_1$ and $VLDL_2$ were separated using consecutive ultra centrifugation, i.e. after preparation the samples were centrifuged and the particles are ordered in the samples according to their density. The top part ($VLDL_1$) is taken away and the procedure is repeated. The apoB and TG pool sizes were analysed from samples obtained at 0, 4, and 8 h. In these samples the concentration of total protein, triglyceride, cholesterol esters, free cholesterol, phospholipid and apoB. Pool sizes for apoB and TG were calculated as the product of plasma volume (4.5% of bw) and the plasma concentration of apoB and TG in $VLDL_1$ and $VLDL_2$. The leucine content of the apoB pool was calculated from the apoB amino acid residue composition. The glycerol content was calculated from the TG concentration using a molecular weight of 885 g/mol for TG and 92 g/mol for glycerol and assuming that one mole of TG equals one mole of glycerol.

3.2.3 Determination of Enrichments of Leucine and Glycerol

We here give a description of the analysis of glycerol enrichment. The enrichment of leucine was determined in a similar manner.

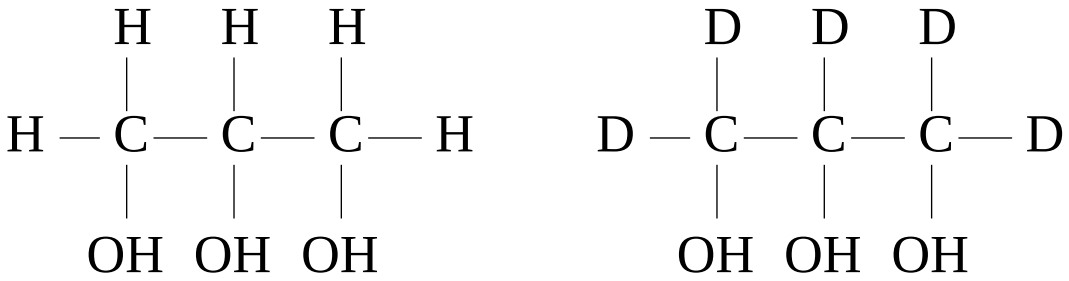

Figure 3.1: **Left:** Unlabelled glycerol molecule, **Right:** Labelled glycerol molecule

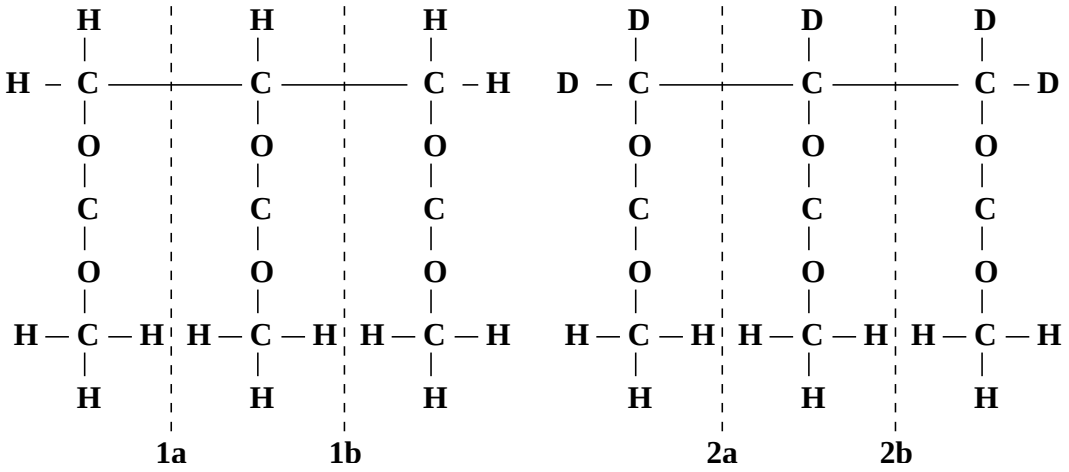

Figure 3.2: **Left:** Unlabelled glycerol triacetate molecule, **Right:** Labelled glycerol triacetate molecule. The molecules are split at either 1a or 1b (or 2a 2b) to form two fragments. The enrichment of the larger fragment is measured.

Glycerol (figure 3.1) was treated with pyridine and acetic anhydride to form glycerol triacetate, $C_9H_{14}O_6$ (figure 3.2). The enrichment was measured using Gas Chromatography/Mass Spectrometry (GC/MS). The molecule is split between carbon 1 and 2 or 2 and 3 in the glycerol backbone to form two fragments, $C_6H_9O_4$ and $C_3H_5O_2$. The split is symmetric so the fragments that are formed are identical, independently of where the molecule is split. The larger fragment has a mass per charge ratio (m/z) of 145 and the smaller fragment has m/z 73. It is the enrichment of the larger fragment that is measured. If the original glycerol molecule was from the tracer, three of the hydrogen atoms would be ^{2}H (deuterium) and the m/z would then be 148.

In the nature, atoms exist in different isotopes, e.g. carbon exists as ^{12}C and ^{13}C. Hence, fractions of the unlabelled glycerol will have a m/z 146, 147, 148 etc. The theoretical abundance of the different isotopomers can be calculated using the natural abundance of the atoms in the molecule. The natural abundance of C, H and O is summarised i table 3.1.

We define the discrete probability density function (pdf) as $P_C(0) = 0.989300$, $P_C(1) = 0.010700$ and $P_C(i) = 0,\ i \neq 0,\ 1$, i.e. $P_C(i)$ is the probability that a carbon atom has atomic weight

	$m+0$	$m+1$	$m+2$
C	0.989300	0.010700	
H	0.999885	0.000115	
O	0.997570	0.000380	0.002050

Table 3.1: Natural abundance of isotopes of carbon, hydrogen and oxygen. m is the natural isotope atomic weight of the corresponding atom (12 for carbon, 1 for hydrogen and 16 for oxygen).

$m+i$, where m is the atomic weight of the most common natural isotope. The pdf's for hydrogen and oxygen are defined analogously. For a molecule, the pdf for the molecular mass can be calculated by taking the discrete convolution of the pdf's of the atoms in the molecule. Hence, the pdf for $C_6H_9O_4$ is

$$\begin{aligned} P_{C_6H_9O_4}(i) &= P_C * P_C * P_C * P_C * P_C * P_C * P_H * P_H * P_H * P_H * P_H * P_H * P_H * P_H * \\ &\quad *P_H * P_O * P_O * P_O * P_O(i) \end{aligned}$$

The labelled fragment has three hydrogen atoms that are known to be ^{2}H. The pdf for these are $P_D(1) = 1,\ P_D(i) = 0,\ i \neq 1$ and we can denote this fragment by $C_6H_6O_4D_3$

$$\begin{aligned} P_{C_6H_6O_4D_3} &= P_C * P_C * P_C * P_C * P_C * P_C * P_H * P_H * P_H * P_H * P_H * P_H * P_D * P_D * \\ &\quad *P_D * P_O * P_O * P_O * P_O(i). \end{aligned}$$

In practice, since the number of atoms in the molecules is quite high and $P_H(1)$ is so small, the probability density function for the labelled fragment is almost a shifted variant of the pdf for the unlabelled fragment, i.e $P_{C_6H_6O_4D_3}(i) \approx P_{C_6H_9O_4}(i+3)$. In figure 3.3 the pdf for the two fragments are shown. The labelled fragment is dashed. In practice we do not use the theoretical values for the pdf's, instead the distribution of the isotopes is approximated through measurements.

The GC/MS the counts the number of molecules having m/z 145, 146, 147, 148 etc. In the samples, the peaks from 145+0, 145+1 and 145+2 originate from the tracee and the 145+3 peak is a combination of molecules from both the tracer and tracee. There is a great difference in the number of molecules in the 145+0 and 145+3 peaks and this can cause problems in the precision in the measurements. Therefore the 145+3 and 145+2 peaks are measured instead, and the 145+0 peak is calculated from a known ratio of the 145+0 and 145+2 peaks.

For a sample taken at time t, the number of particles with m/z 145+i is denoted by $N_i(t)$. Since no tracee can turn up in $N_i(t)$ for $i = 0,\ 1,\ 2$, the ratio of of the 145+2 and 145+0 peaks is constant, and we denote this ratio R_0^2. We now have, for a sample time t_j

$$N_0(t_j) = \frac{N_2(t_j)}{R_0^2}$$

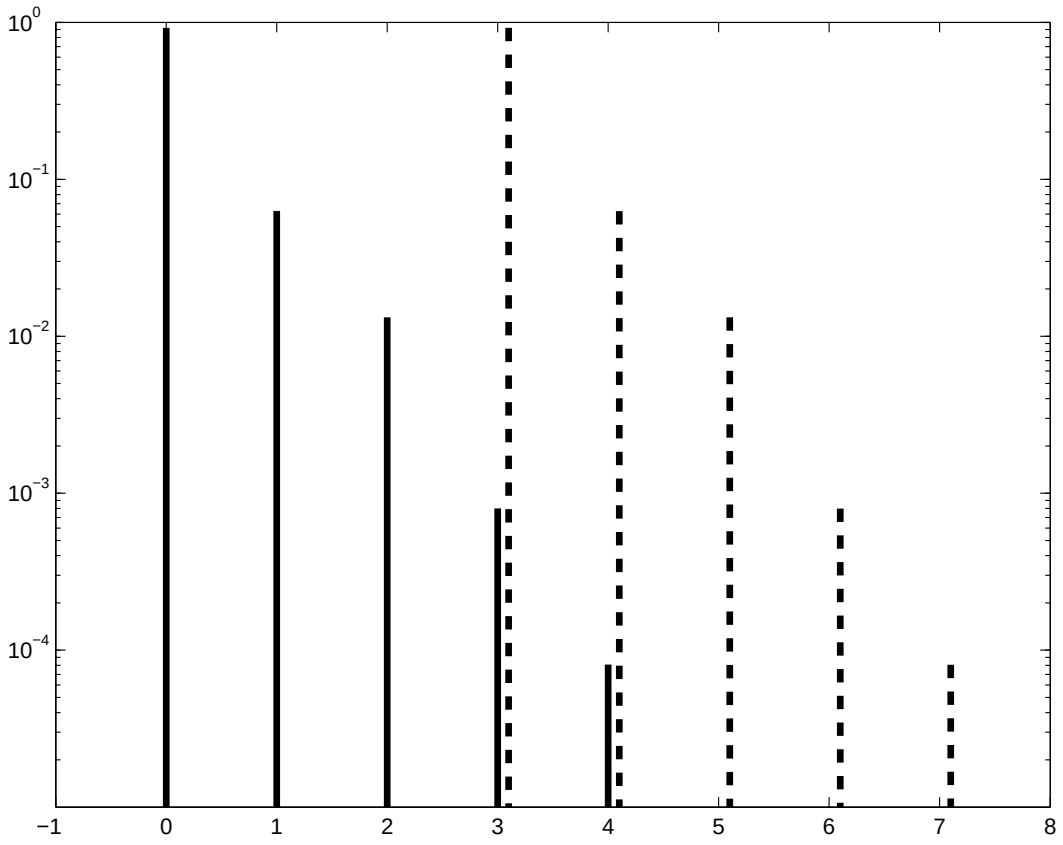

Figure 3.3: The discrete probability density functions for the molecular masses of the fragments. Solid line, $P_{C_6H_9O_4}(i)$ for $i = 0, \ldots, 7$. Dashed line, $P_{C_6H_6O_4D_3}(i)$ for $i = 0, \ldots, 7$.

The 145+3 to 145+0 ratio then is

$$\begin{aligned} R_0^3(t_j) &= \frac{N_3(t_j)}{N_0(t_j)} \\ &= \frac{N_3(t_j)R_0^2}{N_2(t_j)} \end{aligned}$$

The measurement $N_3(t)$ is the sum of the number tracer and tracee particles in the 145+3 peak. Denote the number of tracer particles in the sample taken at t_j by $T_3(t_j)$ and the number of tracee particles by $\hat{N}_3(t_j)$

$$R_0^3(t_j) = \frac{\hat{N}_3(t_j)R_0^2}{N_2(t_j)} + \frac{T_3(t_j)R_0^2}{N_2(t_j)}$$

The ratio $\hat{N}_3(t_j)/N_2(t_j)$ is constant and can be determined from a sample taken before the tracer is injected; we denote this sample time by t_0.

In this sample we have $\hat{N}_3(t_0) = N_3(t_0)$, and then

$$\begin{aligned} R_0^3(t_j) &= \frac{N_3(t_0)R_0^2}{N_2(t_0)} + \frac{T_3(t_j)R_0^2}{N_2(t_j)} \\ &= \frac{N_3(t_j)R_0^2}{N_2(t_j)}, \\ \frac{T_3(t_j)R_0^2}{N_2(t_j)} &= \frac{N_3(t_j)R_0^2}{N_2(t_j)} - \frac{N_3(t_0)R_0^2}{N_2(t_0)}. \end{aligned} \tag{3.1}$$

Equation (3.1) is then corrected by the total number of particles (tracee+tracer) to form the molar percent excess (mpe) equation. First denote

$$IR(t_j) = \frac{N_3(t_j)R_2^0}{N_2(t_j)}.$$

Then

$$\text{mpe}(t_j) = \frac{IR(t_j) - IR(t_0)}{1 + (IR(t_j) - IR(t_0))} 100. \tag{3.2}$$

Standards with enrichments of 0.00-1.00 mpe were included at the beginning and end of each batch of samples and used to correct the calculated mpe values with the calculated recovery rate of the standards. In the experiment care was taken to ensure similar total ion counts in the standards and all samples.

3.3 The Clamp Experiment

The experimental setup is in this case an over night fast, followed by an insulin infusion during the 8.5 hours experiment. The experiment is clamped, i.e. glucose is given intravenously to give a constant plasma glucose level. The insulin is given at -30 minutes, and the apoB and TG pool sizes are measured at -30, 0, 240 and 480 minutes. The enrichments of apoB and TG are measured at 0, 15, 30, 45, 60, 75, 90, 120, and 150 min and 3, 4, 5, 6, 7, and 8 h.

3.4 Error Analysis

It is difficult to to make a completely quantitative estimation of the errors in the measurements. In the preparation and analysis of the samples errors can be introduced. Basically two kinds of data are used, the pool sizes calculated from the measured concentrations and the enrichments.

To measuring the enrichments basically means counting the number of unlabelled and labelled molecules in the sample, as described in section 3.2.3 above. This counting process can be seen as poisson process. For large number of observations the poisson process can be approximated with a normal distribution with mean n and standard deviation $\sqrt{n}$ [38]. In this case the number of particles was 10^6 to 10^9.

As described above all enrichment measurements were corrected with the basal enrichments to give the true enrichment of the introduced tracer. After correction it turned out to be no, very little or negative enrichment in the earliest time points of the VLDL_1 and VLDL_2 samples. Negative enrichments are clearly not physically possible and must be the effect of measurement errors. It would be tempting to use the earliest time points to estimate the variance of the method, however even a negative enrichment could be the measured from a true positive

enrichment (i.e. there are labelled material in the sample) if the measurement error is greater. So it cannot be ruled out that in fact there is some labelled material in samples with negative enrichment.
An error in the basal ($t = 0$) enrichment influence the measurements with low enrichment more than measurements with high enrichment, since the two ratios in equation 3.2 will be of the same magnitude. This only significantly affected the 15 minute sample. Looking at the measured apoB mpe's in seven subjects, at 15 minutes it was -0.01 ± 0.018 (mean $\pm$ SD), at 30 minutes it was 0.37 ± 0.32. The absolute range in the 15 minutes sample were 50-fold, in the 30 minutes sample the range was 10-fold falling to 2-fold in the 8 hour sample. Similarly, in the glycerol samples, the variation was 120-fold in the 15 minutes sample.

Another difficulty with the 15 minutes sample was the use of a delay composed of successive compartments as described in section 4 and section 2.4. Such delays has the property of smoothing out the curve (as seen in figure 2.5 depending on the number of compartments and the delay time. The amount of tracer present in VLDL_1 and VLDL_2 at 15 minutes could not vary as much in the model as it did in the measurements, without altering the number of compartments in the delay. To reduce the complexity of the optimisation we decided not to let the number of compartments in the delay be variable, but to reduce the impact of the 15 minute sample by giving it a lower weight.

Chapter 4

Lipoprotein Models

4.1 Time-independent Models

4.1.1 Multi Compartment Model of Particle Transfer

The basis for the multi compartmental model is an apoB model that was developed by Chris Packard et. al. [33]. The apoB model is built up by three blocks, as in figure 4.1. The blocks are

1. Plasma leucine kinetics (**A**).
2. Assembly of VLDL (**D**).
3. Plasma VLDL kinetics (**E** and **F**).

The first part is specific for the type of experiment that the model describes and models the behavior the tracer before it is incorporated in the apoB molecule. In the tracer-tracee experiment with labelled leucine this block describes the kinetics of leucine before it enters the apoB synthesis mechanism.
The second block is the assembly of apoB molecule and the synthesis of the VLDL particles. In the third block the kinetics of the apoB (and hence the particles) is modelled.
The plasma leucine block consists of four compartments. Compartment 1 corresponds to free leucine in plasma and compartment 3 and 4 are interacting protein-pools, compartment 2 is a hepatic leucine pool that feeds the apoB synthesis machinery.
The apoB and lipoprotein synthesis is modelled by a delay chain, as previously described.
The plasma VLDL kinetics is modelled by a cain of four compartments 5, 6, 8 and 10. These correspond to the successive increase of density as the particle loose TG. Some particles might suffer a different fate, i.e. they might not follow the hydrolysis chain but remain in circulation for some time before being removed. This is implemented as two compartments 7 and 9 which are feed from compartment 5 and 8 respectively. Compartments 5, 6 and 7 correspond to the $VLDL_1$ particles and compartments 8, 9 and 10 corresponds to $VLDL_2$.

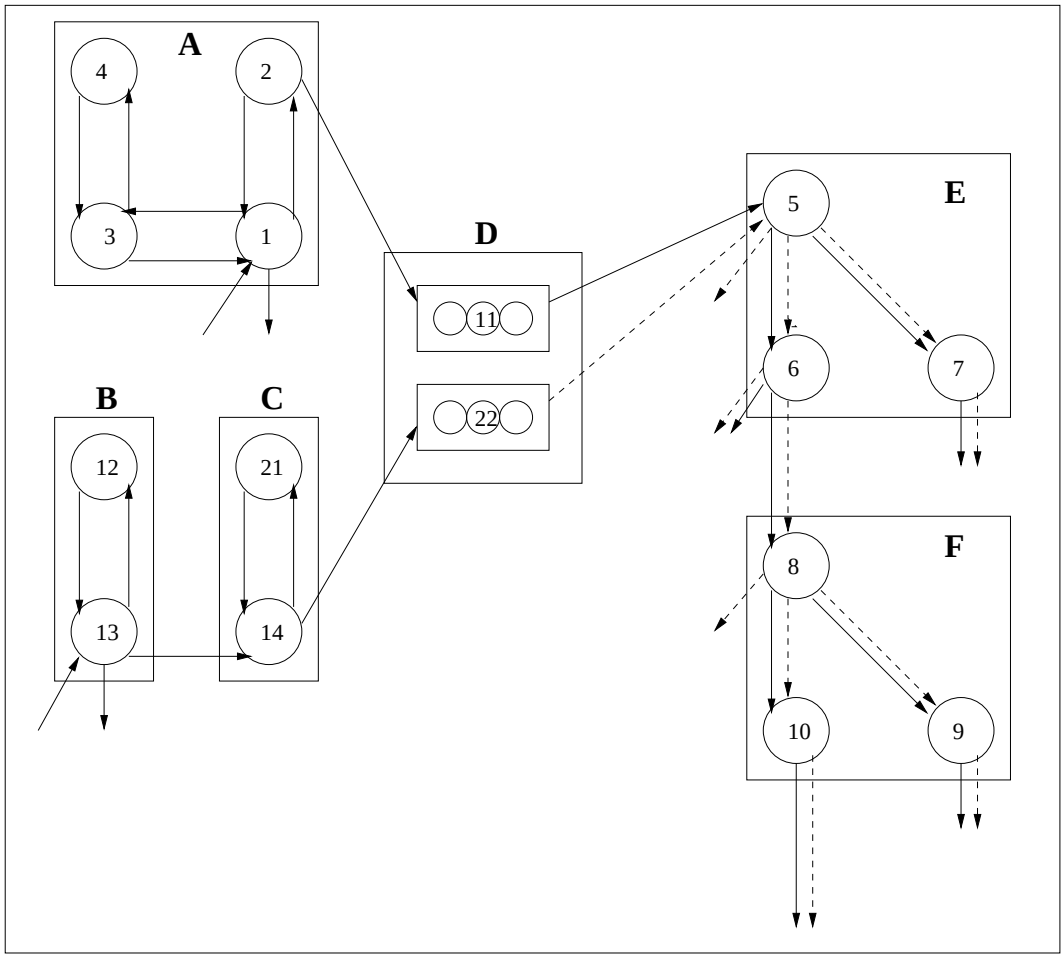

Figure 4.1: Schematic view of the compartmental model. Block **A** is the leucine subsystem, which models the kinetics of the leucine before it enters the apoB-synthesis machinery. **B** is the plasma glycerol subsystem and **C** is the hepatic glycerol-TG conversion. Block **D** models the synthesis of the lipoprotein. Blocks **E** and **F** are the VLDL_1 and VLDL_2 kinetic subsystems.

The apoB model, in matrix form has the following structure. Define

$$\mathbf{Q}^{\text{apoB}} = \begin{pmatrix} Q_1 & Q_2 & Q_3 & Q_4 & D_1^{\text{apoB}} & \cdots & D_{n_1}^{\text{apoB}} & Q_5 & \cdots & Q_{10} \end{pmatrix}^T,$$

and

$$\mathbf{q}^{\text{apoB}} = \begin{pmatrix} q_1 & q_2 & q_3 & q_4 & d_1^{\text{apoB}} & \cdots & d_{n_1}^{\text{apoB}} & q_5 & \cdots & q_{10} \end{pmatrix}^T.$$

This gives a system of the form

$$\begin{aligned} \dot{\mathbf{Q}}^{\text{apoB}} &= \mathbf{K}^{\text{apoB}}\mathbf{Q}^{\text{apoB}} + \mathbf{U}^{\text{apoB}}, \\ \dot{\mathbf{q}}^{\text{apoB}} &= \mathbf{K}^{\text{apoB}}\mathbf{q}^{\text{apoB}}, \qquad (4.1) \\ \mathbf{q}^{\text{apoB}}(0) &= \mathbf{q}_0^{\text{apoB}} = \begin{pmatrix} q_0^{\text{apoB}} & 0 & \cdots & 0 \end{pmatrix}^T. \qquad (4.2) \end{aligned}$$

The matrix $\mathbf{K}^{\text{apoB}}$ is defined as follows.

$$\mathbf{K}^{\text{apoB}} = \begin{pmatrix} \mathbf{K}^{\text{apoB}}_{\text{plasma}} & \mathbf{0} & \mathbf{0} \\ \mathbf{K}^{\text{apoB}}_{1} & \mathbf{K}^{\text{apoB}}_{\text{delay}} & \mathbf{0} \\ \mathbf{0} & \mathbf{K}^{\text{apoB}}_{2} & \mathbf{K}^{\text{apoB}}_{\text{VLDL}} \end{pmatrix},$$

where

$$\mathbf{K}^{\text{apoB}}_{\text{plasma}} = \begin{pmatrix} -k_{2,1} - k_{0,1} - k_{3,1} & k_{1,2} & k_{1,3} & 0 \\ k_{2,1} & -k^{\text{apoB}}_{delay} - k_{1,2} & 0 & 0 \\ k_{3,1} & 0 & -k_{1,3} - k_{4,3} & 0 \\ 0 & 0 & k_{4,3} & -k_{3,4} \end{pmatrix},$$

and

$$\mathbf{K}^{\text{apoB}}_{1} = \begin{pmatrix} 0 & k^{\text{apoB}}_{delay} & 0 & 0 \\ 0 & 0 & 0 & 0 \\ \vdots & \vdots & \vdots & \vdots \\ 0 & 0 & 0 & 0 \end{pmatrix},$$

which is an n_1 by 4 matrix. The delay matrix

$$\mathbf{K}^{\text{apoB}}_{\text{delay}} = \begin{pmatrix} -k^{\text{apoB}}_{D} & 0 & 0 & \cdots & 0 \\ k^{\text{apoB}}_{D} & -k^{\text{apoB}}_{D} & 0 & \cdots & 0 \\ 0 & \ddots & \ddots & \ddots & \vdots \\ \vdots & \ddots & k^{\text{apoB}}_{D} & -k^{\text{apoB}}_{D} & 0 \\ 0 & \cdots & 0 & k^{\text{apoB}}_{D} & -k^{\text{apoB}}_{D} \end{pmatrix}$$

is an n_1 by n_1 matrix. Moreover

$$\mathbf{K}^{\text{apoB}}_{2} = \begin{pmatrix} 0 & \cdots & 0 & d^{\text{a}}_{5} k^{\text{apoB}}_{D} \\ 0 & \cdots & 0 & 0 \\ 0 & \cdots & 0 & 0 \\ 0 & \cdots & 0 & d^{\text{a}}_{5} k^{\text{apoB}}_{D} \\ 0 & \cdots & 0 & 0 \\ 0 & \cdots & 0 & 0 \end{pmatrix},$$

is a 6 by n_1 matrix. Finally

$$\mathbf{K}^{\text{apoB}}_{\text{VLDL}} = \begin{pmatrix} -k_{6,5} - k_{7,5} & 0 & 0 & 0 & 0 & 0 \\ k_{6,5} & -k_{0,6} - k_{8,6} & 0 & 0 & 0 & 0 \\ k_{7,5} & 0 & -k_{0,7} & 0 & 0 & 0 \\ 0 & k_{8,6} & 0 & -k_{9,8} - k_{10,8} & 0 & 0 \\ 0 & 0 & 0 & k_{9,8} & -k_{0,9} & 0 \\ 0 & 0 & 0 & k_{10,8} & 0 & -k_{0,10} \end{pmatrix}.$$

As an alternative to the initial value problem of the tracer system (equations (4.1)-(4.2)) the formulation with inputs can be used. The input distribution matrix is

$$\mathbf{B} = \begin{pmatrix} 1 & 0 & \cdots & 0 \end{pmatrix}^T.$$

And the equations then are

$$\begin{aligned} \dot{\mathbf{q}}^{\text{apoB}} &= \mathbf{K}^{\text{apoB}} \mathbf{q}^{\text{apoB}} + \mathbf{B} q_0^{\text{apoB}} \delta(t), \\ \mathbf{q}^{\text{apoB}}(0) &= \mathbf{0}. \end{aligned}$$

The output matrix is defined as

$$\mathbf{C}^1 = \begin{pmatrix} 1 & 0 & \cdots & 0 & 0 & 0 & 0 & 0 & 0 & 0 \\ 0 & 0 & \cdots & 0 & 1 & 1 & 1 & 0 & 0 & 0 \\ 0 & 0 & \cdots & 0 & 0 & 0 & 0 & 1 & 1 & 1 \end{pmatrix}.$$

This system has been proved to be structurally identifiable in [13], by the concepts described by Saccomani et. al. [39], [2], briefly described in section 2.9. In [2] this particular model is considered as an example.

4.1.2 Glycerol to TG Conversion and Hepatic TG Modelling

Even though our primary interest is the kinetics of the lipoproteins and their components in the plasma, we are faced with the problem of modelling what happens in the experiments before the particles are secreted into the plasma.

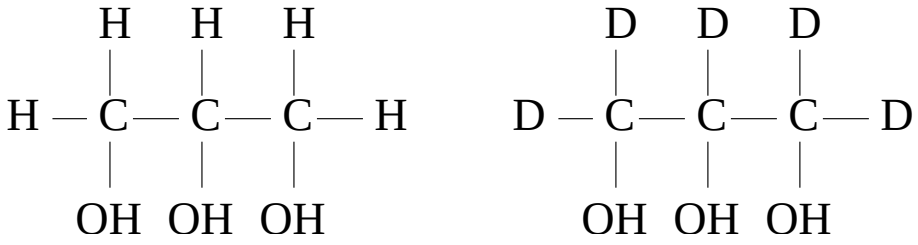

Figure 4.2: To the left, an unlabelled glycerol molecule. On the right a 1,1,2,3,3 D-glycerol molecule.

In the experiments used throughout this thesis the amino acid leucine is used to label the apoB molecules and glycerol to label the TG. To study the kinetics of the TG the TG molecule is labelled by using labelled glycerol. The glycerol molecule (figure 4.2) has deuterium instead of hydrogen at position 1, 2, 3, 4 and 5. The glycerol is esterified in the liver, where the -OH groups are replaced by fatty acid chains to form triglyceride molecules. The labelled glycerol is injected into the plasma.

The plasma is modelled by two interacting compartments (12 and 13 in figure 4.3, block **B** in figure 4.1). Compartment 13 is the free-glycerol plasma compartment and compartment 12 is a glycerol pool. Compartment 13 feeds the hepatic glycerol to TG conversion (compartment 14 and 21), but there is also a loss of glycerol from the plasma. The plasma glycerol model was used in [46].

In [46] the loading of TG into the VLDL particles was modelled with a *fast* and a *slow* pathway. We have interpreted this in another way, using an intrahepatic pool. The main pathway is compartment 14 where the glycerol is esterified to form TG and then is loaded into VLDL particles. We believe that there is a continuous ester- and de-esterification of glycerol in the liver, or at least that there exist internal pools of lipids in the liver. The sources of TG for loading the particles is both the internal pool and the direct pathway. We therefore implemented the slow pathway as a compartment 21 interchanging material with compartment 14, this means that glycerol is internally recycled inside the liver. See figure 4.4 and block **C** in figure 4.1.

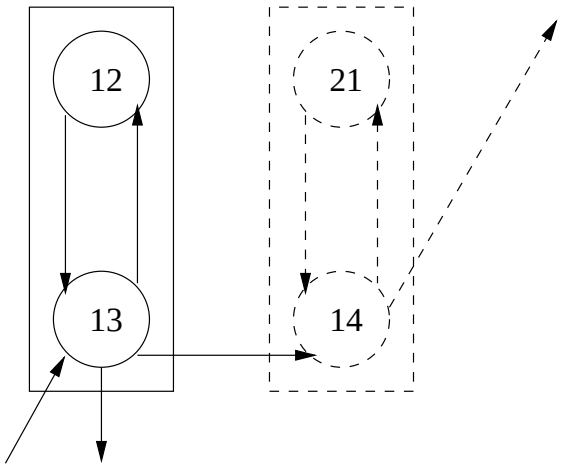

Figure 4.3: The glycerol is injected into the plasma compartment (13), which interacts with a glycerol pool compartment (12). The glycerol to TG conversion is feed from compartment 12. As described in the implementation section, the transfer coefficients $k_{12,12}$, $k_{13,12}$ and $k_{0,13}$ were fixed to population averages from earlier studies ([46]) but also (for comparison) determined using measurements of plasma glycerol enrichments in a few subjects.

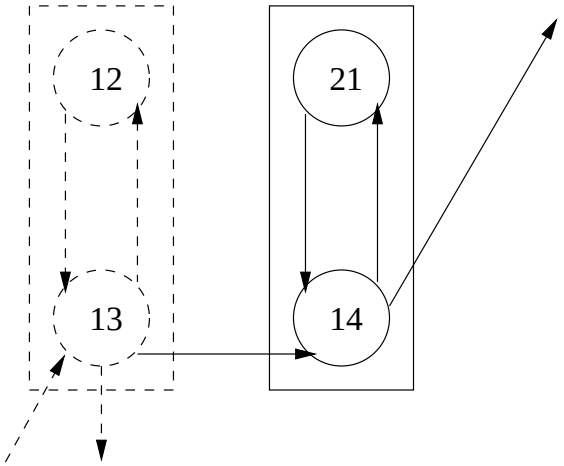

Figure 4.4: Compartment 14 is the main pathway for glycerol to TG conversion, whereas compartment 21 is an intrahepatic glycerol pool.

The hepatic glycerol and TG modelling is limited by the facts that it is difficult to actually measure the hepatic pools. It is possible to get a quantitative measure of the total amount of liver fat but it is not possible to measure the individual pools. Furthermore there is an obvious limitation of the amount of blood that can be drawn from a subject. In order to catch the initial slope and the tail of the curves, samples have to be distributed over the whole time range of the experiment. Therefore it is not possible to sample more often in the early time points, which would otherwise be a way of seeing for instance differences in the secretion of VLDL_1 and VLDL_2.

With emerging knowledge of the hepatic glycerol kinetics this model might have to be revised. With other tracers, such as fatty acids, the modelling of the lipoprotein synthesis will have to be reformulated.

4.1.3 Two Different Models

The basic idea of the compartmental model of lipoprotein is that the TG is transported with the apoB. The change of state of an apoB (i.e. is moved from $VLDL_1$ to $VLDL_2$, or from one compartment to an other) is equivalent to a change (increase) in density. In the current modelling process we only consider apoB and TG, and leave out other proteins, phospholipids, cholesterol and cholesterol esters. By using similar concepts one can extend the model to include other components.
ApoB models are widely used and accepted [27], [28], [29], [30], [33], [32] and [18] and serve as the starting point for the development of a combined TG/apoB model. Based on the apoB model by Packard et. al. described in section 4.1.1, there are several ways of extending this model to also include TG. The apoB model describes the movement of particles between the different density ranges and it is natural to, in some way, assign a TG content to each particle. As described in the previous chapters the lipoproteins in $VLDL_1$ and $VLDL_2$ vary greatly in both size and composition. Most importantly the TG per particle, or TG to apoB ratio, vary widely. A newly secreted $VLDL_1$ particle is large and rich in TG (high TG to apoB ratio) and a $VLDL_1$ particle that is about to become a $VLDL_2$ has a much smaller TG to apoB ratio. However, using linear models, we have to assume that the TG to apoB ratio of the particles in each compartment are uniform .

Given an apoB plasma model, each apoB compartment Q_i is associated with a corresponding TG compartment P_i. Particles in compartment i have an average TG to apoB ratio of $R_i = P_i/Q_i$ and are assumed to have homogenous kinetics. In the first approach we assume the loss of TG from the particles to occur instantly in the transfer between two compartments. Starting with the equations for the apoB system we have

$$\dot{Q}_i = \sum_{\substack{j\neq i \\ j=1}}^{n} k_{i,j}Q_j - \sum_{\substack{j\neq i \\ j=0}}^{n} k_{j,i}Q_i. \tag{4.3}$$

Multiplying equation (4.3) by R_i we get

$$R_i\dot{Q}_i = \sum_{\substack{j\neq i \\ j=1}}^{n} R_i k_{i,j}Q_j - \sum_{\substack{j\neq i \\ j=0}}^{n} k_{j,i}R_i Q_i,$$

$$\dot{P}_i = \sum_{\substack{j\neq i \\ j=1}}^{n} \frac{R_i}{R_j} k_{i,j}P_j - \sum_{\substack{j\neq i \\ j=0}}^{n} k_{j,i}P_i.$$

Defining the transfer rates for TG as

$$l_{i,j} = \frac{R_i}{R_j} k_{i,j}, \quad i \geq 1, \quad i \neq j$$

and

$$l_{0,j} = k_{0,j} + \sum_{\substack{i \neq j \\ i=1}}^{n} (1 - \frac{R_i}{R_j}) k_{i,j},$$

we get a new compartmental system for the TG. The catabolic term $l_{0,j}$ is the sum of the removal of whole particles $k_{0,j}$ and the fractional loss of TG when particles are transferred to other compartments. The total fractional removal is

$$\begin{aligned} l_{i,i} &= -l_{0,i} - \sum_{\substack{j \neq i \\ j=1}}^{n} (1 - \frac{R_i}{R_j}) k_{i,j} \\ &= -k_{i,i}. \end{aligned}$$

The particles in compartment i have TG to apoB ratio R_i, but as a particle enters a new compartment its ratio is the same as in the compartment it is entering. We always assume the ratio to decrease (or at least not increase) as the particle is moved between two compartments. The ratio of particles being transferred from j to i is

$$\begin{aligned} \frac{P_j \; l_{i,j}}{Q_j \; k_{i,j}} &= \frac{R_j \; Q_j \; \frac{R_i}{R_j} k_{i,j}}{Q_j \; k_{i,j}} \\ &= R_i. \end{aligned}$$

The ratio of total outgoing TG and outgoing apoB from a compartment i equals R_i, since the total fractional transfer of apoB and TG from each compartment is equal to

$$\begin{aligned} \sum_{\substack{j \neq i \\ j=0}}^{n} l_{j,i} &= \sum_{\substack{j \neq i \\ j=1}}^{n} \frac{R_j}{R_i} k_{j,i} + l_{0,i} \\ &= \sum_{\substack{j \neq i \\ j=1}}^{n} \frac{R_j}{R_i} k_{j,i} + k_{0,i} + \sum_{\substack{j \neq i \\ j=1}}^{n} (1 - \frac{R_j}{R_i}) k_{j,i} \\ &= k_{0,i} + \sum_{\substack{j \neq i \\ j=1}}^{n} k_{j,i} \\ &= \sum_{\substack{j \neq i \\ j=0}}^{n} k_{j,i}. \end{aligned}$$

Instead of working with R_i or P_i as parameters in the model we introduce $f_{i,j}$ as the fraction of the TG in the particle transferred from compartment j to compartment i that enters compartment i. Since $f_{i,j} = \frac{R_i}{R_j}$ the system of equations is

$$\dot{P}_i = \sum_{\substack{j \neq i \\ j=1}}^{n} f_{i,j} k_{i,j} P_j - \sum_{\substack{j \neq i \\ j=0}}^{n} k_{j,i} P_i.$$

From the definition of $l_{i,j}$ and $f_{i,j}$ we get $l_{i,j} = f_{i,j}k_{i,j}, \quad i \geq 1$ and $l_{0,j} = k_{0,j} + \sum_{\substack{i=1 \\ i \neq j}}^{n}(1 - f_{i,j})k_{i,j}$

and hence

$$\dot{P}_i = \sum_{\substack{j=1 \\ j \neq i}}^{n} l_{i,j}P_j - \sum_{\substack{j=0 \\ j \neq i}}^{n} l_{j,i}P_i.$$

In figure 4.5 we describe the behavior of the model when particles are transported from compartment 5 to compartment 6.

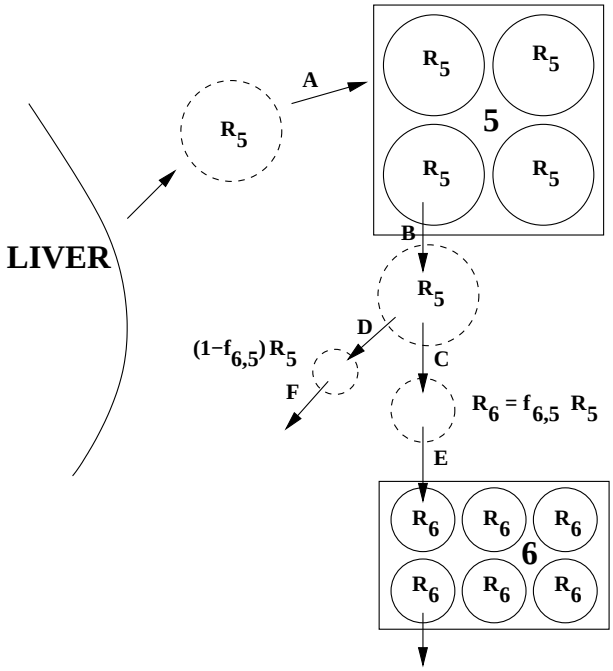

Figure 4.5: The newly produced particles enter compartment 5 (arrow **A**) having the same TG to apoB ratio as the particles in compartment 5. As a particle leaves (arrow **B**) compartment 5, TG corresponding to a whole particle is removed but only a fraction (arrow **C**) enters compartment 6 (arrow **E**). The rest of the TG is removed (**D** and **F**). The transfer between compartments are considered to be instant.

Compartment 8 has an influx of both newly produced VLDL_2 particles and VLDL_2 particles transferred from VLDL_1. The TG to apoB ratio of the particles entering the compartment 8 should be equal independently of their origin, i.e. the particles transferred from compartment 6 to compartment 8 and from the liver to compartment 8 should have the same TG to ratio. Therefore it is necessary to constrain the fluxes. First we assume that the TG to apoB ratio in the compartments are constant during the experiment, i.e. the quotients of P_i and Q_i is constant for $i = 5, \ldots, 10$. Assume $A(t)$ to be the amount of apoB delivered per time unit from the liver at time t and $T(t)$ the amount per time unit of TG. Moreover, let d_5^a be the fraction of apoB going to compartment 5 (VLDL_1) and $d_8^a = 1 - d_5^a$ the fraction going to compartment 8 (VLDL_2), analogously d_5^t is the fraction of TG going into compartment

5 and $d_8^t = 1 - d_5^t$ the fraction going to compartment 8. In this section we assume that the production rates are constant, i.e. $A(t) = A$ and $T(t) = T$.
The equations for compartments 5, 6 and 8 are:

$$\frac{dQ_5}{dt} = d_5^a A - (k_{6,5} + k_{7,5})Q_5, \tag{4.4}$$

$$\frac{dP_5}{dt} = d_5^t T - (k_{6,5} + k_{7,5})P_5. \tag{4.5}$$

Multiplying equation (4.4) by R_5 gives

$$R_5 \frac{dQ_5}{dt} = d_5^a R_5 A - (k_{6,5} + k_{7,5})R_5 Q_5,$$

or

$$\frac{dP_5}{dt} = d_5^a R_5 A - (k_{6,5} + k_{7,5})P_5, \tag{4.6}$$

and hence, comparing equations (4.5) and (4.6) we get $d_5^a R_5 A = d_5^t T$, or

$$R_5 = \frac{d_5^t T}{d_5^a A}. \tag{4.7}$$

For compartment 6 we have

$$\frac{dQ_6}{dt} = k_{6,5} Q_5 - k_{8,6} Q_6, \tag{4.8}$$

$$\frac{dP_6}{dt} = k_{6,5} f_{6,5} P_5 - k_{8,6} P_6. \tag{4.9}$$

Multiplying equation (4.8) with R_6 and comparing with equation (4.9) gives

$$R_6 = f_{6,5} R_5. \tag{4.10}$$

The TG to apoB ratio of the particles entering compartment 8 from compartment 6 should equal the ratio of the particles entering from the liver. Hence,

$$\frac{k_{8,6} f_{8,6} P_6}{k_{8,6} Q_6} = \frac{d_8^t T}{d_8^a A}.$$

Using equation (4.7) we get

$$f_{8,6} R_6 = \frac{d_8^t d_5^a R_5}{d_8^a d_5^t}.$$

Equation (4.10) gives

$$f_{8,6} f_{6,5} = \frac{d_8^t d_5^a}{d_8^a d_5^t}.$$

By the definition of the fractions we get

$$d_5^t = \frac{d_5^a}{d_5^a + f_{8,6} f_{6,5} (1 - d_5^a)}. \tag{4.11}$$

Clearly $d_5^t \geq d_5^a$ and the particles entering compartment 5 have more TG than particles entering compartment 8.
We can now define the system describing the TG model. First we define:

$$\mathbf{P}^{\mathrm{TG}} = \begin{pmatrix} P_{13} & P_{12} & P_{14} & P_{21} & D_1^{\mathrm{TG}} & \cdots & D_{n_2}^{\mathrm{TG}} & P_5 & \cdots & P_{10} \end{pmatrix}^T,$$

and

$$\mathbf{q}^{\mathrm{TG}} = \begin{pmatrix} p_{13} & p_{12} & p_{14} & p_{21} & d_1^{\mathrm{TG}} & \cdots & d_{n_2}^{\mathrm{TG}} & p_5 & \cdots & p_{10} \end{pmatrix}^T.$$

The system is of the form

$$\begin{aligned} 0 &= \mathbf{K}^{\mathrm{TG}}\mathbf{P}^{\mathrm{TG}} + \mathbf{U}^{\mathrm{TG}}, && (4.12)\\ \dot{\mathbf{p}}^{\mathrm{TG}} &= \mathbf{K}^{\mathrm{TG}}\mathbf{p}^{\mathrm{TG}}, && (4.13)\\ \mathbf{p}^{\mathrm{TG}}(0) &= \mathbf{p}_0^{\mathrm{TG}} = \begin{pmatrix} p_0^{\mathrm{TG}} & 0 & \cdots & 0 \end{pmatrix}^T, && (4.14)\\ \mathbf{U}^{\mathrm{TG}} &= \begin{pmatrix} U_0^{\mathrm{TG}} & 0 & \cdots & 0 \end{pmatrix}^T. && (4.15) \end{aligned}$$

$\mathbf{K}^{\mathrm{TG}}$ is defined as follows.

$$\mathbf{K}^{\mathrm{TG}} = \begin{pmatrix} \mathbf{K}^{\mathrm{TG}}_{\mathrm{plasma}} & \mathbf{0} & \mathbf{0} \\ \mathbf{K}^{\mathrm{TG}}_{1} & \mathbf{K}^{\mathrm{TG}}_{\mathrm{delay}} & \mathbf{0} \\ \mathbf{0} & \mathbf{K}^{\mathrm{TG}}_{2} & \mathbf{K}^{\mathrm{TG}}_{\mathrm{VLDL}} \end{pmatrix},$$

where

$$\mathbf{K}^{\mathrm{TG}}_{\mathrm{plasma}} = \begin{pmatrix} -k_{12,13} - k_{14,13} - k_{0,13} & k_{13,12} & 0 & 0 \\ k_{12,13} & -k_{13,12} & 0 & 0 \\ k_{14,13} & 0 & -k_{21,14} - k^{\mathrm{TG}}_{delay} & k_{14,21} \\ 0 & 0 & k_{21,14} & -k_{14,21} \end{pmatrix},$$

and

$$\mathbf{K}^{\mathrm{TG}}_{1} = \begin{pmatrix} 0 & 0 & k^{\mathrm{TG}}_{delay} & 0 \\ 0 & 0 & 0 & 0 \\ \vdots & \vdots & \vdots & \vdots \\ 0 & 0 & 0 & 0 \end{pmatrix},$$

an n_2 by 4 matrix. The TG delay matrix is

$$\mathbf{K}^{\mathrm{TG}}_{\mathrm{delay}} = \begin{pmatrix} -k^{\mathrm{TG}}_D & 0 & 0 & \cdots & 0 \\ k^{\mathrm{TG}}_D & -k^{\mathrm{TG}}_D & 0 & \cdots & 0 \\ 0 & \ddots & \ddots & \ddots & \vdots \\ \vdots & \ddots & k^{\mathrm{TG}}_D & -k^{\mathrm{TG}}_D & 0 \\ 0 & \cdots & 0 & k^{\mathrm{TG}}_D & -k^{\mathrm{TG}}_D \end{pmatrix},$$

which is an n_2 by n_2 matrix. Furthermore we have

$$\mathbf{K}^{t}_{2} = \begin{pmatrix} 0 & \cdots & 0 & d^t_5 k^{\mathrm{TG}}_D \\ 0 & \cdots & 0 & 0 \\ 0 & \cdots & 0 & 0 \\ 0 & \cdots & 0 & d^t_8 k^{\mathrm{TG}}_D \\ 0 & \cdots & 0 & 0 \\ 0 & \cdots & 0 & 0 \end{pmatrix},$$

a 6 by n_2 matrix. The fractional transfers from the delay d^t_5 is defined as in equation (4.11). Finally

$$\mathbf{K}^{\mathrm{TG}}_{\mathrm{VLDL}} = \begin{pmatrix} -l_{6,5} - l_{7,5} - l_{0,5} & 0 & 0 & 0 & 0 & 0 \\ l_{6,5} & -l_{0,6} - l_{8,6} & 0 & 0 & 0 & 0 \\ l_{7,5} & 0 & -l_{0,7} & 0 & 0 & 0 \\ 0 & l_{8,6} & 0 & -l_{9,8} - l_{10,8} - l_{0,8} & 0 & 0 \\ 0 & 0 & 0 & l_{9,8} & -l_{0,9} & 0 \\ 0 & 0 & 0 & l_{10,8} & 0 & -l_{0,10} \end{pmatrix}.$$

By the definition of $l_{i,j}$, i.e. $l_{6,5} = f_{6,5}k_{6,5}$, $l_{7,5} = f_{7,5}k_{7,5}$, $l_{8,6} = f_{8,6}k_{8,6}$, $l_{9,8} = f_{9,8}k_{9,8}$, $l_{10,8} = f_{10,8}k_{10,8}$, $l_{0,5} = (1 - f_{6,5})k_{6,5} + (1 - f_{7,5})k_{7,5}$, $l_{0,6} = (1 - f_{8,6})k_{8,6} + k_{0,6}$, $l_{0,7} = k_{0,7}$, $l_{0,8} = (1 - f_{9,8})k_{9,8}(1 - f_{10,8})k_{10,8}$, $l_{0,9} = k_{0,9}, l_{0,10} = k_{0,10}$

$$, we have \mathbf{K}^{\mathrm{TG}}_{\mathrm{VLDL}} = \begin{pmatrix} -k_{6,5} - k_{7,5} & 0 & 0 & 0 & 0 & 0 \\ f_{6,5}k_{6,5} & -k_{0,6} - k_{8,6} & 0 & 0 & 0 & 0 \\ f_{7,5}k_{7,5} & 0 & -k_{0,7} & 0 & 0 & 0 \\ 0 & f_{8,6}k_{8,6} & 0 & -k_{9,8} - k_{10,8} & 0 & 0 \\ 0 & 0 & 0 & f_{9,8}k_{9,8} & -k_{0,9} & 0 \\ 0 & 0 & 0 & f_{10,8}k_{10,8} & 0 & -k_{0,10} \end{pmatrix}.$$

As an alternative to the initial value problem of the tracer system (4.12) - (4.15) the formulation with inputs can be used. The input distribution matrix is

$$\mathbf{B} = \begin{pmatrix} 1 & 0 & \cdots & 0 \end{pmatrix}^T.$$

And the tracer equation (4.13) and (4.14) is replaced by

$$\begin{aligned} \dot{\mathbf{p}}^{\mathrm{TG}} &= \mathbf{K}^{\mathrm{TG}}\mathbf{p}^{\mathrm{TG}} + \mathbf{B}p_0^{\mathrm{TG}}\delta(t), \\ \mathbf{p}^{\mathrm{TG}}(0) &= \mathbf{0}. \end{aligned}$$

The output matrix is defined as

$$\mathbf{C}^1 = \begin{pmatrix} 1 & 0 & \cdots & 0 & 0 & 0 & 0 & 0 & 0 & 0 \\ 0 & 0 & \cdots & 0 & 1 & 1 & 1 & 0 & 0 & 0 \\ 0 & 0 & \cdots & 0 & 0 & 0 & 0 & 1 & 1 & 1 \end{pmatrix},$$

or

$$\mathbf{C}^2 = \begin{pmatrix} 0 & \cdots & 0 & 1 & 1 & 1 & 0 & 0 & 0 \\ 0 & \cdots & 0 & 0 & 0 & 0 & 1 & 1 & 1 \end{pmatrix}.$$

The output matrix $\mathbf{C}^1$ is used when there exist measurements of plasma glycerol. Then the transfer coefficients $k_{12,12}$, $k_{13,12}$ and $k_{0,13}$ are estimated from the data. If no plasma glycerol data exist the transfer coefficients are fixed to the population averages used in [46] and the output matrix is $\mathbf{C}^2$. This is further discussed in section 7.1.3.

We used the method by Sedoglavic [41] to test if the model was identifiable. Since the apoB model was known to be identifiable we assumed the rate constant determined by the apoB model to be known for the TG model, i.e. d_5^a, $k_{6,5}$, $k_{7,5}$, $k_{8,6}$, $k_{9,8}$, $k_{10,8}$, $k_{0,7}$, $k_{0,8}$, $k_{0,9}$ and $k_{0,10}$. We found the model to be identifiable.

The second approach was to assume that particles enter a compartment having the same ratio as the particles in the source compartment. Using this approach all particles in the destination compartment lose TG in order to keep the TG to apoB ratio intact. In this model, the fractional transfer rates are equal, but there is an additional fractional catabolic term (L_i) in the TG system:

$$\dot{P}_i = \sum_{\substack{j \neq i \\ j=1}}^{n} k_{i,j}P_j - \sum_{\substack{j \neq i \\ j=0}}^{n} k_{j,i}P_i - (k_{0,i} + L_i)P_i$$

In this model formulation, the time in the compartments corresponds to the time it takes for the particle to lose enough TG to reach the TG to apoB ratio of the next compartment.

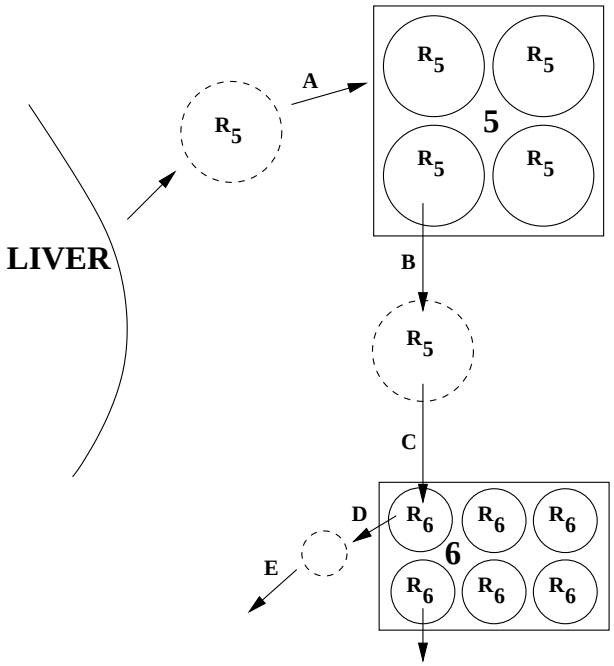

Figure 4.6: The newly produced particles enters compartment 5 (arrow **A**) having the same TG to apoB ratio as the particles in compartment 5. As a particle leaves (**B**) compartment 5, TG corresponding to a whole particle is removed and transferred to compartment 6 (arrow **C**). To balance the TG in compartment 6 a fraction of the TG content is removed (arrows **D** and **E**).

4.1.4 A Combined Model

The interpretation of the first model (model 1) is that the time a particle spends in a compartment corresponds to a circulation time where the TG to apoB ratio does not change. As a particle connects to an LPL it instantly looses TG, hence its density and TG to apoB ratio changes, and is transferred to another compartment - corresponding to a lower TG to apoB ratio.
In model 2 the delipidation of the particles is taking place within the compartments. The TG to apoB ratio of the inflowing particles are greater than the TG to apoB ratio of the outflowing particles. This balanced by a fractional loss of TG from all particles. The transfer between two compartments take place as the particle is released from one LPL site and binds to another.
From this it is possible to build a combined model. In the combined model each compartment is replaced by two compartments where the first compartment corresponds to the circulation time of the particle and the second compartment corresponds to the delipidation process. The second compartment could be a single compartment or a delay compartment.
However the quality (i.e. noise), amount (i.e. total number of sampling points) and scale (i.e $VLDL_1$ and $VLDL_2$) of the current data does not allow for finding all parameters in too complex models.

4.2 Time-Dependent Models

Next the model is extended to include non-steady state situations. The goal is to model the kinetic behavior in the clamp experiment.

4.2.1 The Non-Steady-State Model

The time-dependent model is based on the previously described time-independent model. The structure of the model is considered as a discreteisation of the range of TG to apoB ratios in VLDL. Hence the TG to apoB ratios in the compartments should be fixed during the experimental time for each subject. However, the total TG to apoB ratio in VLDL_1 and VLDL_2 will change since the distribution of the particles over the compartments will change. In section 4.1.3 we assumed $A(t)$ to be the total synthesis rate of apoB in the liver, and distributed to VLDL_1 and VLDL_2. This is not entirely true. The liver also produces small amounts of IDL and LDL particles, so a fraction of the synthesised apoB is secreted into the IDL and LDL ranges. Moreover, there is a degradation of synthesised apoB molecules in the liver.
However, even if the total synthesis rate of apoB is greater than estimated the absolute secretion rate of apoB into VLDL_1 and VLDL_2 is still valid and the ratio of the these secretion rates is also valid. To estimate the secretion rate into IDL and LDL the corresponding pool sizes and enrichments would have to be measured.
To model a change of VLDL_1 and VLDL_2 production we assume the total apoB synthesis to be constant, $A(t) = A$. As before, let the fractional distribution of apoB that goes into VLDL_1 be d_5^a and the fraction going into VLDL_2 be d_8^a. We denote the fraction of the apoB that is degraded by d_0^a.
In section 4.1.3 we assumed that all produced apoB and TG was secreted as VLDL, i.e. that the degradation term was zero, $d_0^a = 0$. We define the time dependent fractions by:

$$\begin{aligned} d_5^a(t) &= d_{5,0}^a f(t), \\ d_8^a(t) &= d_{8,0}^a h(t), \\ d_0^a(t) &= 1 - d_5^a(t) - d_8^a(t), \end{aligned}$$

where $f(t) \in [0,1]$ and $h(t) \in [0,1]$ for $t \in [0, 8.5]$ and $f(0) = h(0) = 1$. Moreover f and h should be chosen so that $d_0^a(t) \geq 0$.
Our assumption on the model is that it represents a discretisation of the range of TG to apoB ratios in VLDL. Hence we assume the TG to apoB ratios in each compartment to be constant. Moreover, we assume that the size of the particles that are transferred between compartments is constant. This amounts to keeping the ratio of the fluxes constants.
As for the apoB, the we assume that the amount of TG is constant $T(t) = T$ but the fraction going to VLDL_1, VLDL_2 and degradation are modified by the same function as for the apoB, i.e.

$$\begin{aligned} d_5^t(t) &= d_{5,0}^t f(t), \\ d_8^t(t) &= d_{8,0}^t h(t), \\ d_0^t(t) &= 1 - d_5^t(t) - d_8^t(t). \end{aligned}$$

This allows the ratios of TG to apoB of particles that are transferred from the liver to compartments 5 and 8 to be constant. It may seem that this idea contradicts the observation

that the plasma FFA levels are decreased during the insulin infusion. However, we are actually modelling the glycerol (since it is the glycerol that is labelled) and it is reasonable to assume that the availability of glycerol is constant and that it is the lack of FFA that cause the removal/degradation of glycerol from the TG loading mechanism.
Changing the fractional transfer rates in a similar way, i.e. defining

$$k_{i,j}(t) = k_{i,j,0}g_{i,j}(t),$$

gives constant TG to apoB ratios in each compartment. The $g_{i,j}$ functions should fulfill $g_{i,j}(t) > 0$, $g_{i,j}(0) = 1$. We denote the primitive function of $g_{i,j}$ as $G_{i,j}$. The constant TG to apoB ratio is a consequence of the *downstream* structure of the model, i.e the mass in a compartment is only dependent on the compartments above. Hence, for the compartments we have

$$\frac{dQ_5}{dt} = Ad^a_{5,0}f(t) - (k_{6,5}g_{6,5}(t) + k_{7,5}g_{7,5}(t))Q_5(t), \tag{4.16}$$

$$\frac{dP_5}{dt} = Td^t_{5,0}f(t) - (k_{6,5}g_{6,5}(t) + k_{7,5}g_{7,5}(t))P_5(t). \tag{4.17}$$

Let $H(t) = k_{6,5}G_{6,5}(t) + k_{7,5}G_{7,5}(t)$. Then the solutions equations (4.16) and (4.17) are

$$Q_5(t) = e^{-H(t)}(Ad^a_{5,0}\int_0^t e^{H(s)}f(s)ds + Q_5(0)),$$

and

$$P_5(t) = e^{-H(t)}(Td^t_{5,0}\int_0^t e^{H(s)}f(s)ds + P_5(0)).$$

The ratio in compartment 5 is

$$\frac{P_5(t)}{Q_5(t)} = \frac{e^{-H(t)}(Td^t_{5,0}\int_0^t e^{H(s)}f(s)ds + P_5(0))}{e^{-H(t)}(Ad^a_{5,0}\int_0^t e^{H(s)}f(s)ds + Q_5(0))},$$

i.e.

$$R_5(t) = \frac{Td^t_{5,0}\int_0^t e^{H(s)}f(s)ds + P_5(0)}{Ad^a_{5,0}\int_0^t e^{H(s)}f(s)ds + Q_5(0)}.$$

Since it was assumed that the system is at steady-state for $t \leq 0$, equation (4.7) gives $Td^t_{5,0}Q_5(0) - Ad^a_{5,0}P_5(0) = 0$. Therefore,

$$R_5(t) = \frac{Td^t_{5,0}(\int_0^t e^{H(s)}f(s)ds + \frac{Q_5(0)}{Ad^a_{5,0}})}{Ad^a_{5,0}(\int_0^t e^{H(s)}f(s)ds + \frac{Q_5(0)}{Ad^a_{5,0}})}.$$

Hence,

$$R_5 = \frac{P_5(t)}{Q_5(t)} = \frac{Td^t_{5,0}}{Ad^a_{5,0}}, \tag{4.18}$$

i.e. the ratio R_5 is constant also in the time dependent case.

Continuing with compartment 6 we have similarly

$$\begin{aligned}
\frac{dQ_6}{dt} &= k_{6,5}g_{6,5}(t)Q_5(t) - k_{8,6}g_{8,6}(t)Q_6(t),\\
\frac{dP_6}{dt} &= k_{6,5}f_{6,5}g_{6,5}(t)P_5(t) - k_{8,6}g_{8,6}(t)P_6(t),\\
Q_6(t) &= e^{-(k_{8,6}G_{8,6}(t))}(k_{6,5}\int_0^t g_{6,5}(s)e^{k_{8,6}G_{8,6}(s)}Q_5(s)ds + Q_6(0)),\\
P_6(t) &= e^{-(k_{8,6}G_{8,6}(t))}(f_{6,5}k_{6,5}\int_0^t g_{6,5}(s)e^{k_{8,6}G_{8,6}(s)}P_5(s)ds + P_6(0)).
\end{aligned}$$

The system is considered to be in steady state for $t = 0$, therefore equation (4.10) holds for $t = 0$ and $R_6(0) = f_{6,5}R_5$ or $P_6(0) = Q_6(0)f_{6,5}R_5$. Equation (4.18) gives $P_5(t) = R_5Q_5(t)$, and then

$$\begin{aligned}
P_6(t) &= e^{-(k_{8,6}G_{8,6}(t))}(f_{6,5}k_{6,5}\int_0^t g_{6,5}(s)e^{k_{8,6}G_{8,6}(s)}R_5Q_5(s)ds + Q_6(0)f_{6,5}R_5)\\
&= R_5f_{6,5}e^{-(k_{8,6}G_{8,6}(t))}(k_{6,5}\int_0^t g_{6,5}(s)e^{k_{8,6}G_{8,6}(s)}Q_5(s)ds + Q_6(0))\\
&= R_5f_{6,5}Q_6(t).
\end{aligned}$$

Hence,

$$R_6 = \frac{P_6(t)}{Q_6(t)} = R_5f_{6,5}.$$

Therefore also the ratio R_6 is constant and

$$R_6 = \frac{P_6(t)}{Q_(t)} = f_{6,5}R_5 = R_6 = \frac{Td^t_{5,0}f_{6,5}}{Ad^a_{5,0}}.$$

Similar calculations show that R_7, R_8, R_9 and R_{10} are constant with the definition of the fractional transfer rates above. Hence the model defines a fixed structure, where each compartment corresponds to a fixed particle TG to apoB ratio. The changes in the fractional distribution and the changes in fractional transfer rates will cause a shift in the distribution among these fixed TG to apoB ratios.

As in the analysis in section 4.1.3 we must ensure that TG to apoB ratio of the streams that enter the compartment 8 are equal, i.e. that the TG to apoB ratio of the fluxes from compartment 6 to compartment 8 and from the liver to compartment 8 is equal. This is the case since

$$\frac{d^t_{8,0}h(t)T}{d^a_{8,0}h(t)A} = \frac{k_{8,6}f_{8,6}P_6}{k_{8,6}Q_6}$$

and

$$\frac{d^t_{8,0}T}{d^a_{8,0}A} = f_{8,6}f_{6,5}\frac{Td^t_{5,0}}{Ad^a_{5,0}} \Leftrightarrow \frac{d^t_{8,0}}{d^a_{8,0}} = f_{8,6}f_{6,5}\frac{d^t_{5,0}}{d^a_{5,0}}.$$

Therefore, the initial fractions can be determined (as in equation (4.11)) by assuming the degradation terms to be zero at $t = 0$, then $d^a_{8,0} = 1 - d^a_{5,0}$ and $d^t_{8,0} = 1 - d^t_{5,0}$.

4.2.2 Discussion of the Time Dependent- Model

In the clamp experiments, the typical response to the insulin infusion was a reduction of the $VLDL_1$ and $VLDL_2$ pools of both apoB and TG. The reduction was most pronounced

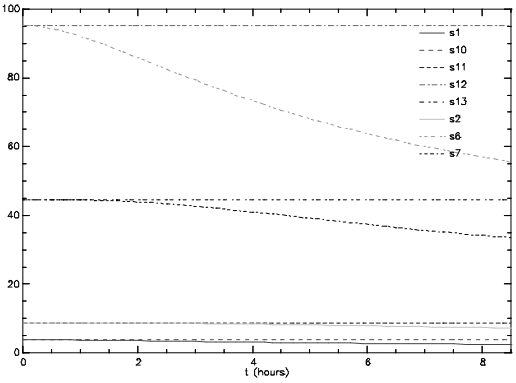

(a) Basal pools compared to pools when the $VLDL_1$ production is decreased by $e^{-0.2t}$

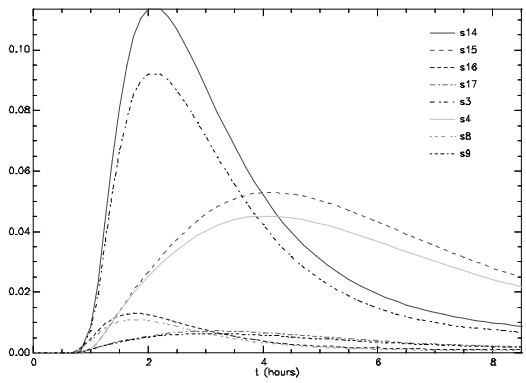

(b) Basal enrichment curves compared to enrichment curves when the $VLDL_1$ production is decreased by $e^{-0.2t}$

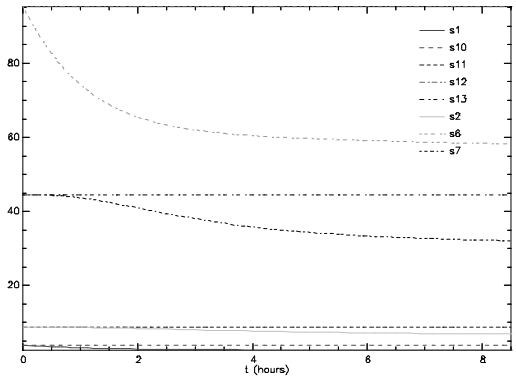

(c) Here the $VLDL_1$ production is instantly decreased to 0.3 of its original value. The $VLDL_1$ pool almost reach it's new steady state within the experimental time of 8 hours.

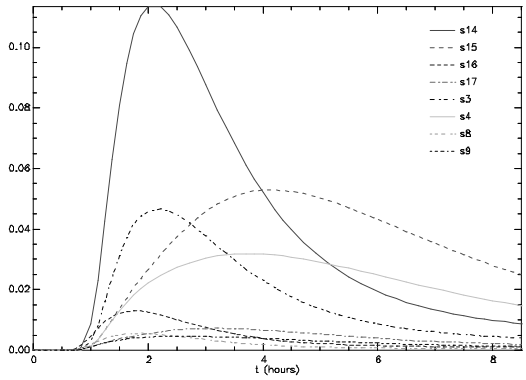

(d) Enrichments curves for the same change of $VLDL_1$ production

Figure 4.7: Pools and enrichment curves when the $VLDL_1$ production is suppressed. In (a) and (b) the production is slowly decreasing with an exponential decay. In (c) and (d) the $VLDL_1$ production is instantly decreased to 1/3 of the original value. Before the change the system is in steady state. (a) and (c) s1 - $VLDL_1$ apoB steady state, s10 - $VLDL_1$ apoB time dependent, s2 - $VLDL_2$ apoB steady state, s11 - $VLDL_2$ apoB time dependent, s6 - $VLDL_1$ TG steady state, s12 - $VLDL_1$ TG time dependent, s7 - $VLDL_2$ TG steady state, s13 - $VLDL_2$ TG time dependent. (b) and (d) s3 - $VLDL_1$ apoB steady state, s14 - $VLDL_1$ apoB time dependent, s4 - $VLDL_2$ apoB steady state, s15 - $VLDL_2$ apoB time dependent, s8 - $VLDL_1$ TG steady state, s16 - $VLDL_1$ TG time dependent, s9 - $VLDL_2$ TG steady state, s17 - $VLDL_2$ TG time dependent. These figures are also attached in the appendix B.

for $VLDL_1$. Assuming that the pools were in steady-state when the insulin was infused the reduction of the pools has to be due to either reduced production, increased clearance or a combination of these.

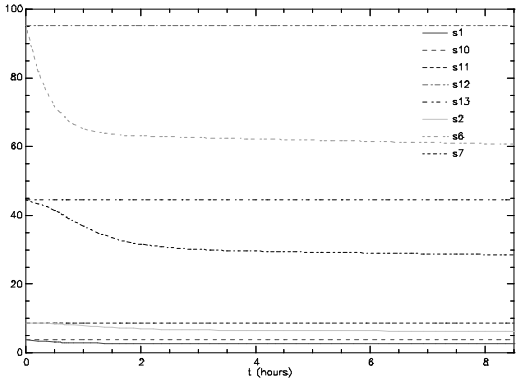

(a) Pools sizes when $VLDL_1$ and $VLDL_2$ FTR is increased, the fractional transfer rates $k_{6,5}, k_{8,6}, k_{10,8}$ and $k_{0,10}$ were tripled

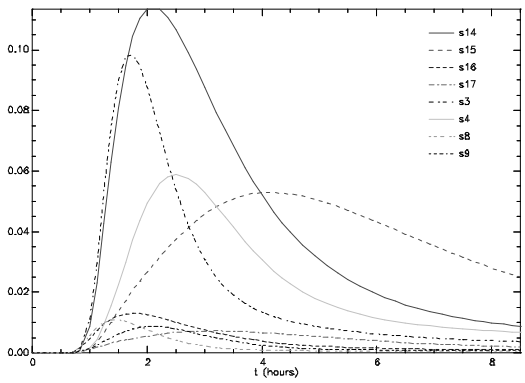

(b) Enrichment curves when $VLDL_1$ and $VLDL_2$ FTR were increased

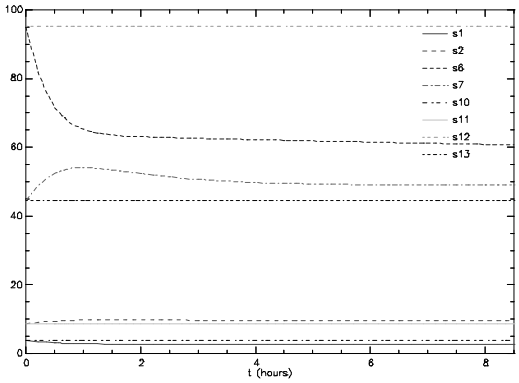

(c) Pools sizes when $VLDL_1$ FTR is increased, the fractional transfer rates $k_{6,5}$ and $k_{8,6}$ were tripled

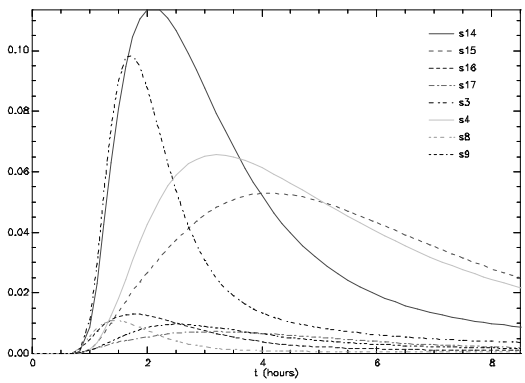

(d) Enrichment curves when $VLDL_1$ FTR was increased

Figure 4.8: Pools and enrichment curves when FTR parameters are changed. Before the change, the system is in steady state. (a) and (c) s1 - $VLDL_1$ apoB steady state, s10 - $VLDL_1$ apoB time dependent, s2 - $VLDL_2$ apoB steady state, s11 - $VLDL_2$ apoB time dependent, s6 - $VLDL_1$ TG steady state, s12 - $VLDL_1$ TG time dependent, s7 - $VLDL_2$ TG steady state, s13 - $VLDL_2$ TG time dependent. (b) and (d) s3 - $VLDL_1$ apoB steady state, s14 - $VLDL_1$ apoB time dependent, s4 - $VLDL_2$ apoB steady state, s15 - $VLDL_2$ apoB time dependent, s8 - $VLDL_1$ TG steady state, s16 - $VLDL_1$ TG time dependent, s9 - $VLDL_2$ TG steady state, s17 - $VLDL_2$ TG time dependent. These figures are also attached in the appendix B.

To investigate how to simulate such response in the model and in order to get a feeling of the qualitative behavior of the model and its dependence on the parameters we carried out a number of simulations where one parameter at a time was changed. Figures 4.7(a) - 4.7(d) shows the change in pool sizes and enrichment curves when the synthesis rate of $VLDL_1$ is

decreased. In a slow suppression of the synthesis, with an exponentially decaying rate ($e^{-0.2t}$, figures 4.7(a) and 4.7(b)) the $VLDL_1$ pool shows a steady decay. The lack of particles in $VLDL_1$ introduces a decreased transfer rate of particles into $VLDL_2$, hence the $VLDL_2$ pools shows a slowly increasing decay. The enrichment curves are similar to the basal curve but with lower maximal enrichments. In 4.7(c) and 4.7(d) the production of $VLDL_1$ is instantly suppressed to 30% of its original value, which causes a rapid decay of the $VLDL_1$ pool. Due to the circulation time of $VLDL_1$ particles, which is a few hours, the pools starts to flatten out and the system almost reaches a new steady-state.
In 4.8(a) both the $VLDL_1$ and the $VLDL_2$ FTRs were changed. The $k_{6,5}, k_{8,6}, k_{10,8}$ and $k_{0,10}$ were tripled at $t = 0$. We observe an rapid change in the pools and after 2 hours the pools starting to stabilise. The initial slope of the $VLDL_1$ enrichment (figure 4.8(b)) is close to the slope in the basal experiment but since the turnover rate is tripled the enrichment reach it's peak earlier and the decay is more rapid than for the basal curve. The enriched material reaches $VLDL_2$ more rapidly and hence the slope of the $VLDL_2$ curve is steeper than the basal curve. The increased transfer rate results in a steeper decay of the curve.

4.2.3 Implementation of Non Steady-State Models in SAAMII

In SAAMII, time dependent transfer coefficients can be introduced either by defining the equation directly or by introducing a *change condition* to give an instant changes in parameters. However, for tracer/tracee experiments the tracee is assumed to be in steady state.
The common way work around this is construct two tracer experiments in the same model. One corresponds to the actual tracer (experiment T1) and one corresponds to the tracee (T2). The T1 experiment is designed by defining the input functions corresponding to the injected tracers. The T2 experiment is defined by a constant inputs. The compartmental system is integrated for a period of time (i.e loading time) until all compartments have reached steady state. The loading time should be chosen so that the masses in all compartments are constant when the T1 experiment starts. This is implemented by starting the experiment at, say, $h = -50$ hours. The constant input will then assure the system to be close to a steady-state at $t = 0$ hours.

We have modified this approach. Instead of a loading phase of the T2 experiment, we use the steady state solution from the model as a start solution to the T2 experiment. Hence, there are actually three systems of equations. The steady-state system only holds for $t = 0$

$$\dot{\mathbf{Q}} = \mathbf{0} = \mathbf{K}(0)\mathbf{Q} + \mathbf{U}.$$

The solution ($\mathbf{Q}$) to this system is then used as initial condition to the tracee experiment, T2. Let $\mathbf{q}_2$ denote the vector of tracee masses, then

$$\begin{aligned} \dot{\mathbf{q}}_2(t) &= \mathbf{K}(t)\mathbf{q}_2(t) + \mathbf{U}, \\ \mathbf{q}_2(0) &= \mathbf{Q}. \end{aligned}$$

This is achieved by defining $q_2^i = Q_i$ at time $t = 0$ by using *Change Condition* in SAAMII. The T1 experiment is defined as usual. Let $\mathbf{q}_1$ denote the tracer mass vector

$$\begin{aligned} \dot{\mathbf{q}}_1(t) &= \mathbf{K}(t)\mathbf{q}_1(t) + \mathbf{u}(t), \\ \mathbf{q}_1(0) &= \mathbf{0}. \end{aligned}$$

The system still has to be integrated for a period of time, since the delay compartments cannot be assigned an initial value.

4.3 Outputs From the Models

From the calculated solution to the models, we have estimated the following parameters:

Production The absolute production of apoB and TG was calculated as the fluxes from the delays to $VLDL_1$ and $VLDL_2$. The production is presented in milligrams per day [mg day^{-1}] and relative the body weight in milligrams per kg body weight per day [mg $kgbw^{-1}$ day^{-1}].

Fractional Transfer Rate The fractional transfer rate (FTR) was calculated as fractional transfer of material from $VLDL_1$ to $VLDL_2$. The FTR is expressed in pools per day [day^{-1}].

Fractional Catabolic Rate The fractional catabolic rate (FCR) was calculated as the fractional removal (transfer and direct removal) of material from $VLDL_1$ and $VLDL_2$. The FCR is expressed in pools per day [day^{-1}].

Fractional Direct Catabolic Rate The fractional direct catabolic rate was calculated as the fractional removal of material from $VLDL_1$ and $VLDL_2$ due to catabolism. The FDCR is expressed in pools per day [day^{-1}].

For model 1 and 2 the calculated parameters are defined as

$$
\begin{aligned}
\mathrm{Prod}_1^{\mathrm{apoB}} &= \mathrm{FLUX}^{\mathrm{apoB}}(5,11),\\
\mathrm{FTR}^{\mathrm{apoB}} &= \frac{\mathrm{FLUX}^{\mathrm{apoB}}(8,6)}{Q_5+Q_6+Q_7},\\
\mathrm{FDCR}^{\mathrm{apoB}} &= \frac{\mathrm{FLUX}^{\mathrm{apoB}}(0,6)+\mathrm{FLUX}^{\mathrm{apoB}}(0,7)}{Q_5+Q_6+Q_7},\\
\mathrm{FCR}_1^{\mathrm{apoB}} &= \frac{\mathrm{FLUX}^{\mathrm{apoB}}(0,6)+\mathrm{FLUX}^{\mathrm{apoB}}(0,7)+\mathrm{FLUX}^{\mathrm{apoB}}(8,6)}{Q_5+Q_6+Q_7},\\
\mathrm{Prod}_2^{\mathrm{apoB}} &= \mathrm{FLUX}^{\mathrm{apoB}}(8,11),\\
\mathrm{FCR}_2^{\mathrm{apoB}} &= \frac{\mathrm{FLUX}^{\mathrm{apoB}}(0,9)+\mathrm{FLUX}^{\mathrm{apoB}}(0,10)}{Q_8+Q_9+Q_{10}},\\
\mathrm{Prod}_1^{\mathrm{TG}} &= \mathrm{FLUX}^{\mathrm{TG}}(5,11),\\
\mathrm{FTR}^{\mathrm{TG}} &= \frac{\mathrm{FLUX}^{\mathrm{TG}}(8,6)}{P_5+P_6+P_7},\\
\mathrm{FDCR}^{\mathrm{TG}} &= \frac{\mathrm{FLUX}^{\mathrm{TG}}(0,6)+\mathrm{FLUX}^{\mathrm{TG}}(0,7)}{P_5+P_6+P_7},\\
\mathrm{FCR}_1^{\mathrm{TG}} &= \frac{\mathrm{FLUX}^{\mathrm{TG}}(0,6)+\mathrm{FLUX}^{\mathrm{TG}}(0,7)+\mathrm{FLUX}^{\mathrm{TG}}(8,6)}{P_5+P_6+P_7},\\
\mathrm{Prod}_2^{\mathrm{TG}} &= \mathrm{FLUX}^{\mathrm{TG}}(8,11),\\
\mathrm{FCR}_2^{\mathrm{TG}} &= \frac{\mathrm{FLUX}^{\mathrm{TG}}(0,9)+\mathrm{FLUX}^{\mathrm{TG}}(0,10)}{P_8+P_9+P_{10}}.
\end{aligned}
$$

The above definitions hold if the time scale of the model is days, i.e. the experimental time is 8/24 days and the transfer coefficients are in [day^{-1}]. For the time dependent model the above definitions gives functions of time. In the literature both [day^{-1}] and [h^{-1}] are used. Depending on the situation different parameters could be calculated, for instance how fast the response is (the drop of production the first hour etc.).
The size of newly produced particles are estimated from the quotient of the TG and apoB productions and gives the TG to apoB ratio.

4.4 Dealing With Tracer-Loss

In a recent paper by Patterson et.a. [34] it was discovered that there can be an exchange of hydrogen atoms of the glycerol during the esterification of the glycerol molecules in the liver. The effect of this is that a labelled 1,1,2,3,3-D-glycerol may loose one ore more deuterium atoms during the esterification in the liver. In that paper the authors directly measured the enrichment of isotopomers with mass m+1, m+2, m+3, m+4 and m+5 vs m+0. The clearance rates appeared to be identical for all the isotopes - suggesting that it is in the esterification that the atoms are replaced.
In the tracer/tracee application this such loss of label will not be a problem. The measured the m+5 vs m+0 ratio will be less than the true tracer/tracee ratio since some of the injected tracer will be put as unlabelled material. This could be taken care of by introducing an extra loss term in the liver model.

However, in this project the analysis the glycerol enrichment was not measured directly. As described in section 3, the m+3 and m+2 enrichment of a fragment of the glycerol triacetate was measured and the m+3 to m+0 ratio was estimated by multiplying the m+3 to m+2 ratio by the basal ($t = 0$) m+2 to m+0 ratio. The problem that may occur is that if one or more deuterium atoms are replaced by hydrogen atoms then it can be measured as m+2, hence the m+2 to m+0 ratio will not be constant.

# D	145+3	145+2	145+1	145	P
5	100	0	0	0	$(1-p)^5$
4	40	60	0	0	$5p(1-p)^4$
3	10	60	30	0	$10p^2(1-p)^3$
2	0	30	60	10	$10p^3(1-p)^2$
1	0	0	60	40	$5p^4(1-p)$
0	0	0	0	100	p^5

Table 4.1: Percent detected fragments if one or more deuterium atoms are exchanged to hydrogen atoms. Left column; number of intact deuterium atoms. Column 2-5; percent of fragments 148, 147, 146 and 145 detected. Column 6 (rightmost), probability of event to occur, p is the probability of exchange of a deuterium atom.

In the analysis we first assume that all other atoms are in their most common natural isotopes. If the exchanged deuterium atom was attached to carbon 1 or 3 (4 out of 5 cases) the MS will detect a m/z 145+3 fragment in 50% of the cases and a m/z 145+2 fragment in 50%. If the exchanged atom is at carbon 2 (1 out of 5 cases) the MS always detects a m/z 147. If each atom is replaced with probability p, all five deuterium atoms are intact with probability $(1-p)^5$. In this case the MS always detects a m/z 145+3 fragment. The different fragments that are detected if one or more atoms are exchanged are summarised in table 4.1.
However, as described in figure 4.9 the measured molecule is not the glycerol triacetate molecule $C_9H_{14}O_6$, but the fragment $C_6\ H_9\ O_4$. Hence, we can consider the smaller problem of one or more of the three deuterium atoms being exchanged. Therefore we have the probability $(1-p)^3$ to detect 145+3, $3p(1-p)^2$ to detect 145+2, $3p^2(1-p)$ to detect 145+1 and p^3 to detect 145. We verify this by summarising the probabilities in table 4.1:

$$\begin{aligned}
1(1-p)^5 + \frac{4}{10}5p(1-p)^4 + \frac{1}{10}10p^2(1-p)^3 &= (1-p)^3 \\
\frac{6}{10}5p(1-p)^4 + \frac{6}{10}10p^2(1-p)^3 + \frac{3}{10}10p^3(1-p)^2 &= 3p(1-p)^2 \\
\frac{3}{10}10p^2(1-p)^3 + \frac{6}{10}10p^3(1-p)^2 + \frac{6}{10}5p^4(1-p) &= 3p^2(1-p) \\
\frac{1}{10}10p^3(1-p)^2 + \frac{4}{10}5p^4(1-p) + 1p^5 &= p^3
\end{aligned}$$

We now move on to consider the case where all the other atoms in the molecule are naturally distributed isotopes. Considering the three deuterium atoms, the molecular weight is distributed with $f(i) = \binom{3}{i}p^i(1-p)^{3-i}$, $i = 0, 1, 2, 3$ and $f(i) = 0$. The total probability density function for the whole molecule therefore is

$$\begin{aligned}
P_{C_6H_6O_4\hat{D}_3}(i) &= f * P_C * P_C * P_C * P_C * P_C * P_C * P_H * P_H * P_H * P_H * P_H * P_H * \\
&* \quad P_O * P_O * P_O * P_O(i),
\end{aligned}$$

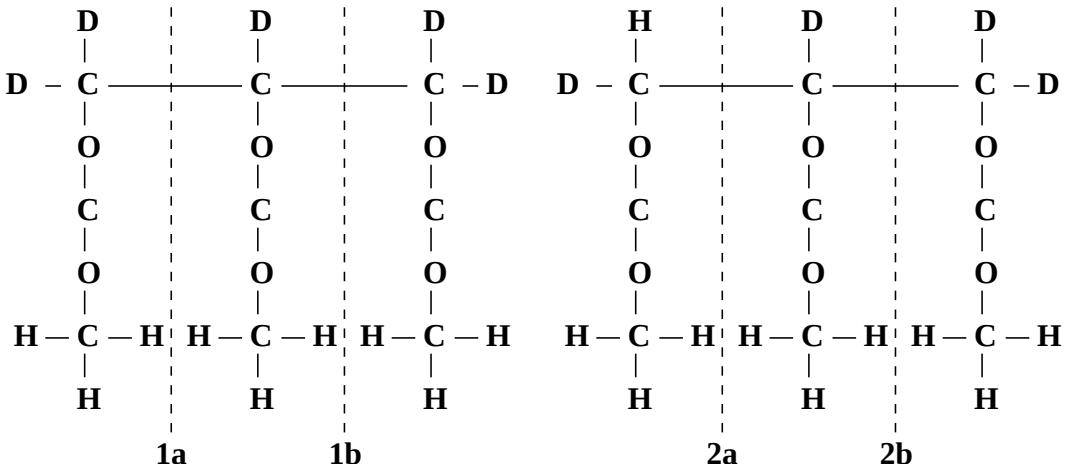

Figure 4.9: In the GC the glycerol triacetate molecule is split between carbon 1 and 2 (1a or 2a) or between 2 and 3 (1b or 2b). In an un-labelled molecule, these splits form one fragment with m/z 73 (the smaller fragment) and one fragment with m/z 145 (the larger fragment). The split is symmetric, so the there is no difference in the fragments if the split is between carbon 1 and 2 or 2 and 3. The MS measures the intensity of the larger fragment. **Left**: A fully labelled glycerol molecule, a split at 1a or at 1b and forms one fragment with m/z 73+2 and one with m/z 145+3. **Right**: One deuterium atom is exchanged to a hydrogen atom. If the split is at 2a the MS will measure a m/z 145+3 fragment, but if the split is at 2b the MS will measure a m/z 145+2 fragment.

where f_C, f_H and f_O is defined as in section 3 and $\hat{D}$ refers to a deuterium atom that could be replaced by a hydrogen atom. The probability to measure the different masses is displayed in figure 4.10.
Let $P^U(i)$ be the abundance of m+i in the unlabelled fragment (which is the tracee). Fix p and let, $P^T(i)$ be the abundance of the tracer. The goal now is to simulate the analysis procedure, which was presented in section 3.
The measured quantities are the m/z 145+3 fragments, $N_3(t_j)$, and the m/z 145+2 fragment, $N_2(t_j)$, where t_j is the sample time. Furthermore, the ratio of m/z 145+2 and m/z 145, R_0^2, is estimated in the t_0 sample. Assuming $T(t_j)$ to be the true amount of tracer and $Q(t_j)$ the true amount of tracee in the sample taken at time t_j, we have

$$\begin{aligned} N_3(t_j) &= T(t_j)P^L(3) + Q(t_j)P^U(3) \\ N_2(t_j) &= T(t_j)P^L(2) + Q(t_j)P^U(2) \end{aligned}$$

Hence, the adjusted mpe (molar percent excess) as in equation (3.2) is

$$\hat{\text{mpe}} = \frac{R_0^2 \frac{T(t_j)P^T(3)+Q(t_j)P^Q(3)}{T(t_j)P^T(2)+Q(t_j)P^Q(2)} - R_0^2 \frac{T(t_0)P^T(3)+Q(t_j)P^Q(3)}{T(t_0)P^T(2)+Q(t_j)P^Q(2)}}{1 + R_0^2 \frac{T(t_j)P^T(3)+Q(t_j)P^Q(3)}{T(t_j)P^T(2)+Q(t_j)P^Q(2)} - R_0^2 \frac{T(t_0)P^T(3)+Q(t_j)P^Q(3)}{T(t_0)P^T(2)+Q(t_j)P^Q(2)}} 100.$$

Since there should be no tracer in the t_0 sample, $T(0) = 0$ and

$$\hat{\text{mpe}} = \frac{R_0^2 \frac{T(t_j)P^T(3)+Q(t_j)P^Q(3)}{T(t_j)P^T(2)+Q(t_j)P^Q(2)} - R_0^2 \frac{Q(t_j)P^Q(3)}{Q(t_j)P^Q(2)}}{1 + R_0^2 \frac{T(t_j)P^T(3)+Q(t_j)P^Q(3)}{T(t_j)P^T(2)+Q(t_j)P^Q(2)} - R_0^2 \frac{Q(t_j)P^Q(3)}{Q(t_j)P^Q(2)}} 100. \tag{4.19}$$

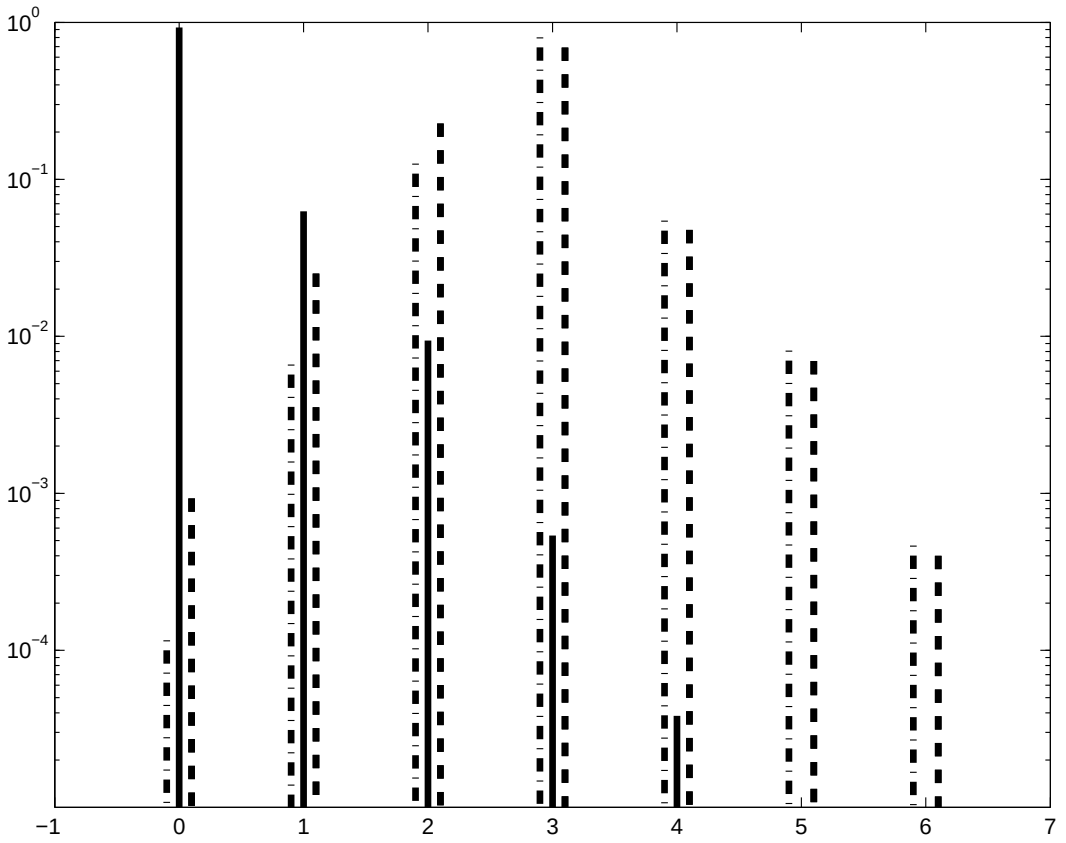

Figure 4.10: Solid line, pdf for unlabelled fragment. Dashed line, pdf for tracer with loss of deuterium, p=0.05. Dash-dotted line, pdf for tracer with loss of deuterium, p=0.1

If there is no loss of label, then $P^T(2) = 0$ and equation (3.2) is identical to equation (4.19).

To test the impact of the loss of tracer we simulated the measurement procedure from the solution to the compartmental model.For VLDL_1 we defined $T(t) = q_5(t) + q_6(t) + q_7(t)$ and $Q(t) = Q_5(t) + Q_6(t) + Q_7(t)$. For VLDL_2 similar definitions was made. In figure 4.11 the original and adjusted tracer curves are shown. The implementation and impact of the tracer loss is summarised in section 7.1.4, where we conclude that in most cases the loss of tracer did not influence the result.

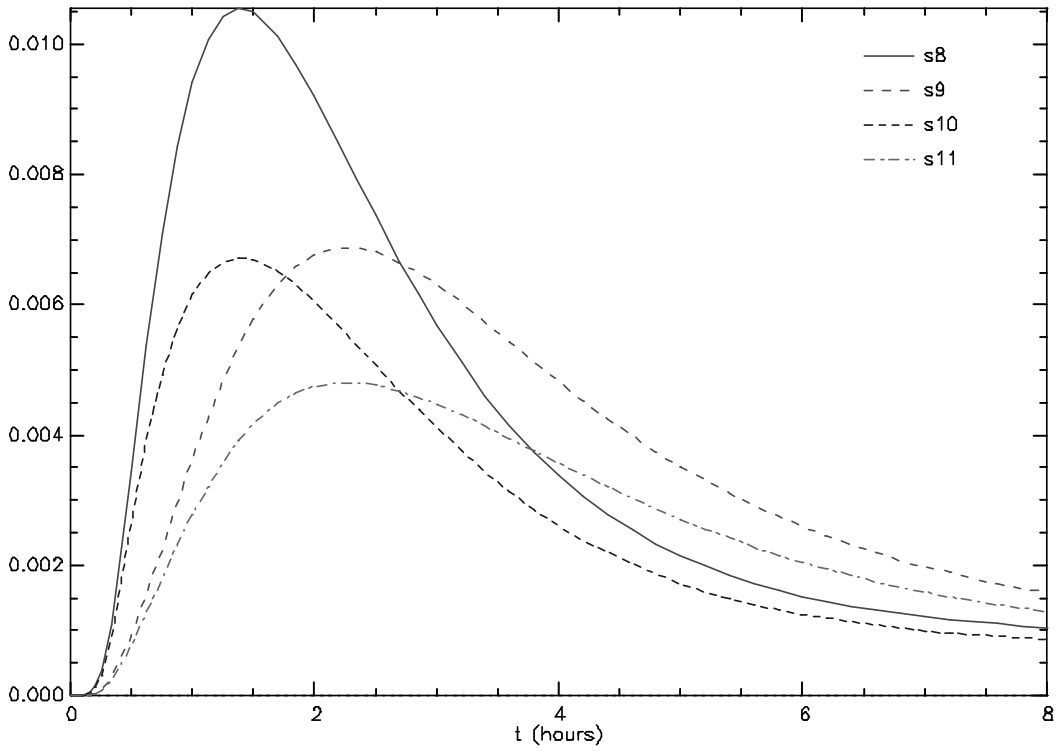

Figure 4.11: Simulation of adjusted tracer/tracee ratios from the model. The solution to the tracer equation (s8 - $VLDL_1$ and, s9 - $VLDL_2$) was adjusted using equation 4.19, using a p value of 0.05. The adjusted enrichment curves are s10 - $VLDL_1$ and s11 -$VLDL_2$.

Chapter 5

Limitations of the Compartmental Model, A Stochastic Approach

There are some limitations of the compartmental model. We here describe some concepts that are not possible to implement in compartmental models or would give very complex models.

Structural aging The kinetic properties of a circulating particle could change with the time. We know that the protein content is dependent on time, but there could be other effects as well. For instance the surface proteins could be oxidised and the concentration of the surface lipids could be changed as some of the surface lipids has to be removed when the TG and CE content is changed. On a more speculative matter, the TG and CE concentrations in outer part of the core is changed as the TG is hydrolysed. This could lead to a slower hydrolysation since less TG is exposed.

Density distribution of new particles As discussed in section 1.3 there exist particles with a wide range of S_f , densities and diameters. This suggests that the distribution of the newly produced particles is continuous and spread out over the whole VLDL density range.

Hydrolysation The loss of TG molecules due to hydrolysation by LPL is most likely not constant, i.e. the number of molecules that is lost is random.

Implementation of structural aging would include a non-exponentially distributed holding time in a compartment. It would also include *memory*, i.e. the time spent in previous states influence the behavior in the current state. Here it would be a great advantage in using a stochastic model. The problem is of course to experimentally verify and quantify structural aging in this sense.
In the compartmental model, movement between compartments is associated with a fixed loss of TG. In reality, the number of TG molecules being hydrolysed by LPL could vary. Moreover, the number of simultaneously active LPL determines the speed and total loss of TG. Again, this would be difficult to in verify by experiments *in vivo*. However, it could be possible to quantitatively verify *in vitro*.
A continuous distribution of particle size and composition would not be possible to implement in the compartmental model. However, a nice way to open up for implementation of these

and other concepts is stochastic modelling. As it turns out, compartment modelling may be seen as a special case of such a model.

In the most general case, we consider a (VLDL) lipoprotein as a pre-VLDL particle that is loaded by stochastic amounts of TG and cholesterol esters, as well as being equipped with other apolipoproteins such as apoC and apoE. The amounts of phospholipids and cholesterol esters (i.e. the shell components) are more or less determined by the total particle size. Once the particle is released into the plasma it is open for reactions, such as binding to LPL and exchange of apoE and apoC with HDL. In the general case, the time between two events are random, as well as the results of the event. For instance, if the event is loss of TG, the amount of removed TG is random. An example of the life of a particle is shown if figure 5.1. A pseudo simulation-code for such stochastic model is fairly simple and straight forward.

```
Structure Particle
  Time;
  Mass;
End;

For each particle P Do
 P.Time=GetStartTime;
 P.Mass=GetStartTGMass;
 While (P.Time < ExperimentTime) OR (P.Mass>MinumTGMass)
  T1=getTimeToEvent(1);
  ...
  Tn=getTimeToEvent(n);
  [T,I]=Min([T1,...,Tn]);
  Save(P.Time,P.Time+T,P.Mass);
  PerformEvent(P,I); % i.e. remove mass etc
  P.Time+=T;
 End
End
```

A detailed analysis of the general stochastic model above is complicated if the loss of TG (the *di* in figure 5.1) is random. For the analysis we assume the loss of TG to be deterministic but dependent of the TG mass, likewise we assume that TG added to each particle follows a discrete distribution with two possible outcomes, e.g. VLDL_1 or VLDL_2. Such scheme is displayed in figure 5.2.
We assume that the loss of TG is positive in each step and that there can only be a finite number of losses until the particle is removed from the VLDL density range. This is not an over simplification since in reality several LPL simultaneously acts on the particle, as described in section 1.2. This is very much like the different compartments in the compartmental model. In fact, as pointed out by several authors (a few are mentioned in [15]), the linear time-invariant system with initial condition;

$$\dot{\mathbf{Q}} = \mathbf{KQ},\ \mathbf{Q}(0) = \mathbf{Q}_0, \tag{5.1}$$

where $\mathbf{K}$ is a compartmental matrix, has a probabilistic interpretation. In fact, the matrix $\mathbf{K}$ can be regarded as the intensity matrix of the transition matrix $P(t) = e^{t\mathbf{K}}$ of a Markovian

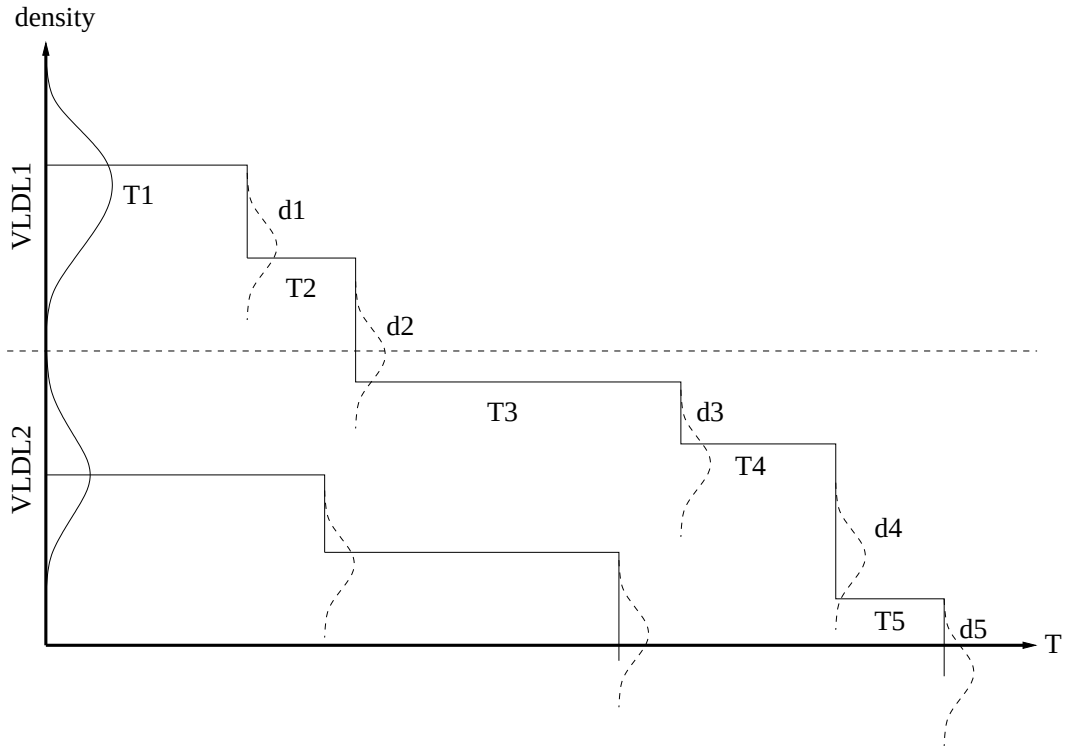

Figure 5.1: The upper graph displays the behavior of a VLDL_1 particle. The initial TG content is drawn from the distribution on the y-axis. The time between the events $T1, \ldots, T5$ is stochastic and determined from a distribution wish can depend on the TG content (i.e. size). The loss of TG, $d1, \ldots, d5$, is also stochastic and is drawn from the distributions in the figure.

stochastic process [15]. The compartments correspond to the states of the systems and an element $p_{i,j}(t)$ of $P(t)$ is the probability that a particle is in state i given that it started in state j.

Assume that the holding time T_i in state i is a stochastic variable, distributed with $f_i(t)$. Under the assumption that the holding times are independent, the probability for a particle to be in state i at time is $p(T_0 + T_1 + \cdots + T_{i-1} < t < T_0 + T_1 + \cdots + T_i)$, where T_0 is the time until the particle is secreted. T_0 is distributed with $f_0(t)$. Since T_i is distributed with f_i the sum $T_0 + \cdots + T_i$ is distributed with $f_0(t) * \cdots * f_i(t) \equiv g_i(t)$.

$$\begin{aligned} p(T_0 + T_1 + \cdots + T_{i-1} < t < T_0 + T_1 + \cdots + T_i) &= \\ p(t < T_0 + T_1 + \cdots + T_i) - p(t < T_0 + T_1 + \cdots + T_{i-1}) &= \int_0^t g_{i-1}(s) - g_i(s) ds \end{aligned} \quad (5.2)$$

It is natural to assume that the time interval between to interactions with LPL is exponentially distributed, or if the case of saturation - at least only depending on the concentration of lipoprotein and the number of LPL.
The time between the collisions can be estimated as follows. Assume C to be a constant which depends on the velocity and size of the particle and on the number of particles in the system. The probability of no collision in the short time interval Δt is $p(\text{no collision in } \Delta t) = (1 -$

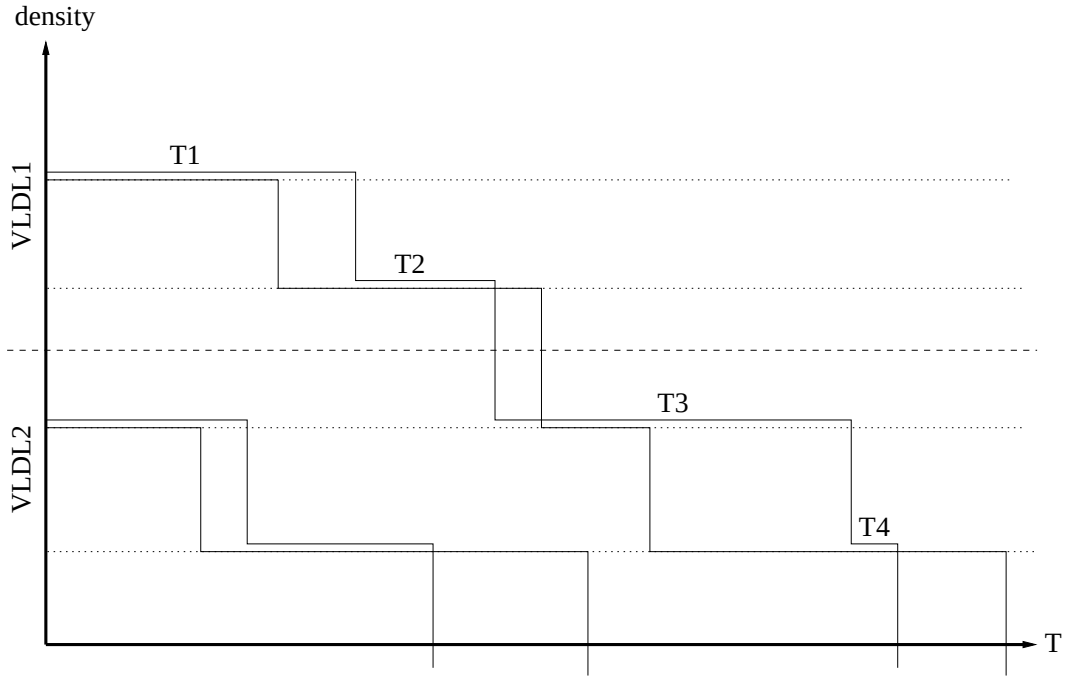

Figure 5.2: The upper graphs displays the behavior of two VLDL_1 particles (the curves are slightly shifted). The initial TG content is fixed. The time between the events $T1, \ldots, T4$ is stochastic and determined from a distribution wish can depend on the TG content (i.e. size).

$C\Delta t$), for a longer time of m intervals ($t = m\Delta t$) the probability is $p(\text{no collision in } m\Delta t) = (1 - C\Delta t)^m = (1 - Ct/m)^m \approx e^{-tC}$, if the interactions are assumed to be independent. Hence the probability that at least one collision occurs is $1 - e^{-Ct}$. Taking the derivative gives the probability distribution $f(t) = Ce^{-tC}$. This reasoning assumes that the particle does not age, i.e. that the circulation itself does not alter the kinetic properties of the particle. Furthermore it assumes linearity, i.e. that the number of particles does not influence the kinetics. This allows for modelling of one particle at a time.
The amount of TG that is lost once a interaction with LPL has started could depend on several factors - such as particle size and the amount (or lack thereof) apoC and apoE.
The time between interactions with HDL (exchange of apolipoproteins) should also be exponentially distributed. Results of the interaction could be loss or gain of apoE or apoC, a result that could be dependent on the amount of apoE and apoC as well as on the particle size.

5.1 Modelling tracer-tracee experiments

When modelling tracer-tracee experiments, there are not many things that differ from the background particle model. All tracer particles are assumed to be labelled, and they are put into the system according to some distribution. In this case the distribution of starting times is modelled by the four-compartment leucine model and the four-compartment glycerol-TG model respectively.

We first consider an irreversible catenary system of n compartments, with one exit from compartment n. Assume that one particle enters the first compartment at time T_0, which is random and has probability density function $f_0(t)$. The time spent in compartment i is T_i, which is random and has probability density function $f_i(t)$. From equation (5.2) we have the probability for the particle to be in compartment i at time t

$$\begin{aligned} p(i,t) &= \int_0^t g_{i-1}(s) - g_i(s)ds \\ &= \int_0^t (f_0 * \cdots * f_{i-1} * (\delta - f_i))(s)ds \\ &= \int_0^t (g_{i-1} * (\delta - f_i))(s)ds. \end{aligned} \tag{5.3}$$

Taking the Laplace transform, and assuming $f_i(t) = \lambda_i e^{-\lambda_i t}$,

$$\begin{aligned} \mathcal{L}(p(i,t)) &= F_0 \frac{\lambda_1}{\lambda_1 + s} \cdots \frac{\lambda_{i-1}}{\lambda_{i-1} + s}(1 - \frac{\lambda_i}{\lambda_i + s})\frac{1}{s} \\ &= F_0 \frac{\lambda_1}{\lambda_1 + s} \cdots \frac{\lambda_{i-1}}{\lambda_{i-1} + s}\frac{1}{\lambda_i + s}. \end{aligned}$$

The solution to the ODE formulation of the catenary system can be calculated inductively.

$$\begin{aligned} q_0(t) &= \int_0^t f_0(s)e^{-\lambda_1(t-s)}ds = f_0(t) * e^{-\lambda_1 t}, \\ q_i(t) &= \lambda_{i-1}\int_0^t q_{i-1}(s)e^{-\lambda_i(t-s)}ds = \lambda_{i-1}q_{i-1}(t) * e^{-\lambda_i t} \\ &= \lambda_{i-2}\lambda_{i-1}q_{i-2}(t) * q_{i-1}(t) * e^{-\lambda_i t} \\ &= \lambda_1 \cdots \lambda_{i-1} f_0(t) * e^{-\lambda_1 t} * \cdots * e^{-\lambda_i t}. \end{aligned}$$

Taking the laplace transform we get

$$\mathcal{L}(q_0(t)) = \lambda_1 \cdots \lambda_{i-1} F_0 \frac{1}{\lambda_1 + s} \cdots \frac{1}{\lambda_i + s}.$$

Hence, for this almost closed irreversible catenary system the solution to the ODE system and the solution for the stochastic model are identical in the sense that the expected number of particles in each compartment satisfies the compartmental system.

This can be extended to general irreversible systems by introducing paths, which are a linear sequences of states. Assume that from state i the particle can go to a collection of different states, A_i. The time $T_{j,i}$ before the particle changes to state $j \in A_i$ is exponentially distributed with $\lambda_{j,i}$. The time in state i therefore is $T_i = \min(T_{j,i}, j \in A_i)$ which is exponentially distributed with $\lambda_i = \sum_{j \in A_i} \lambda_{j,i}$. The probability that the particle changes to state j then is $p(i \to j) = \lambda_{j,i}/\lambda_i$.
The probability for a particle in i to be in state j is the sum of the probabilities following all paths from i to state j. Let $i, n_{1,k}, \ldots, n_{n_k,k}, j$ for $k = 1 \ldots K$ be all K paths from i to j. For path k from i to j we define

$$g_{j,i,k}(t) \equiv (f_0 * f_i * f_{n_{1,k}} * \cdots * f_{n_{n_k,k}})(t)p(i \to n_{1,k}) \cdots p(n_{n_{k-1},k} \to n_{n_k,k}),$$

where f_0 is the distribution of the starting time in state i, According to equation (5.3) the probability that a particle is in state j at time t, starting in state i at time 0, following path k then is

$$p(i \to j,k) \quad = \quad \int_{t_0}^{t} (g_{j,i,k} * (\delta - f_i))(s)ds.$$

Taking the sum over all paths K we get

$$p(i \to j) \quad = \quad \sum_{k=1}^{K} p(i \to j,k).$$

5.2 Implementation

A stochastic model was implemented in Matlab and C++. The steady-state was simulated by starting the experiment at -8 hours, which gave an approximate steady-state in the 0 to 8 hour range (figure 5.3). The release of enriched material was simulated by the four compartment leucine subsystem. The enrichment in compartment 2 (which feeds the apoB synthesis mechanism) was used to approximate the random release time of the labelled particles (figure 5.4).

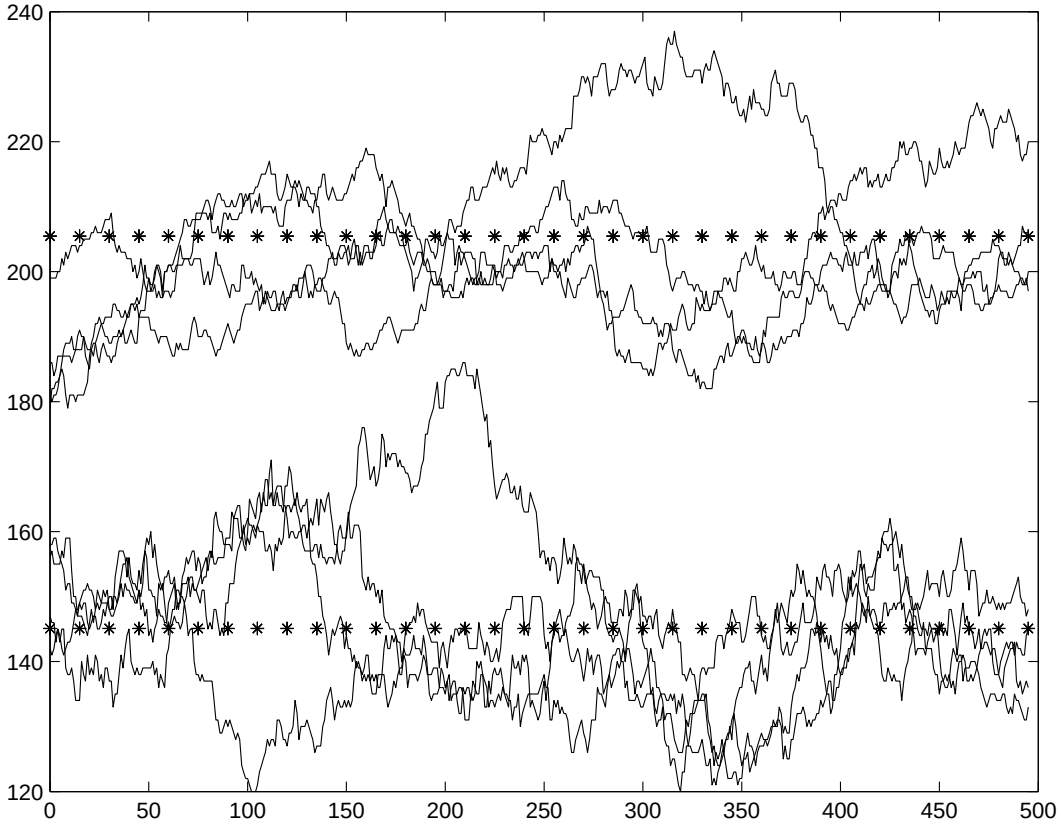

Figure 5.3: Stochastic simulation of 2000 particles (four repetitions), uniformly distributed on the interval -8 to 8 hours. The asterisks are the solution to the compartmental model. Upper curves $VLDL_1$, lower curves $VLDL_2$.

Even with a low number of particles the stochastic simulation gave results close to the solution to the compartmental model.

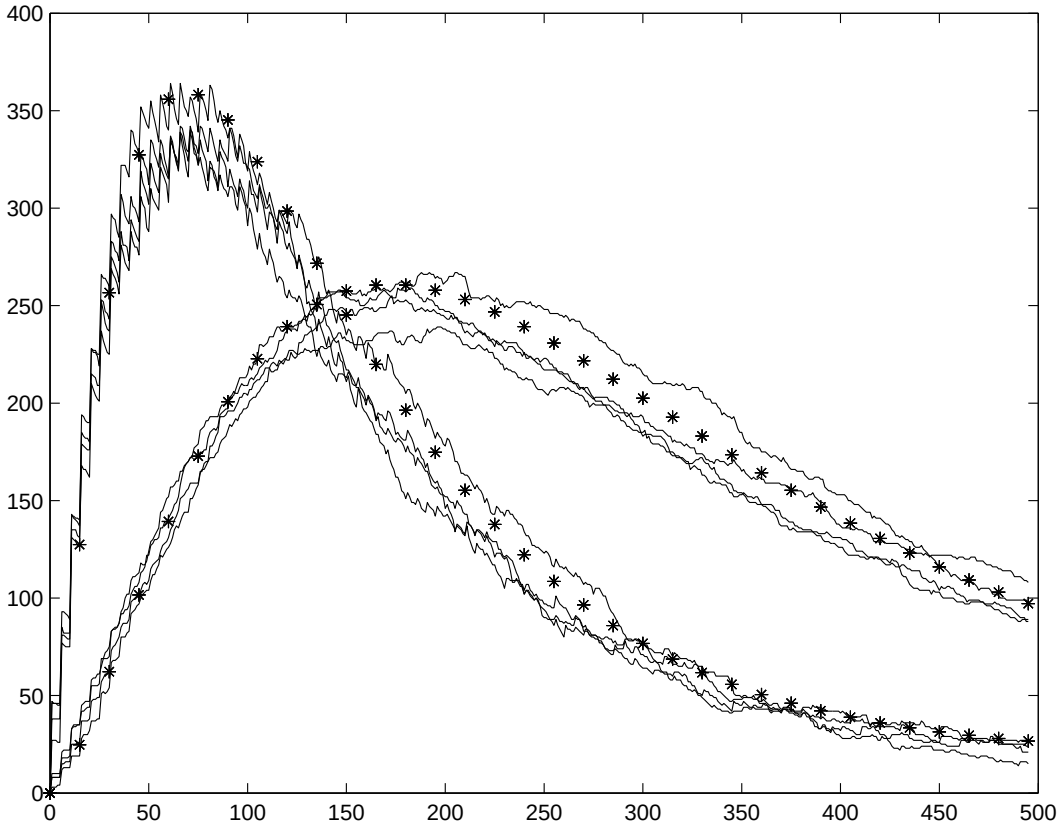

Figure 5.4: Stochastic simulation of 1000 labelled particles (repeated four times). The solution to the compartmental model is plotted with asterisks '*'.

Chapter 6

Parameter-free Analysis

In this chapter we describe methods to analyse the data without using any detailed mathematical calculations. It is possible to extract some information from the plots of the measured data directly.

From the enrichment curves we can estimate the fraction of TG and apoB that is secreted into VLDL_1 and VLDL_2. To do this, we investigate the curves and identify three important regions. The first region is the rapid increase of enrichment, the second region is the area where the curve is fairly flat and the third region is the region of rapid decay, as described in figure 6.1.
In region **A** little or no labelled material has left VLDL_1 (or VLDL_2). Let $L(t)$ be the total amount of labelled material that has been secreted into VLDL_1 and VLDL_2 at time t. With the notations in chapter 4, d_5 is the fraction of material secreted into VLDL_1 and $d_8^a = 1 - d_5$ is the fraction secreted into VLDL_2. Also, $L_1(t) = d_5 L(t)$ is the total amount of material secreted into VLDL_1 and $L_2 = (1 - d_5)L(t)$ the total amount secreted into VLDL_2. If t is in region **A** then little labelled material has left VLDL_1 and VLDL_2 and the enrichments in VLDL_1 and VLDL_2 can be expressed as $E_1(t) = L_1(t)/P_1$ and $E_2(t) = L_2(t)/P_2$ respectively, where P_1 and P_2 is the pool size of VLDL_1 and VLDL_2. We have

$$\frac{E_1(t)}{E_2(t)} = \frac{d_5 L(t) P_2}{(1 - d_5) L(t) P_1},$$

that is

$$d_5 = \frac{E_1(t) P_1}{E_1(t) P_1 + E_2(t) + P_2}.$$

From the, curves we can estimate $\hat{E}_1$ and $\hat{E}_2$ and from the pool measurements we can estimate the pool sizes $\hat{P}_1$ and $\hat{P}_2$, and compute

$$\hat{d}_5 = \frac{\hat{E}_1(t) \hat{P}_1}{\hat{E}_1(t) \hat{P}_1 + \hat{E}_2(t) + \hat{P}_2}$$

This estimation gave a good approximation of the calculated fractions. In the subjects ($n = 25$, two subjects had to be excluded since crucial data points were missing) both the apoB and TG fractions going to VLDL_1 were slightly overestimated (paired t-test). The average overestimation of the fraction of apoB going to VLDL_1 was 2.0 percent units, and 1.3 percent units for TG.

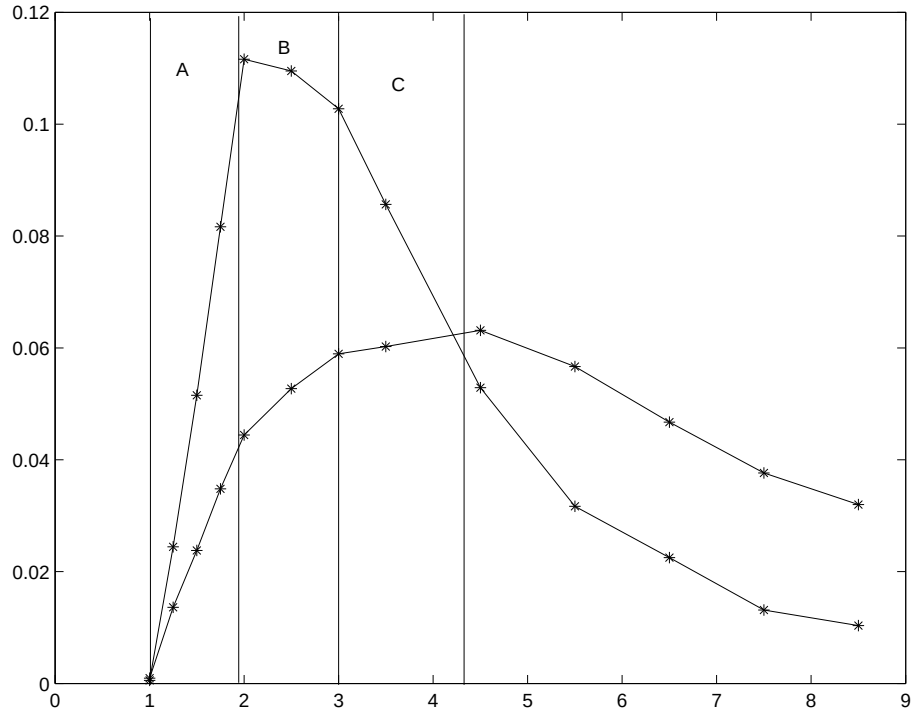

Figure 6.1: For the $VLDL_1$ (upper) curve, **A** is the region where the inflow of labelled material is greater then the outflow. In region **B** the inflow and outflow of labelled material is in balance and in region **C** the outflow dominates the inflow. The corresponding regions for the $VLDL_2$ can also be defined.

Chapter 7

Application

We start this chapter with describing the implementation of the combined model in SAAMII and discuss the impact of the usage of population averages in some kinetic parameters. Then we summarise the two medical papers that are attached in the end of this thesis. These papers are focused on the medical results and do not include the detailed description of the model as presented here in this thesis.
We will also present the results of the non-steady-state model applied to a few subjects.

7.1 Implementation

The models were implemented in SAAMII as well as in Matlab. SAAMII is the a commonly used program in compartmental modelling, especially in biochemistry and biomedicine. The functionality is less general than that in Matlab but, at least for the steady-state modelling, it has sufficient capacity to handle a complex model. For the non-steady-state there are potential problems which only can be taken care of by some tricks.
The advantage of SAAMII is it's widespread acceptance in the field and its graphical interface which makes it easy to communicate the modelling to non-mathematicians. Furthermore it is accepted by editors of journals of medical research, which allows for simpler manuscripts for the non-mathematic reader.

7.1.1 Steady State Model

The steady state model in section 4.1.3 was implemented as two separate models as in figures 7.1 (apoB) and 7.2 (TG). For the apoB model the delay compartment (11) was a seven compartment linear chain delay (section 2.4) and the fractional distribution was selected so that the fraction of apoB going to compartment 5, $d(5,11)$, was an unknown parameter and $d(8,11) = 1 - d(5,11)$. Naturally $d(5,11)$ was constrained to be in $[0,1]$. The TG delay (compartment 22) was a five compartment linear delay. The fraction of the TG going to $VLDL_1$ and $VLDL_2$ was defined as in section 4.1.3. The compartments corresponding to $VLDL_1$ was 5, 6, and 7 (apoB) and 15, 16 and 17 (TG) and for $VLDL_2$ it was compartments 8, 9 and 10 (apoB) and 18, 19 and 20 (TG).
The plasma model was constrained by defining $k(3,4) = 0.1\ k(4,3)$ and $k(2,1) = k(1,2)$ as described in [13]. The plasma kinetics were constrained by letting $k(8,6) = k(6,5)$ and $k(0,10) = k(10,8)$, other constrains has also been used [13].

The TG model was constrained by defining the plasma glycerol transfer coefficients to be the population means used in [46], i.e. $k(0,13) = 19, k(12,13) = 12$ and $k(13,12) = 5$. The impact of the use of population means is discussed in section 7.1.3.

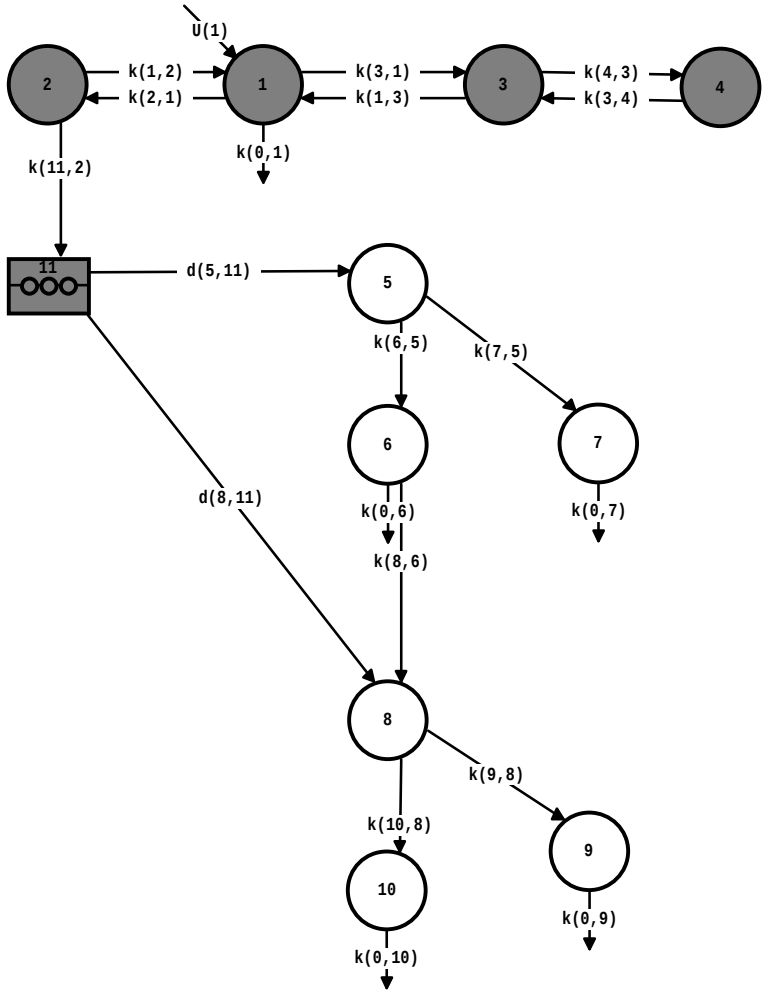

Figure 7.1: The apoB model, as implemented in SAAMII. The highlighted section (compartments 1, 2, 3, 4 and 11) is the free leucine and liver system. Constraints of the parameters are discussed in the text.

The transfer coefficients was defined as defined in section 4.1.3:

$$\begin{aligned}
k(0,15) &= (1-f_{6,5})k(6,5) + (1-f_{7,5})k(7,5)\\
k(0,16) &= k(0,6) + (1-f_{8,6})k(8,6)\\
k(0,17) &= k(0,7)\\
k(0,18) &= (1-f_{10,8})k(10,8) + (1-f_{9,8})k(9,8)\\
k(0,19) &= k(0,9)\\
k(0,20) &= k(0,10)\\
k(17,15) &= k(7,5)f_{7,5}\\
k(16,15) &= k(6,5)f_{6,5}\\
k(18,16) &= k(8,6)f_{8,6}\\
k(19,18) &= k(9,8)f_{9,8}\\
k(20,18) &= k(10,8)f_{10,8}\\
d(15,22) &= d(5,11)/(d(5,11) + (1-d(5,11))f_{8,6}f_{6,5})\\
d(18,22) &= 1-d(15,22)
\end{aligned}$$

The unknown parameters were: $k(0,1)$, $k(1,2)$, $k(1,3)$, $k(3,1)$, $k(4,3)$, $k(11,2)$, $d(5,11)$, $k(6,5)$, $k(7,5)$, $k(0,7)$, $k(10,8)$, $k(9,8)$, $k(0,9)$, the delay time for apoB, T_a, and the plasma leucine, PL. Moreover, for the TG model the unknown parameters were: $k(14,13)$, $k(14,21)$, $k(21,14)$, $k(22,14)$, $f(6,5)$, $f(7,5)$, $f(8,6)$, $f(9,8)$, $f(10,8)$, the delay time for TG, T_b, and the plasma glycerol, PG.
The $VLDL_1$ and $VLDL_2$ apoB pools were converted into leucine pools by multiplication of 0.12 (leucine is 12% of the apoB) and the TG pools were converted into glycerol pools by multiplying with 92/885 (the molecular weight of glycerol is 92 g/mol and the average molecular weight of TG is 885 g/mol).
The tracee experiment with constant inflow of material inflow into compartments 1 and 13 was solved as well as the tracer experiment with bolus injection of tracers into compartments 1 and 13. The solution to the system was assigned to fit the data by the following equations. The compartmental masse in compartment i is denoted Q_i for the tracee and q_i for the tracer.

$$\begin{aligned}
Q_5+Q_6+Q_7 &= \text{VLDL}_1\text{leucine mass}\\
\frac{q_5+q_6+q_7}{Q_5+Q_6+Q_7} &= \text{VLDL}_1\text{leucine enrichment}\\
Q_8+Q_9+Q_{10} &= \text{VLDL}_2\text{leucine mass}\\
\frac{q_8+q_9+q_{10}}{Q_8+Q_9+Q_{10}} &= \text{VLDL}_2\text{leucine enrichment}\\
Q_{15}+Q_{16}+Q_{17} &= \text{VLDL}_1\text{glycerol mass}\\
\frac{q_{15}+q_{16}+q_{17}}{Q_{15}+Q_{16}+Q_{17}} &= \text{VLDL}_1\text{glycerol enrichment}\\
Q_{18}+Q_{19}+Q_{20} &= \text{VLDL}_2\text{glycerol mass}\\
\frac{q_{18}+q_{19}+q_{20}}{Q_{18}+Q_{19}+Q_{20}} &= \text{VLDL}_2\text{glycerol enrichment}\\
\frac{q_1}{Q_1} &= \text{leucine plasma enrichment}\\
\frac{q_{13}}{Q_{13}} &= \text{glycerol plasma enrichment}
\end{aligned}$$

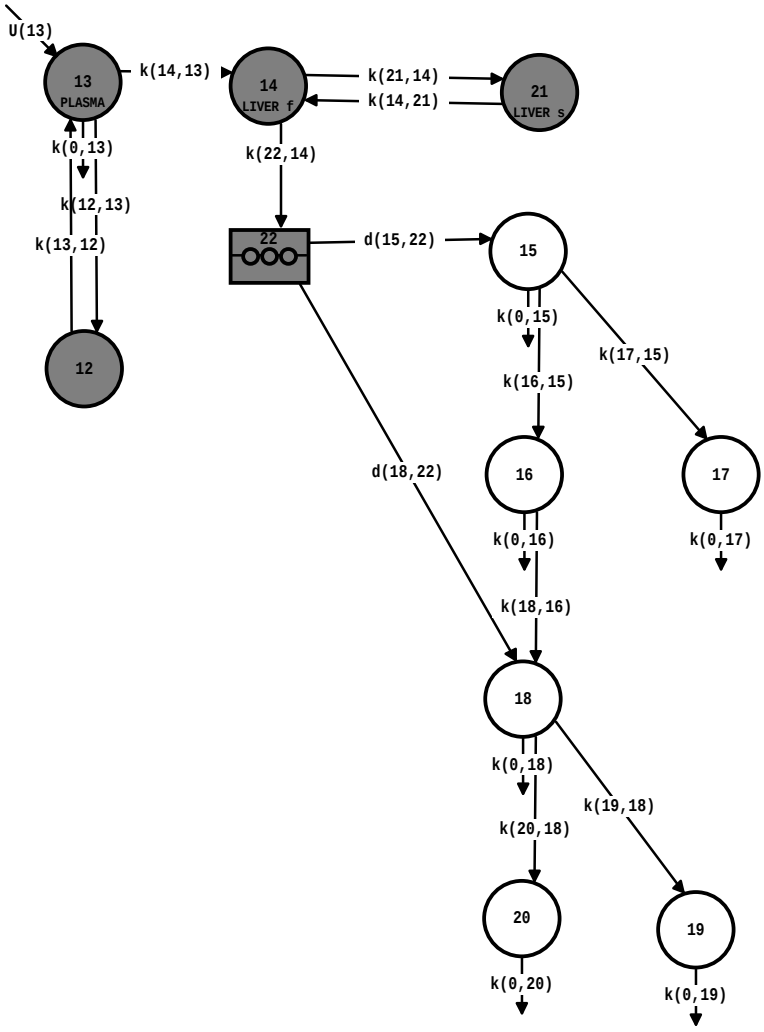

Figure 7.2: The triglyceride model as implemented in SAAMII. The transfer coefficients were constrained as described in the text. The highlighted section is the plasma glycerol subsystem (compartments 13 and 12), the glycerol to TG conversion (compartments 14 and 21) and the delay compartment 22.

Enrichments and masses were fitted with fractional standard deviational weights with a relation 1 (enrichments) to 10 (masses). The first measurements of the enrichments were taken relatively early. If no enrichment has entered the system then the measurements will measure the basal enrichment of the isotopes and due to small errors the estimated enrichments could appear negative (section 3 shows how the enrichments were calculated). Negative enrichments were disregarded.
Both model 1 and model 2 was implemented and the results were comparable. We believe that model 1 has a better description of the VLDL kinetics.

7.1.2 Data

Data was analysed as described in sections 3 and appendix A. Control and diabetes mellitus type-2 (DM2) subjects were compared using t-test, i.e. testing if the parameters and calculated variables came from the same population.

7.1.3 Impact of Population Averages

In most of the subjects the enrichment of plasma glycerol was not measured. We therefore used the population averages $k_{0,13} = 19$, $k_{12,13} = 12$ and $k_{13,12} = 5$, determined from a normal population in [26] and used in TG models in for instance [46]. In the rest of the subjects the plasma enrichment was measured and in those subjects we used both methods to estimate the parameters. In table 7.1 the estimated parameters for six subjects (three controls and three DM2 subjects) from the two methods are summarised.

	$VLDL_1$				$VLDL_2$			
	FCR[a]	FDCR[a]	FTR[a]	Prod[b]	FCR[a]	T. Prod[b]	Prod[b]	VLDL Prod[b]
subj. 1	10.760	7.689	3.071	38878	12.579	14377	3281	42159
PG	10.162	7.146	3.016	36722	12.230	13983	3085	39808
subj. 2	10.009	6.810	3.198	28946	12.658	13500	4249	33195
PG	10.049	7.078	2.971	29308	11.740	12631	3966	33274
subj. 3	3.367	1.583	1.784	17123	6.221	10574	1502	18625
PG	3.688	1.773	1.915	18757	6.696	11362	1623	20380
subj. 4	7.185	4.793	2.393	28545	8.968	12587	3082	31626
PG	7.879	5.057	2.822	31337	10.509	14757	3534	34871
subj. 5	11.546	9.425	2.121	40612	11.506	9872	2412	43024
PG	10.447	8.161	2.286	36866	12.081	10387	2321	39187
subj. 6	8.737	5.467	3.269	22954	14.179	10847	2257	25211
PG	8.226	5.155	3.071	21612	13.370	10227	2159	23771

Table 7.1: Comparison of results from model with parameters; First line, population averages, and; Second line, determined by plasma glycerol enrichment. [a] [day^{-1}], [b] [mg kg^{-1} day^{-1}]. $VLDL_2$ T. Prod. refers to total $VLDL_2$ production, i.e. direct production from the liver and transfer from $VLDL_1$. Direct $VLDL_2$ production is denoted $VLDL_2$ Prod. [a] [day^{-1}], [b] [mg kg^{-1} day^{-1}].

We found a quite good agreement in the results from the two implementations. Studying the difference between the estimated parameters in the two implementation in each subjects revealed no systematic difference. Neither did we observe any difference between control and DM2 subjects.
In the appended papers and the summary all numbers are from the model with population averages, since it not would make sense to mix results from different models.

7.1.4 Implementation of Tracer Loss

Using the theory described in section 4.4 we implemented the tracer loss mpe equation (4.19) instead of the regular mpe equation (3.2).
In the implementation we defined $f(i,p) = \binom{3}{i} p^i (1-p)^{3-i}$, $i = 0,1,2,3$ and $f(i,p) = 0$

and computed $P_{C_6H_6O_4}(i)$ for $i = 0,1,2,3$ and $P^U(i) = P_{C_6H_9O_4}(i)$ for $i = 0,1,2,3$ as in section 4.4. We define

$$P^T(3,p) = P_{C_6H_6O_4}(3)f(0,p) + P_{C_6H_6O_4}(2)f(1,p) + P_{C_6H_6O_4}(1)f(2,p) + P_{C_6H_6O_4}(0)f(3,p),$$
$$P^T(2,p) = P_{C_6H_6O_4}(2)f(0,p) + P_{C_6H_6O_4}(1)f(1,p) + P_{C_6H_6O_4}(0)f(2,p).$$

Define R_0^2 as $P^U(2)/P^U(0)$, i.e. the ratio of m/z 145+2 and m/z 145+0 peaks. In equation (4.19), we corrected the tracer to tracee ratio to form the tracer to (tracer + tracee) ratio. This is not necessary in the compartmental case since the tracer can be assumed to be part of the tracee system. Hence, we define the output function

$$S_k(t) = R_0^2\left(\frac{T_k(t_j)P^T(3) + \Phi_k P^Q(3)}{T_k(t_j)P^T(2) + \Phi_k P^Q(2)} - \frac{P^Q(3)}{P^Q(2)}\right).$$

For $\Phi_1 = Q_{15} + Q_{16} + Q_{17}$, $T_1(t) = q_{15}(t) + q_{16}(t) + q_{17}(t)$, $\Phi_2 = Q_{18} + Q_{19} + Q_{20}$ and $T_2(t) = q_{18}(t) + q_{19}(t) + q_{20}(t)$

The probability for loss of deuterium was first chosen to be $p = 0.05$, in the next step we allowed p to be determined by the optimiser.

	VLDL$_1$				VLDL$_2$			
	FCR^a	FDCR^a	FTR^a	Prod^b	FCR^a	T. Prod^b	Prod^b	VLDL Prod^b
Subj. 1	18.653	16.514	2.139	22865	10.937	4315	1694	24558
p=0.05	18.653	16.514	2.139	22856	10.937	4314	1693	24549
p=0.1073	18.652	16.512	2.140	22834	10.937	4313	1693	24527
Subj. 2	11.086	6.438	4.649	29159	21.144	15598	3371	32530
p=0.05	11.141	6.578	4.563	29298	20.747	15309	3309	32607
p=0.1199	10.968	6.668	4.301	28845	19.555	14429	3119	31963
Subj. 3	23.430	16.281	7.149	23321	18.863	10956	3840	27161
p=0.05	23.737	17.073	6.664	23626	17.583	10213	3580	27206
p=0.0000	23.443	16.315	7.128	23334	18.808	10925	3829	27163
Subj. 4	8.737	5.467	3.269	22954	14.179	10847	2257	25211
p=0.05	9.842	6.453	3.390	25858	14.698	11245	2340	28197
p=0.16	14.764	10.820	3.943	38728	17.114	13062	2718	41446
Subj. 5	3.367	1.583	1.784	17123	6.221	10574	1502	18625
p=0.05	3.496	1.685	1.811	17778	6.314	10734	1524	19302
p=0.1983	3.945	2.075	1.870	19896	6.555	10992	1561	21457
Subj. 6	16.668	11.596	5.072	44018	23.683	18773	5378	49396
p=0.05	16.759	11.740	5.019	44259	23.437	18577	5322	49581
p=0.1949	16.980	12.106	4.874	44321	22.767	17830	5108	49429

Table 7.2: The estimated parameters in six subjects. First line; Regular model. Second line; The tracer loss model with fixed $p = 0.05$. Third line; Tracer loss model with variable p. VLDL$_2$ T. Prod. refers to total VLDL$_2$ production, i.e. direct production from the liver and transfer from VLDL$_1$. Direct VLDL$_2$ production is denoted VLDL$_2$ Prod. ^{a} [day^{-1}], ^{b} [mg kg^{-1} day^{-1}].

In one subject (subject 4) the optimiser failed to find a optimum with variable parameter p. In the subjects where a good fit was achieved the difference between the regular model and the tracer loss (TL) model was quite good. Most importantly the FCR and production rates showed good agreement, the numbers for six subjects are presented in table 7.2. In [34] the

enrichments of the different isotopomers varied between the subjects, in some subjects the m+5 fragment was the dominant curve, whereas other fragment dominated in other subjects. This is reflected in our analysis by the different p values found to best fit the data.

Even though the numbers showed good agreement this is still a potential source of error. The best way to work around this would be to directly measure the m/z 145+3 and m/z 145+0 peaks. However, one can perhaps gain information about the esterification of glycerol in the liver by these experiments. For instance, if the m/z 145+3, m/z 145+2, m/z 145+1 and m/z 145 peaks were measured, then one could try to find the p that best fits the model to the three enrichment curves. For instance, hydrogen atoms at different places might have different probability of being replaced.

7.2 Presentation of some Modelled data

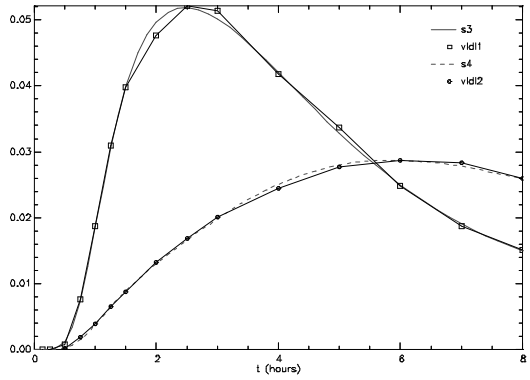

(a) Leucine enrichment curves. □ $VLDL_1$, and ∘ $VLDL_2$ measured data.

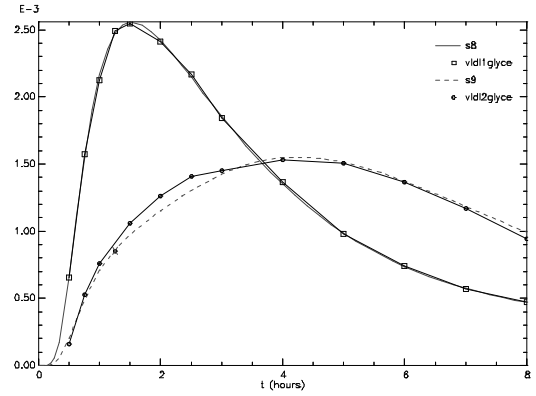

(b) Glycerol enrichment curves. □ $VLDL_1$, and ∘ $VLDL_2$ measured data.

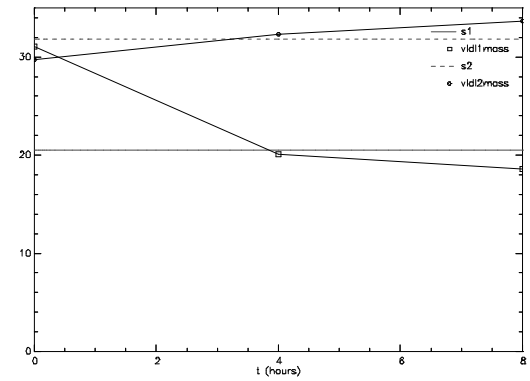

(c) Leucine pool sizes. □ $VLDL_1$, and ∘ $VLDL_2$ measured data.

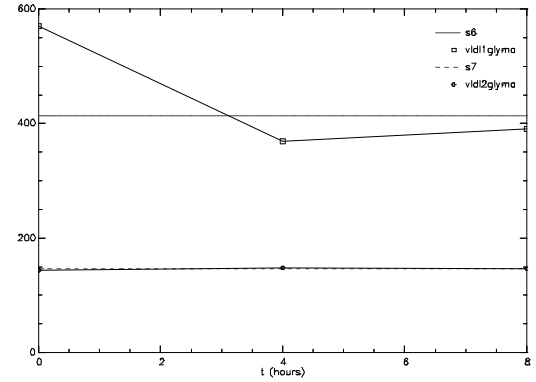

(d) Glycerol pool sizes. □ $VLDL_1$, and ∘ $VLDL_2$ measured data.

Figure 7.3: Enrichment curves for control subject 16. Larger figures are attached in the appendix.

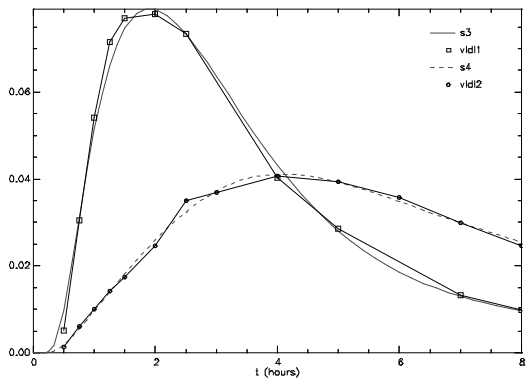

(a) Leucine enrichment curves. □ $VLDL_1$, and ∘ $VLDL_2$ measured data.

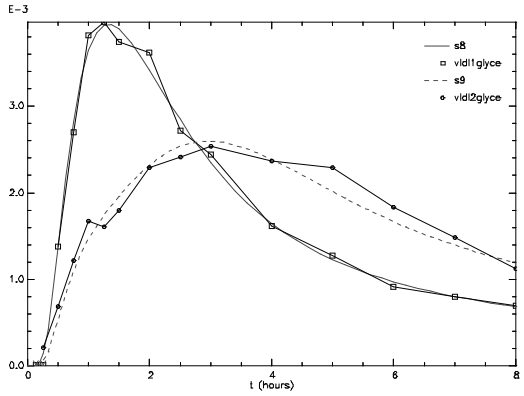

(b) Glycerol enrichment curves. □ $VLDL_1$, and ∘ $VLDL_2$ measured data.

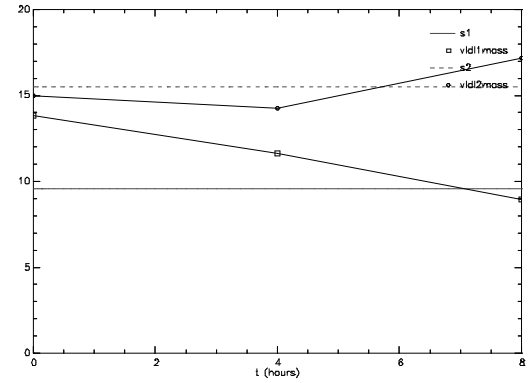

(c) Leucine pool sizes. □ $VLDL_1$, and ∘ $VLDL_2$ measured data.

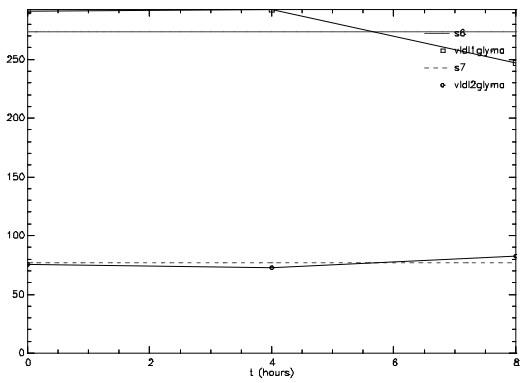

(d) Glycerol pool sizes. □ $VLDL_1$, and ∘ $VLDL_2$ measured data.

Figure 7.4: Enrichment curves for healthy control subject 17. Larger figures are attached in the appendix.

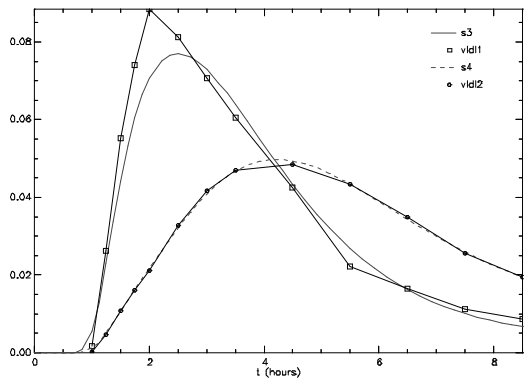

(a) Leucine enrichment curves. □ $VLDL_1$, and ∘ $VLDL_2$ measured data.

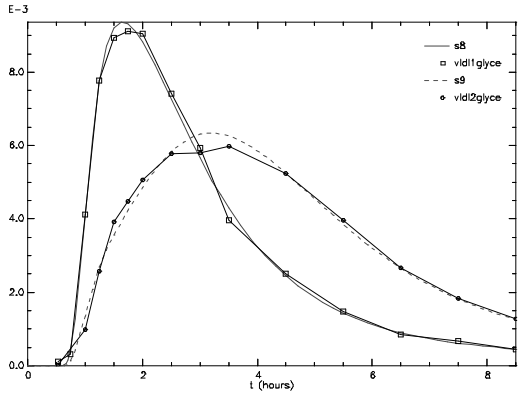

(b) Glycerol enrichment curves. □ $VLDL_1$, and ∘ $VLDL_2$ measured data.

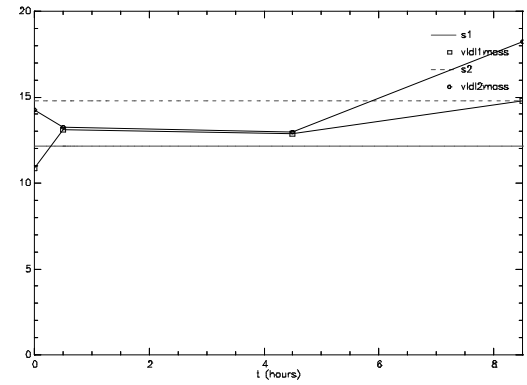

(c) Leucine pool sizes. □ $VLDL_1$, and ∘ $VLDL_2$ measured data.

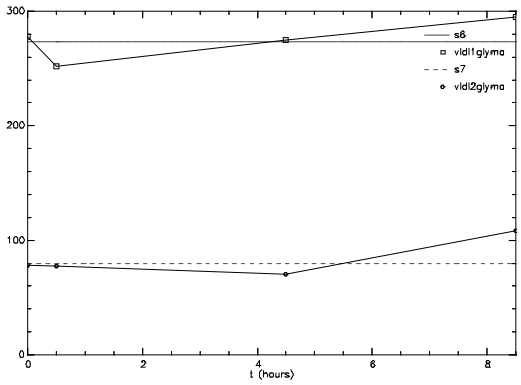

(d) Glycerol pool sizes. □ $VLDL_1$, and ∘ $VLDL_2$ measured data.

Figure 7.5: Enrichment curves for DM2 subject 10. Larger figures are attached in the appendix.

7.3 Summary of Paper I and II

The two papers appended to this thesis are written in a medical perspective. The first article presents the model and summarise its application to seventeen healthy control subjects. The second article covers the application of the model to the seventeen control subjects as well as to ten DM2 subjects. We here summarise the results from the second paper, without going to much into details.

	Control Subjects(n=17)		DM2 Subjects (n=10)	
	Mean ± SD	Range	Mean ± SD	Range
Age, [years]	49±9	25-59	54±9	38-67
Weight, [kg]	82±9	69-98	89±12	76-106
BMI, [kg m^{-2}]	26±2	22-30	28±5	23-35
Insulin, [mU L^{-1}]	6.5±3.1	2.8-15.0	9.8±3.8∗	6.0-16.0
Plasma glucose, [mg dL^{-1}]	105±11	87-130	173±40†	123-239
Hemoglobin A1c,			7.4±1.1	6,1-9.6
HOMA-IR	1.73±0.72	0.46-2.96	4.19±1.59†	2.21-6.84
TG, [mmol L^{-1}]	1.54±0.46	0.99-2.59	1.84±0.75	0.64-2.77
Chol, [mmol L^{-1}]	5.23±0.95	4.00-7.51	5.14±0.72	4.10-6.40
HDL, [mmol L^{-1}]	1.34±0.23	0.93-1.68	0.97±0.30‡	0.75-1.68
FFA, [μmol L^{-1}]	520±98	319-648	668±189∗	373-1075
ApoB, [mg dL^{-1}]	105±23	66-140	119±21	87-156

Table 7.3: Basal characteristics of control and DM2 subjects. $*P < 0.05$, $\dagger P < 0.001$, $\ddagger P < 0.01$ versus control subjects.

The basal characteristics of the subjects are summarised in table 7.3. As suspected the insulin, FFA and plasma glucose levels were significantly higher in the DM2 subjects and the HDL were significantly lower.
The particle composition (table 7.4) did not show any significant difference between control and DM2 subjects. The two groups were compared by testing the hypothesis that data from two groups of subjects were from the same population, the alternative hypothesis was that they have different means but the same variance.
Table 7.5 shows the mean and standard deviation of the estimated parameters for all the subjects.
Both the TG and the apoB $VLDL_1$ and $VLDL_2$ pools were higher in the DM2 subjects compared to the control group, which reflects the higher plasma TG levels. However, the apoB and TG pool variations were closely related (figure 7.6) and the TG to apoB ratio did not show any significant difference in neither $VLDL_1$ or $VLDL_2$. Together with the compositional data of CE, FC and PL this suggests that the particles are similar in size and composition in DM2 and control subjects.
There seems to be a shift in the distribution between $VLDL_1$ and $VLDL_2$ particles, i.e. there are relatively more $VLDL_1$ particles than $VLDL_2$ particles in DM2 subjects. Previous studies of VLDL size and composition have observed larger VLDL particles (higher TG to apoB ratio) in DM2 subjects. Our findings implies that is an effect of the shift of particle distribution.

	Particle Composition (% of Total)	
	Control Subjects (n=17)	DM2 Subjects (n=10)
$VLDL_1$		
TG	64.64±1.85	64.93±2.18
FC	5.43±0.39	5.15±0.76
CE	5.17±1.55	5.65±1.61
PL	16.26±1.01	15.70±0.65
Protein	8.49±0.72	8.57±0.70
ApoB	2.41±0.28	2.56±0.24
$VLDL_2$		
TG	41.47±3.13	41.60±3.94
FC	8.23±0.57	7.91±0.44
CE	15.82±3.21	16.17±3.40
PL	20.87±1.23	20.47±0.88
Total protein	13.61±1.03	13.85±0.88
ApoB	6.94±0.74	6.99±0.77

Table 7.4: The relative composition of the $VLDL_1$ and $VLDL_2$ particles. The total protein fraction includes apoB. FC indicates total free cholesterol; CE, cholesterol esters; PL, phospholipids.

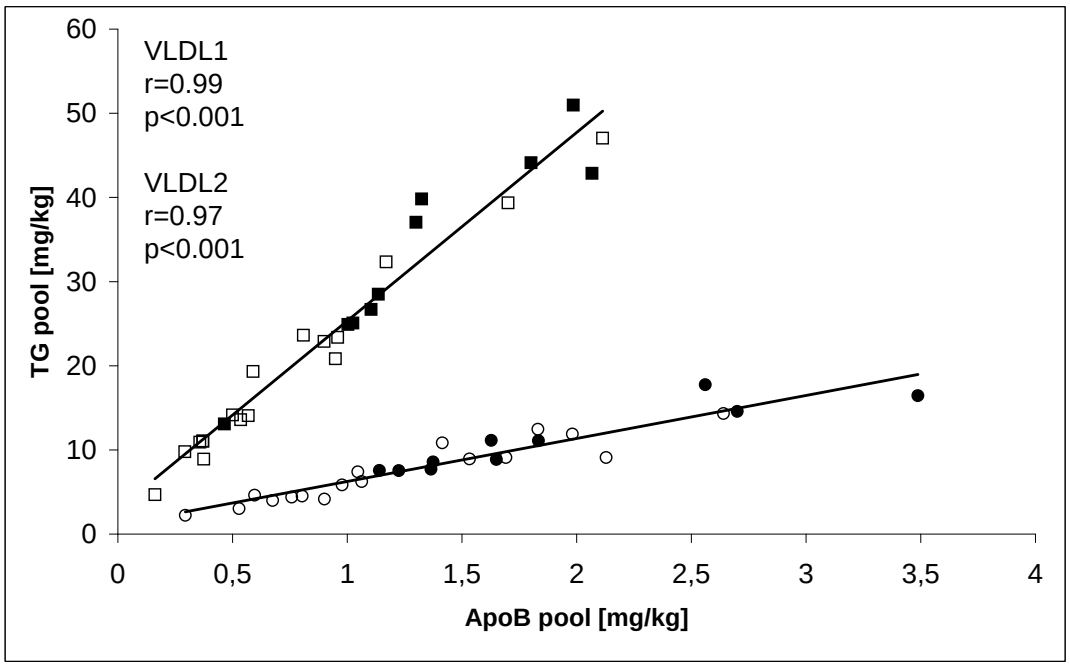

Figure 7.6: Correlation of the measured TG and apoB pools in $VLDL_1$ (upper curve) and $VLDL_2$ (lower curve). Black boxes (■) - DM2 subjects and white boxes (□) - control subjects.

	Control Subjects (n=17)		DM2 Subjects (n=10)	
	Mean ± SD	Range	Mean ± SD	Range
TG				
$VLDL_1$ FCR, [day^{-1}]	15.20±8.91	5.69-35.50	12.52±5.45	3.37-23.43
$VLDL_1$ FDCR, [day^{-1}]	11.47±8.62	4.15-33.01	8.98±4.05	1.58-16.28
$VLDL_1$ FTR, [day^{-1}]	3.73±1.84	1.53-8.62	3.54±1.60	1.78-7.15
$VLDL_1$ Prod, [mg kg^{-1} day^{-1}]	217.7±76.3	107.3-347.1	369.9±116.3∗	173.8-495.3
$VLDL_2$ FCR, [day^{-1}]	14.02±7.81	5.76-39.42	14.01±4.76	6.22-23.68
$VLDL_1$ to $VLDL_2$, [a]	61.16±36.77	20.91-145.6	102.6±17.62†	80.89-131.3
$VLDL_2$ Prod, [mg kg^{-1} day^{-1}]	27.24±11.56	9.53-51.76	33.41±12.24	15.24-51.22
Total FCR, [day^{-1}]	10.96±5.45	4.50-25.82	10.19±4.78	2.78-19.80
Total Prod, [g day^{-1}]	20.34±7.31	10.71-32.53	35.11±9.30∗	18.62-49.40
ApoB				
$VLDL_1$ FCR, [day^{-1}]	12.66±7.46	4.31-31.05	9.09±3.78	3.09-17.23
$VLDL_1$ FDCR, [day^{-1}]	5.32±6.28	0.00-23.28	2.61±2.29	0.00-5.88
$VLDL_1$ FTR, [day^{-1}]	7.34±3.44	2.08-13.54	6.47±4.06	2.89-16.93
$VLDL_1$ Prod, [mg kg^{-1} day^{-1}]	6.93±2.89	2.88-12.46	10.81±3.75†	6.22-16.52
$VLDL_2$ FCR, [day^{-1}]	5.95±2.74	2.12-12.34	5.52±2.09	2.62-8.92
$VLDL_1$ to $VLDL_2$, [a]	4.36±2.45	1.79-9.99	7.03±1.18†	5.82-9.54
$VLDL_2$ Prod, [mg kg^{-1} day^{-1}]	1.92±0.65	1.01-3.01	2.34±1.00	0.96-4.16
Total FCR, [day^{-1}]	8.23±4.34	2.94-18.03	6.38±2.15	2.30-9.50
Total Prod, [mg day^{-1}]	741.1±319.8	283.0-1321	1152±302.9†	707.4-1532
Pool Sizes				
TG $VLDL_1$ pool, [mg kg^{-1}]	19.2±11.5	4.68-47.0	33.3±11.5∗	13.1-51.0
TG $VLDL_2$ pool, [mg kg^{-1}]	7.24±3.62	2.24-14.3	11.12±3.85‡	7.54-17.8
ApoB $VLDL_1$ pool, [mg kg^{-1}]	0.75±0.52	0.16-2.11	1.32±0.50∗	0.46-2.07
ApoB $VLDL_2$ pool, [mg kg^{-1}]	1.23±0.65	0.29-2.64	1.90±0.77 ‡	1.14-3.49
TG to apoB ratios				
$VLDL_1$ TG to apoB pool	27.2±3.58	22.0-33.6	25.6±2.67	20.7-30.1
$VLDL_2$ TG to apoB pool	6.08±1.00	4.27-7.76	6.00±0.71	4.72-6.93
$VLDL_1$ TG to apoB Prod	33.4±8.44	19.7-49.4	34.7±6.64	28.0-49.9
$VLDL_2$ TG to apoB Prod	14.3±4.00	6.94-21.3	14.9±3.02	10.8-18.7

Table 7.5: Summary of estimated parameters from the model. Pool sizes are the average of the three measurements. The control and DM2 subjects were compared using t-test, to test for significant differences. $*P < 0.001$, $\dagger P < 0.01$, $\ddagger P < 0.05$. [a], [mg kg^{-1} day^{-1}].

7.3.1 Kinetic Parameters

The estimated $VLDL_1$ production rates of apoB and TG were significantly higher in the DM2 subjects than in the control group (figure 7.7). The $VLDL_2$ direct productions were comparable in the two groups.

The combined TG and apoB model allowed us to estimate the apoB to TG ratio of newly synthesised particles, i.e. the ratio of the production rates. We observed no significant difference in the TG to apoB ratio between the two groups of subjects, as seen in figure 7.7. This further

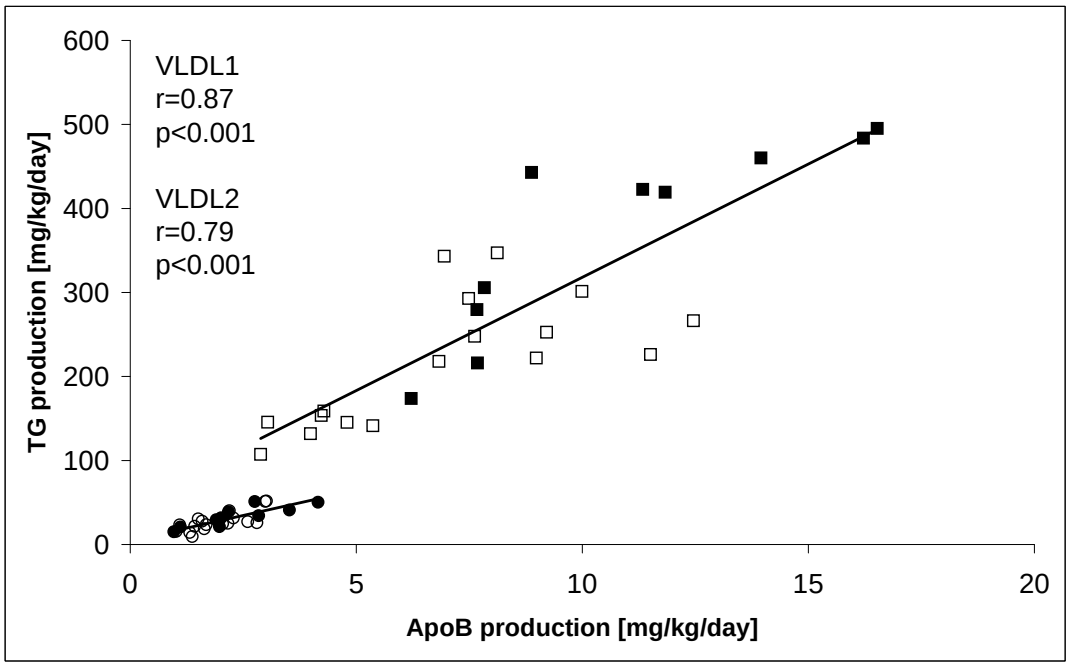

Figure 7.7: Correlation of the calculated TG and apoB production rates in $VLDL_1$ (upper curve) and $VLDL_2$ (lower curve). Black boxes (■) - DM2 subjects and white boxes (□) - control subjects.

strengthens the conclusion that there is little difference in composition and size. However, there still exists the possibility of different compositions of lipoproteins on the surface.
In these subjects we observed no significant difference in the clearance rates (FTR, FCR or FDCR), but an increased production of both $VLDL_1$ apoB and TG. We observed no significant difference in direct $VLDL_2$ production, however the increased $VLDL_1$ pools created an increased transfer of apoB and TG from $VLDL_1$ to $VLDL_2$. Hence the major difference lies in the increased $VLDL_1$ production which induces increased $VLDL_1$ pools and increased transfer to $VLDL_2$ and therefore the $VLDL_2$ pools are increased.

7.3.2 Determinants of Production and Clearance Rates

Both the $VLDL_1$ TG and apoB productions were correlated with plasma glucose, fasting insulin levels and HOMA-index (which is the product of plasma glucose and fasting insulin). The $VLDL_1$ TG production was also correlated to plasma FFA. The $VLDL_2$ productions was only correlated with the HOMA-index. Moreover, the FCRs were not correlate to neither plasma glucose, HOMA-index, fasting insulin or FFA. We also investigated the correlation in the groups of control and DM2 subjects but the strongest correlations was found in the combined group, since the range of the variables were much greater.

7.3.3 Determinants of Pool Sizes

In the combined group of subjects the $VLDL_1$ pool sizes were correlated to both the FCR (figure 7.8) and production rate (figure 7.9). The pool sizes were also correlated to insulin

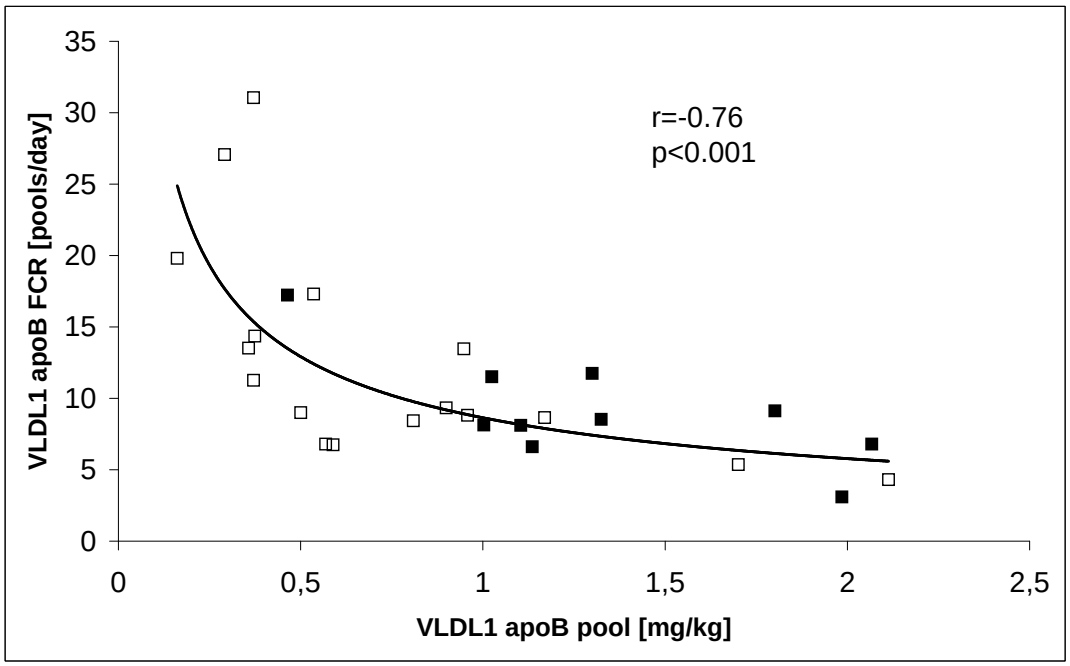

Figure 7.8: Correlation of apoB FCR and pool in $VLDL_1$. Black boxes (■) - DM2 subjects and white boxes (□) - control subjects.

and HOMA-IR, only the TG pool size was correlated to the plasma glucose. For $VLDL_2$ pool sizes similar correlations were observed.

7.3.4 Determinants of Plasma TG

In the combined group of subjects, both the apoB and TG FCR were negatively correlated to the plasma TG. For $VLDL_2$ apoB FCR showed a significant correlation, and a trend was observed for $VLDL_2$ TG FCR.

7.3.5 Discussion

This study shows that the overproduction of VLDL particles in DM2 is entirely accounted for by enhanced secretion of $VLDL_1$ particles due to increased production of both $VLDL_1$ apoB and TG. Diabetes per se did not influence the direct production of $VLDL_2$ apoB and TG. The production rates of $VLDL_1$ TG and apoB were closely related, as were the pool sizes of $VLDL_1$ TG and apoB (figure 7.7). Importantly, there was no significant difference in particle composition of either $VLDL_1$ or $VLDL_2$ between DM2 and control subjects, and the TG/apoB ratio of newly synthesised particles was very similar in both groups (table 7.4). These findings indicate that DM2 and insulin resistance are associated with excess hepatic production of $VLDL_1$ particles that are similar in size and composition to those of non-DM2 subjects.

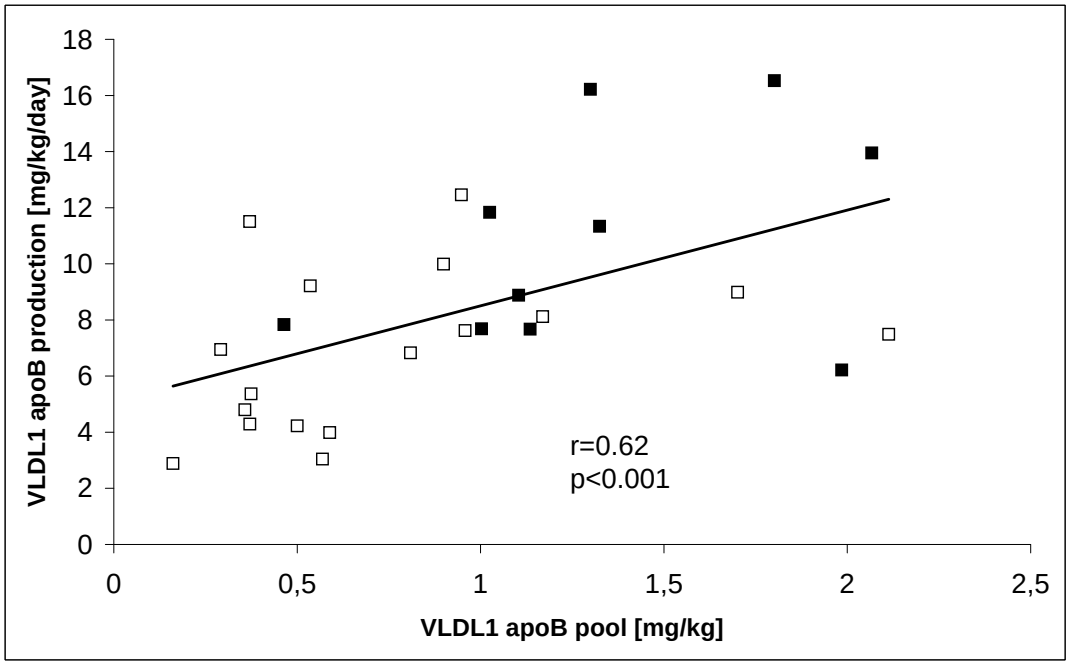

Figure 7.9: Correlation of apoB production rates and pool $VLDL_1$. Black boxes (■) - DM2 subjects and white boxes (□) - control subjects.

7.4 The Clamp Experiment

After the over night fast the production and clearance (lipolytic rate) are in balance, i.e. we assume that the experiment starts at a steady state. By analysing the measurement curves we can identify some characteristic behavior of the kinetics.

Plasma FFA In both healthy controls and subjects, the plasma FFA is remarkably decreased during the first 30 to 60 minutes. The concentration drops to $20 - 40\%$ of the initial value. The decrease was somewhat slower in DM2 subjects, although the total decrease was similar in both cases. Figure 7.12(a).

Drastic drop in pool sizes In several subjects there was a drastic drop in $VLDL_2$ within the first 30 minutes of the experiment, figure 7.10(a).

Overall drop of $VLDL_1$ pool sizes In most subjects we observed an decrease of $VLDL_1$ pool sizes. Figures 7.10(a), 7.10(c) and 7.10(b).

$VLDL_2$ pools The $VLDL_2$ pools behaved differently and in some subjects followed the $VLDL_1$ pools (figure 7.10(b)), in other subjects the $VLDL_2$ pools actually increased during the experiment (figure 7.10(c)).

The concentration of plasma FFA flattens out after 60 minutes and is fairly constant thereafter. It is not known whether plasma FFA concentration is a driving force of $VLDL_1$ (and $VLDL_2$) production, however the availability of FFA decreases and the lack of substrate could be a factor that down-regulates $VLDL_1$ and $VLDL_2$ production.
The decrease of $VLDL_1$ apoB and TG pools could come from either a decrease of $VLDL_1$ production, an increase of the removal rate or a combination of these two factors:

1. Decreased production of $VLDL_1$ particles would lower the $VLDL_1$ pool and consequently lower the absolute transfer to $VLDL_2$, which leads to lowering the $VLDL_2$ pools.

2. Increased direct removal of $VLDL_1$ particles would decrease the $VLDL_1$ pool, and induce a lowering of the $VLDL_2$ pools.

3. Increased transfer rate from $VLDL_1$ to $VLDL_2$ would lower the $VLDL_1$ pool and, initially, increase the $VLDL_2$ pool. But as the $VLDL_1$ pools shrinks the absolute transfer from $VLDL_1$ to $VLDL_2$ decrease and the $VLDL_2$ pools decrease as well.

The most surprising observation was the rapid removal of $VLDL_2$ particles in some subjects. This was surprisingly fast and happened within 30 minutes. To study the exact behavior one would need to sample the pool sizes more frequently than has been done in the experiments described here.

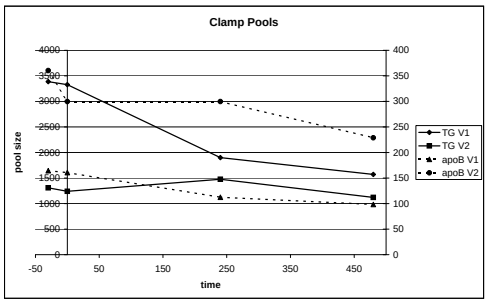

(a) Here there is a fast initial drop of $VLDL_2$ pools, most pronounced for apoB. The $VLDL_1$ pools decay slowly.

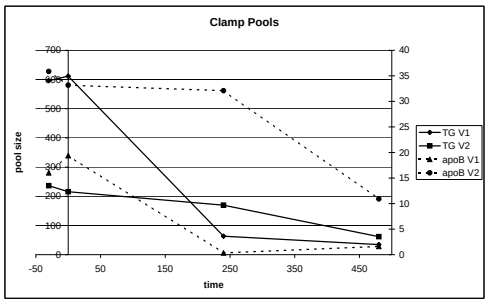

(b) The pools of TG and apoB. In this particular subject the concentrations of $VLDL_1$ fell drastically, where as the falls of $VLDL_2$ were slower.

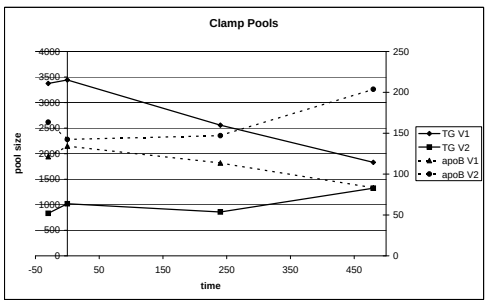

(c) The TG and apoB pools. Here the $VLDL_1$ pools decrease but the $VLDL_2$ actually increase.

Figure 7.10: TG and apoB pool sizes from the basal and clamp studies. Data from three subjects.

In figures 7.11 and 7.12 the measurements from both the basal and the clamp study are presented. One clearly sees that the $VLDL_1$ apoB and TG pools are decreasing during the study (figures 7.11(a) and 7.11(b)). Moreover, the enrichments of both apoB and TG were lower in both $VLDL_1$ and $VLDL_2$ in the clamp study (figures 7.11(c) and 7.11(d)). There is a difference in the TG to apoB ratio between the two studies , but the ratios are almost constant during the experiments (figure 7.12(b)).

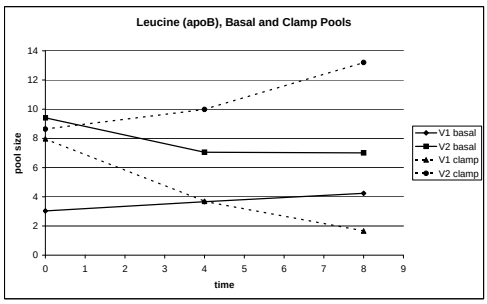

(a) The leucine pools in $VLDL_1$ and $VLDL_2$ in both the clamp and basal studies. In the clamp study there is a clear drop in the $VLDL_1$ pool and an increase of the $VLDL_2$ pool.

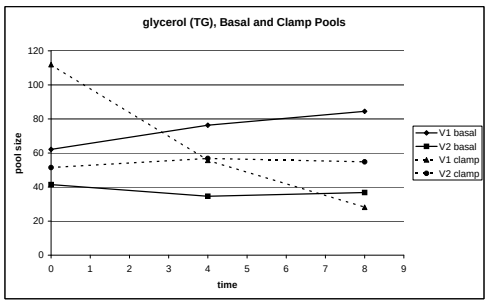

(b) The basal and clamp glycerol pools for $VLDL_1$ and $VLDL_2$. As for apoB there is a clear decrease of the $VLDL_1$ pool in the clamp study.

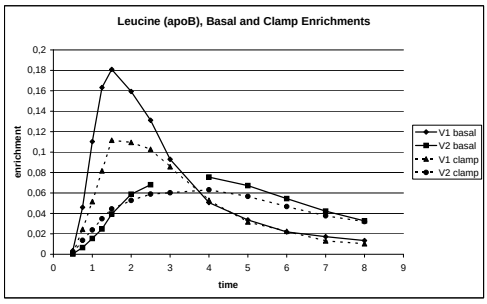

(c) The apoB enrichment for the same subject. In the clamp study the maximal apoB enrichment is less than for the basal study.

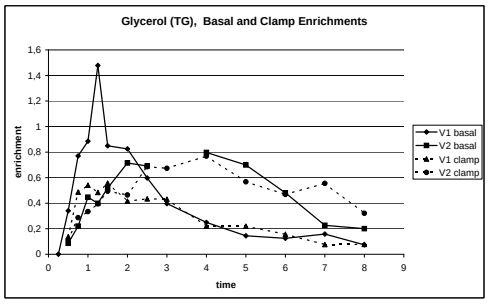

(d) As for the apoB, the TG enrichment was lower in clamp study than in the basal study.

Figure 7.11: Comparison of basal and clamp measurements for one subjects. The leucine pool is 0.1212 % of the apoB pool and the glycerol pool is 92/885 times the TG pool.

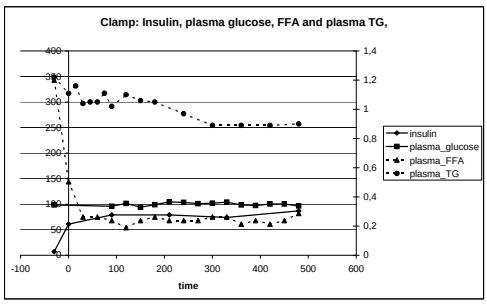

(a) The concentration of FFA decreases rapidly during the first hour of the experiment. The insulin is given with an instant injection followed by a constant infusion, and the concentration is fairly constant during the experimental time. Plasma glucose levels are kept constant by giving glucose intravenously. The total plasma TG level (right axis) is decreasing.

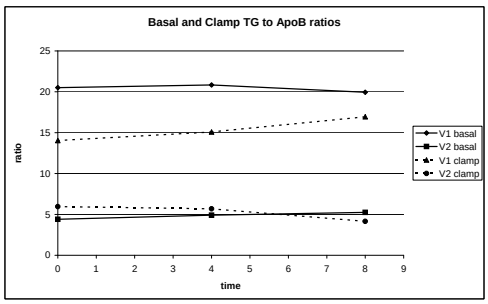

(b) The TG to apoB ratios of the $VLDL_1$ and $VLDL_2$ pools in the basal and clamp studies

Figure 7.12: Measurements for one subjects.

7.4.1 Implementation of Time Dependent Model

The time dependent, non-steady state model was implemented as described in section 4.2.3. We tried different approaches on how to introduce the time dependency as discussed in section 4.2.
It was difficult to find an explanation, valid for all subjects, for the variation of the kinetics during the clamp. In most subjects only suppression of $VLDL_1$ production was enough to explain the variation in the apoB pools and good agreement with measured data was achieved. However for the TG it was not always enough to only vary the $VLDL_1$ production.

We here present two subjects, one where a satisfactory fit was achieved and one where a typical under estimation of $VLDL_2$ enrichments was observed. This further discussed in the next chapter.

Subject 1

In this subject it was sufficient to introduce the time dependency only on VLDL_1 production. This was done by a piecewise linear function f defined as

$$f(t) = \begin{cases} 1 & t \leq 20 \\ 1 - a(t-20)/4.5 & 20 < t \leq 24.5 \\ (1-a)(1-b(t-24.5)/4) & 24.5 < t \leq 28.5. \end{cases} \tag{7.1}$$

We then defined $d_5^a(t) = d_{5,0}^a f(t)$.

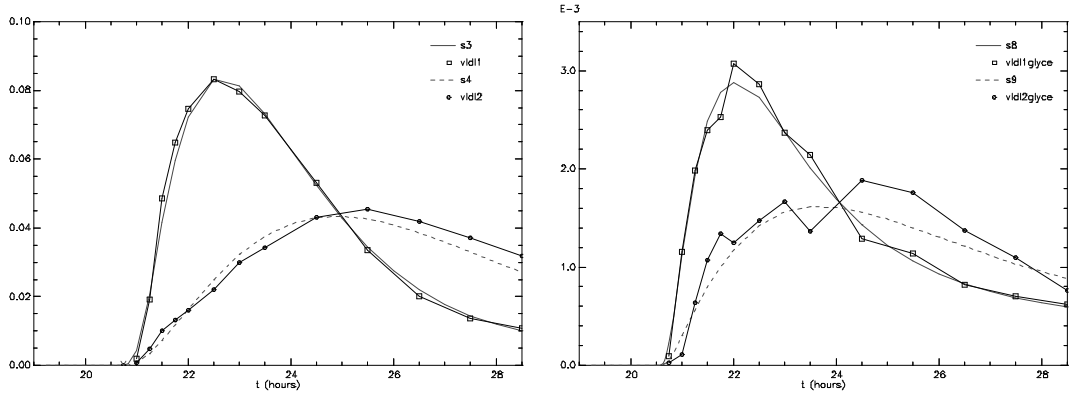

(a) The fit to the apoB enrichment curve.

(b) TG enrichment curves.

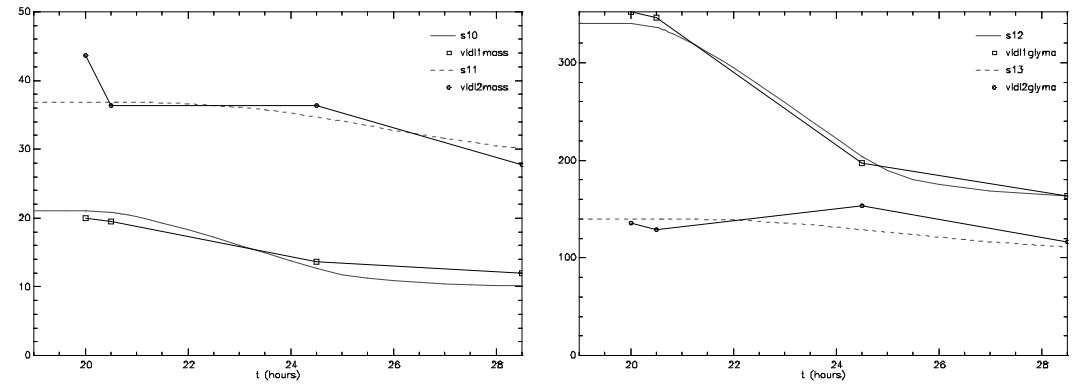

(c) The fit to the decaying apoB curves.

(d) The fit to the decaying TG curves.

Figure 7.13: Measured enrichments and pools and solutions to the clamp model. Subject 1.

Subject 2

In a majority of the subjects the $VLDL_2$ TG enrichment curve was under-estimated, or the $VLDL_1$ curve over-estimated. Comparing the enrichment curves for the basal and clamp experiments we can conclude that in subjects with large response in the pool measurements the maximal enrichments were lower in the clamp than in the basal study, see figures 7.11(d) and 7.11(c). Moreover, the $VLDL_2$ TG enrichment was relatively larger than that of $VLDL_1$, as in figure 7.11(d). In subject 2, we used the same time dependence as in subject one, i.e. a piecewise linear variation of $VLDL_1$ productions.

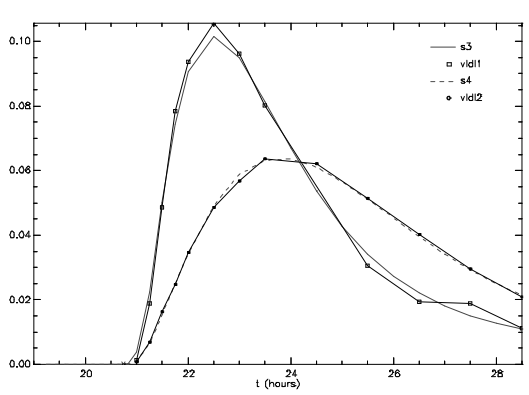

(a) The fit to the apoB enrichment curve.

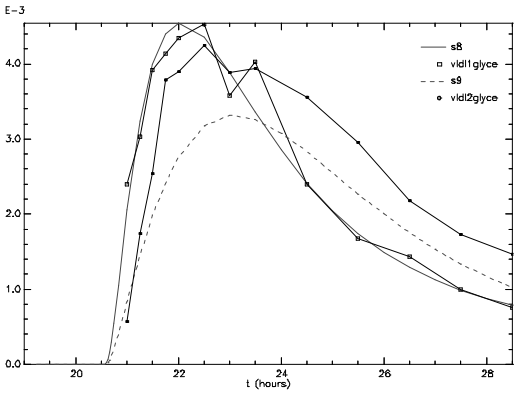

(b) TG enrichment curves.

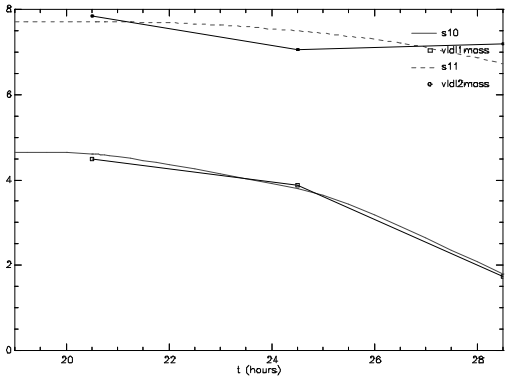

(c) The fit to the decaying apoB curves.

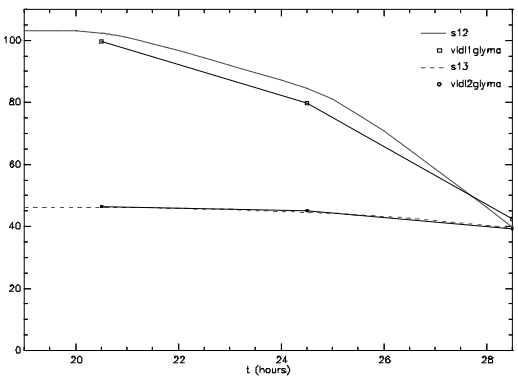

(d) The fit to the decaying TG curves.

Figure 7.14: Measured enrichments and pools and solutions to the clamp model. Subject 2.

Chapter 8

Discussion and Future Directions

The model presented in this thesis has proven to give a good description of the $VLDL_1$ and $VLDL_2$ metabolism, at least for healthy control and DM2 subjects and in a steady-state situation. It still has to be investigated if it is applicable to subjects with more severe diabetes and other lipid disorders.

8.1 Tracers

Here leucine has been used as tracer for apoB and glycerol has been used as tracer for TG. We see no reason for using other tracers than leucine for apoB. However, for glycerol the protocol for measurement of enrichment (section 7.1.4) has some drawbacks as discussed in section 4.4.

8.1.1 1,1,2,3,3 -D_5 glycerol

In the paper by Patterson et. al. [34] a method measuring the whole glycerol fragment was used and all the peaks m/z m+0, m+1, m+2, m+3, m+4 and m+5 were measured (recall that m+j denotes the m/z of a molecule with j labels, m+0 is the unlabelled molecule). In [34] it is pointed out that in some subjects, the enrichment m+5/m+0 was in fact less than that of m+1 and m+2 vs m+0.
In our analysis we assumed that the removed deuterium atom was replaced by a hydrogen atom with mass 1. The removed deuterium could in fact be replaced by a new deuterium atom (with probability $p_{DD} \geq 0.000115$, table 3.1[1]) but this could be included in the probability of being replaced.
Moreover, we assumed all hydrogen atoms could be replaced with the same probability. It might be the case that the atoms at carbon 1 and 3 are replaced with a different probability than that on carbon 2. At least the hydrogen atoms at carbon 1 and 3 can be replaced.
It appears as the transformation of the glycerol molecule occur prior the recruitment of glycerol to form TG that is incorporated into VLDL [34], hence the effect on the modelling should be small.

[1] It is possible that the local concentration of deuterium atoms is increased.

8.1.2 Other Tracers for TG-kinetics.

TG kinetics has been estimated with radio-active tracers, such as 2-^{3}H- and ^{14}C, as well as stable isotopes such as 1,1,2,3,3 -D_5 glycerol used here. There are also methods with labelled fatty acids. Fatty acids (FA) recycle more than glycerol, and therefore this has to be accounted for in the modelling.

8.2 Extending the Model

The model, as presented in this thesis, only includes TG and apoB and does only model the $VLDL_1$ and $VLDL_2$ particles. In this section we discuss extension of the model.

8.2.1 Extending the Density Range

In the model we have only included $VLDL_1$ and $VLDL_2$ but the technique with coupled transfer rates is readily applicable to include the whole density range, i.e. the intermediate- and low density lipoproteins (IDL and LDL).
Including IDL would make it possible to differentiate between the fractional transfer rate (FTR) and the fractional direct catabolic rate (FDCR) from $VLDL_2$, these are now combined into the FCR. If IDL and LDL were included, then the sampling time has to be extended since the tracer enrichment curves peak after 8 hours.

8.2.2 Adding More Layers

In the proposed model we can interpret the apoB model as the underlying model and the added TG model, which is coupled by the fractional transfer coefficients, as a second layer on the model. It would of course be possible to also include other components into the model. In theory it would be possible to include the cholesterol esters (CE) but also the phospholipids and free cholesterol in the shell of the particle. We here briefly describe how CE could be incorporated into the model.

The current analysis is much based on the TG to apoB ratio. The core also consists of CE and to get a better description of metabolism it would be appealing to also label the CE. In the early stages of the lipoprotein metabolism the CE content is preserved but at the later stages the CE content is altered by the cholesterol ester transfer protein (CETP). In fact, a quantitative measure of the CE kinetics could be estimated without introducing any new tracers, since the CE to apoB ratio is preserved if no CE is lost.
A CE layer can be implemented as the TG model. The plasma kinetics for the selected tracer has to be modelled separately, just as the glycerol and leucine sub-systems.

8.2.3 Separation of Pathways

We have not at all taken into account a fact that is of great importance in cardiovascular disease (CVD) and that is the formation of small, dense LDL. As briefly mentioned in the section 1.2 the LDL exists in different pools. These pools arise from different sources, i.e. particles secreted from the liver as $VLDL_1$ has a different fate than $VLDL_2$ particles secreted directly from the liver.
In a study by Packard et. al. [33], $VLDL_1$ and $VLDL_2$ particles were separated from plasma

and labelled with Na[^{131}I] and Na[^{125}I] respectively. The labelled lipoproteins were injected 3 days after the plasma donation and blood samples were collected for 14 hours and at 24 hours and then daily.
By labelling $VLDL_1$ and $VLDL_2$ with different labels it was possible to see that $VLDL_1$ and $VLDL_2$ followed different pathways. ^{125}I labelled $VLDL_2$ particles included particles both formed by $VLDL_1$ and secreted from the liver. Since $VLDL_1$ was labelled with a different label it was possible to determine the kinetics of $VLDL_1$ and their remnants. A fraction of the ^{125}I labelled $VLDL_2$ particles was then modelled to follow the $VLDL_1$ pathway whereas the rest followed a separated pathway. The LDL particles that is formed from the different pathways are in metabolically distinct pools.

This raises the question; *What is the difference in $VLDL_2$ formed from $VLDL_1$ and $VLDL_2$ secreted directly from the liver?*
These particles are in the same density range, but they still have some different characteristics that makes them behave differently. We have already briefly mentioned possible causes one of being structural ageing (section 5).

The reason for not taking separated pathways into account is that it difficult to determine the kinetic differences without the individual labelling. It could be that the kinetics are so similar at the $VLDL_1$ and $VLDL_2$ stage so that it actually can be modelled with the same subsystems. It could, however, be possible to separate the pathways if the CE is labelled as well.
If the CE to apoB ratio is different in the $VLDL_1$ and $VLDL_2$ particles produced from the liver, then the $VLDL_2$ formed from $VLDL_1$ and native $VLDL_2$ would have different CE to apoB ratio. The CE to apoB ratio in the $VLDL_1$ and $VLDL_2$ formed from $VLDL_1$ would then be identical and can be determined from the $VLDL_1$ pools.

8.3 Stochastic Modelling and Particle Density

In section 5 we showed a relationship between a discrete stochastic model and compartmental modelling. There is a relation between the continuous stochastic model (figure 5.1) and a continuous model of the particle density. We consider a irreversible catenary system.
Let $f(m,t)$ be the particle density with mass m at time t. Then

$$\int_{m_1}^{m_2} f(m,t)dm,$$

is the number of particles in the mass interval $m_1 < m < m_2$ at time t.
Let $S(m,t)$ be the number of particles secreted with mass m at time t and define $k(m_1,m_2,t)$ as the fraction of particles with mass m_2 that is transferred to mass m_1 at time t. We then have the following equation that describes the evolution of the particle density.

$$\frac{\partial f(m,t)}{\partial t} = \int_m^\infty k(m,s)f(s,t)ds - \int_0^m k(s,m)ds f(m,t) + S(m,t).$$

The change of particle density at mass m is the the sum of all particles entering from the mass range *above*, i.e. having higher mass, and the sum of all losses to density ranges *below*, i.e. having lower. The compartmental formulation is a special case where f is discrete.

Introducing metabolic different particles, i.e. the particles in compartments 7 and 9 in the compartmental model, could be easily done by introducing a discrete parameter.

The inverse problem, which corresponds to identifying parameters in the compartmental model, is then to determine k from measurements.

8.4 Discussion on the Time Dependent Model

Introducing time-dependency in the model gives more unknown parameters, this can make some parameters unidentifiable. However, in the time dependent case there is more information in the pool size measurements than in the steady state case. In the steady state case, the four measurements only determines the constant pool size, whereas in the time dependent case the four measurements determines a varying pool size.
It still remains to be investigated which parameters are preserved between the basal and clamp models. Some parameters, or relation between parameters, from the basal modelling can perhaps be used in the clamp modelling. This would improve the performance of the clamp modelling since the number of unknown is reduced.

As mentioned in the implementation section in the previous chapter, the $VLDL_2$ TG enrichment was typically under-estimated or the TG $VLDL_1$ enrichment was over-estimated. This goes hand in hand with the fact that the $VLDL_2$ enrichment was high, in relation to the $VLDL_1$ enrichment, in some cases even greater then the $VLDL_1$ enrichment. This was never observed in the basal enrichments curves.
A possible explanation to this behavior is that the recruitment of TG to $VLDL_1$ and $VLDL_2$ partly are from different pools, i.e that pre-VLDL particles are formed with TG from one pool, and the addition of extra TG to form $VLDL_1$ particles is from another pool. Under normal circumstances these pools interact. In [46] the hepatic TG pools were implemented as a *fast* and a *slow* pathway that both produced VLDL particles (no subdivision into $VLDL_1$ and $VLDL_2$). Such implementation could be applicable to $VLDL_1$ and $VLDL_2$ as well, but most likely the interaction of the pools has to be determined by new experiments.

Appendix A

Methods

A.1 ApoB and TG turnover protocol

All subjects were admitted at 7:30 a.m. to the metabolic ward of the Helsinki University Central Hospital after a 12-h overnight fast. An indwelling cannula was inserted into an antecubital vein for infusions. A second cannula was inserted retrogradely into a heated hand vein to obtain arterialised venous blood for sampling. A saline infusion was started. Thirty minutes later, leucine (5,5,5-D^3), 7 mg/kg body weight (bw), and glycerol (1,1,2,3,3-D^5), 500 mg (Isotec, Miamisburg, OH), were injected as a bolus. For measurement of free $^2H_3$-leucine concentration in plasma, blood samples were taken before the tracer injection and at 2, 4, 6, 8, 10, 12, 15, 20, 30, and 45 min and 1, 2, 3, 4, 6, and 8 h. For measurement of $^2H_3$-leucine and $^2H_5$-glycerol in VLDL1 and VLDL2, blood samples were taken before the injection of tracers and at 15, 30, 45, 60, 75, 90, 120, and 150 min and 3, 4, 5, 6, 7, and 8 h. In some subjects, additional samples were taken at 8 minutes. The particle composition and apoB mass of the $VLDL_1$ and $VLDL_2$ fractions were determined 30 min before and 0, 4, and 8 h after the injection. The subjects continued to fast until 5 p.m., when the last blood sample was taken.

A.2 Isolation of lipoproteins

$VLDL_1$ and $VLDL_2$ were isolated from 8.4 ml of plasma as described [24]. The apoB and TG pool sizes were analysed from samples obtained at 0, 4, and 8 h and prepared as described [24]. Pool sizes for apoB and TG were calculated as the product of plasma volume (4.5% of bw) and the plasma concentration of apoB and TG in $VLDL_1$ and $VLDL_2$. The leucine content of the apoB pool was calculated from the apoB amino acid residue composition. The glycerol content was calculated from the TG concentration using a molecular weight of 885 g/mol for TG and 92 g/mol for glycerol and assuming that one mole of TG equals one mole of glycerol.

A.3 Biochemical analyses

TG and cholesterol concentrations in total plasma and in all lipoprotein fractions were determined by automated enzymatic methods (Cobas Mira analyser, Hoffman-La Roche, Basel, Switzerland). ApoB was analysed in the plasma lipoprotein fractions as described [31]. Serum

glucose, insulin, free fatty acids, and alanine transaminase were analysed as described [42]. Protein concentrations in lipoprotein fractions were measured by the method of Kashyap et al. [21].

A.4 Determination of leucine enrichment in apoB

The samples were precipitated with isopropanol, delipidated with ethanol-diethyl ether, dried, and hydrolysed with 6 M HCl at 110C for 22-24 h [24]. The samples were then prepared for analysis of leucine enrichment [16], and the $^2H_3$-leucine enrichments in protein hydrolysates and plasma amino acids were performed as described [13]. Enrichments were determined by gas chromatography mass spectrometry (GC/MS) with a quadrupole GC/SM instrument (MD 800, Fisons, Manchester, UK).

A.5 Determination of glycerol enrichment in TG

The samples were precipitated with isopropanol and delipidated twice with ethanol-diethyl ether as described [16]. The supernatants were combined, and the volume was increased to 20 ml with isopropanol. To remove phospholipids, 2 g of activated zeolite (product no. 96096, Fluka Biochemika, Buchs, Switzerland) was added to each tube and mixed for 20 min. After centrifugation, the supernatants were evaporated under N2 at 80C. Isopropanol (1 ml) was added to each tube, transferred into a 1.5 ml vial, and dried on a heating block at 80C. The glycerol samples were stored at -80C. The amount of diacylglycerol and monoacylglycerols not extracted in the supernatant was not determined. This has been reported to be a minor contaminant, accounting for 2-10% of the total plasma triglyceride [44]. Immediately before analysis, the glycerol extracts were saponified with 250 ml of 2% KOH in ethanol, incubated at 60C for 2 h, and dried under N2 at 70C for 2 h.
In three subjects, glycerol was isolated as described by Patterson et al. [35]. Briefly, plasma proteins were precipitated with ice-cold acetone, equal volumes of hexane and water were added to the supernatant, and the upper phase (hexane) was dried in a centrifugal evaporator.
Glycerol was derivatised to its 1,2,3 triacetate ester by adding equal volumes of pyridine and acetic anhydride [6]. Enrichments were determined with a quadrupole GC/MS instrument (Trio-1000, Fisons, Manchester, UK) under electron ionisation conditions within 24 h after saponification. Samples (1-3 l) were injected automatically into a 30 m x 0.25 mm (I.D.) x 0.25 mm DB5MS capillary column fitted with a 2-m plain silica guard column (J&W, Folsom, CA), which was run isothermally at 195C, using a split ratio of 1:50, helium as the carrier gas, and a head pressure of 70 kPa (10 psi). The glycerol derivative eluted at approximately 3.5 min. Under these conditions, the derivative fragments between carbons 1 and 2 or 2 and 3 of the glycerol backbone resulted in the formation of two symmetrical fragments of m/z 145 and two symmetrical fragments of m/z 73 for the unlabelled derivative [6].
The penta-deuterated derivative formed a tri-deuterated fragment at m/z 148 and a bi-deuterated fragment at m/z 75. Monitoring the larger fragment (m/z 148) allowed measurements to be made against a very low natural background, resulting in greater sensitivity than monitoring the smaller ion fragment. Ion mass fragments at m/z 147 and 148 were monitored in the selective ion recording mode. Ion peaks areas were integrated and quantified in arbitrary units with the LabBase GC/MS data management system (Fisons).

To calculate isotope enrichments, the average value of the m/z 147:m/z 145 ratio was determined in the baseline sample. This value was multiplied by the m/z 148:m/z 147 ratio, and the resulting m/z 148:m/z 145 values were expressed as molar percent excess (mpe) by the following formula:

$$\text{mpe} = \frac{IR(t) - IR(b)}{1 + (IR(t) - IR(b))} 100 \tag{A.1}$$

where $IR(t)$ is the m/z 148:m/z 145 peak area ratio for the enriched sample at time t and $IR(b)$ is the equivalent ratio for the baseline (0 h) sample.
Monitoring of the m+3 and m+2 peaks permitted greater loading of the GC/MS and enhanced the ability to detect low enrichments with good precision, as we do for leucine enrichment in apoB [13]. Standards with enrichments of 0.00-1.00 mpe were included at the beginning and end of each batch of samples and used to correct the calculated mpe values with the calculated recovery rate of the standards. Care was taken to ensure similar total ion counts in the standards and all samples.

Appendix B

Figures

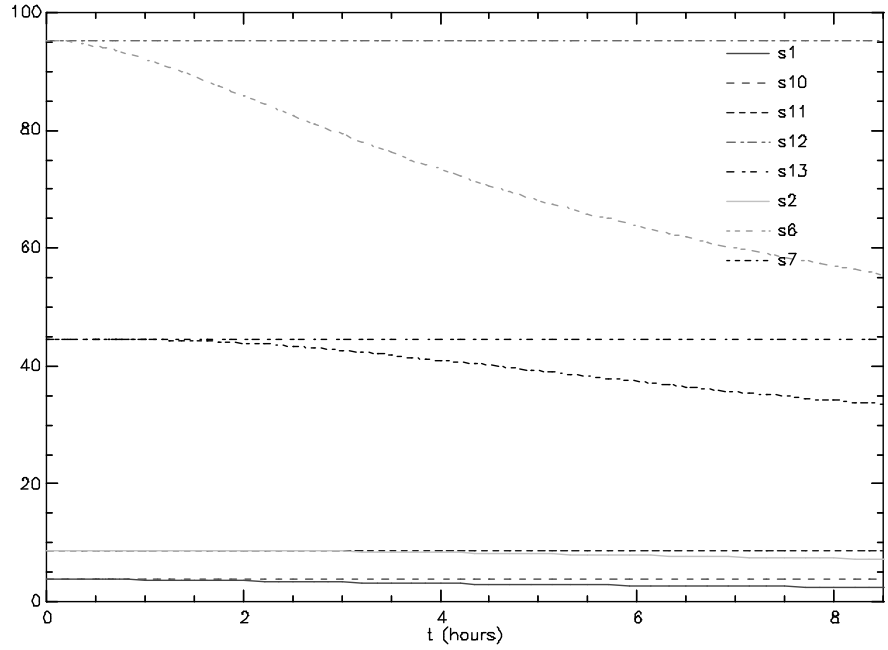

Figure B.1: 4.7(a). Pools: s1/s10 - apoB $VLDL_1$, s2/s11 - apoB $VLDL_2$, s6/s12 - TG $VLDL_1$ and s7/s13 - TG $VLDL_2$.

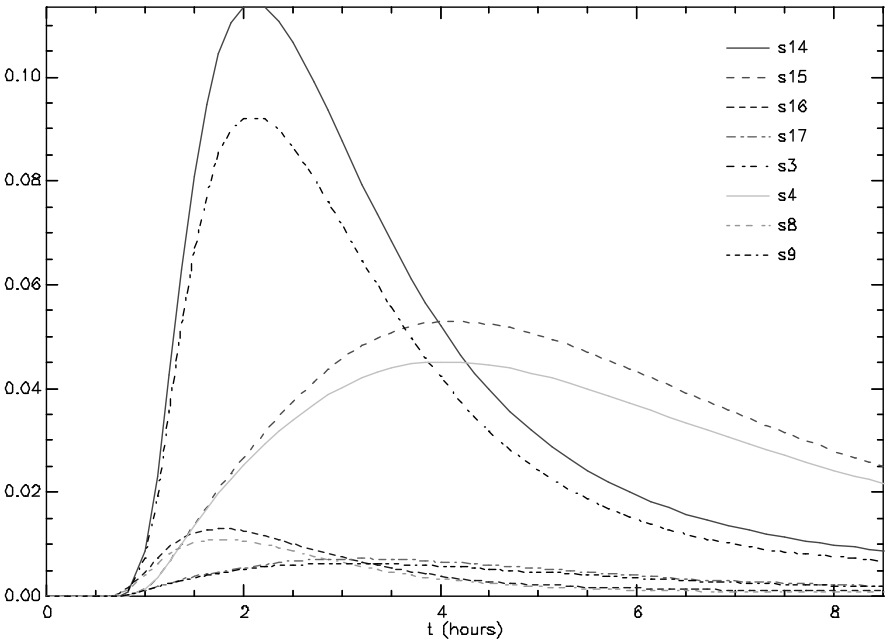

Figure B.2: 4.7(b). Enrichments: s3/s14 - apoB $VLDL_1$, s4/s15 - apoB $VLDL_2$, s8/s16 - TG $VLDL_1$ and s9/s17 - TG $VLDL_2$.

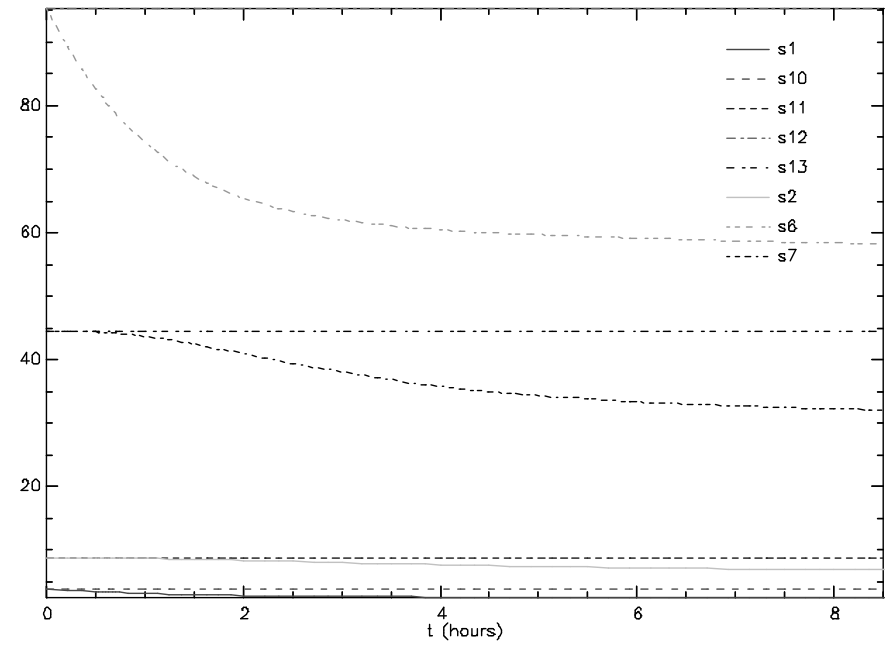

Figure B.3: 4.7(c). Pools: s1/s10 - apoB $VLDL_1$, s2/s11 - apoB $VLDL_2$, s6/s12 - TG $VLDL_1$ and s7/s13 - TG $VLDL_2$.

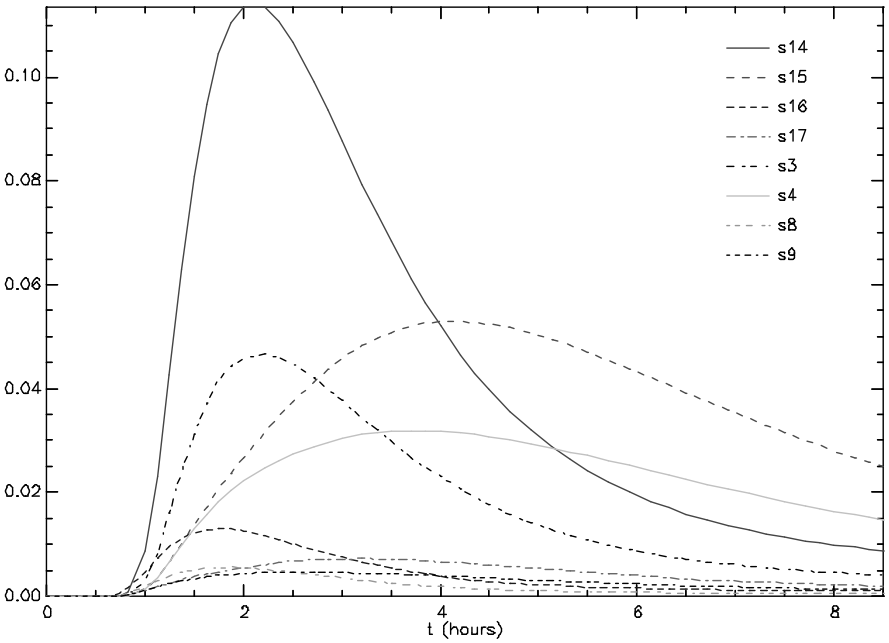

Figure B.4: 4.7(d). Enrichments: s3/s14 - apoB $VLDL_1$, s4/s15 - apoB $VLDL_2$, s8/s16 - TG $VLDL_1$ and s9/s17 - TG $VLDL_2$.

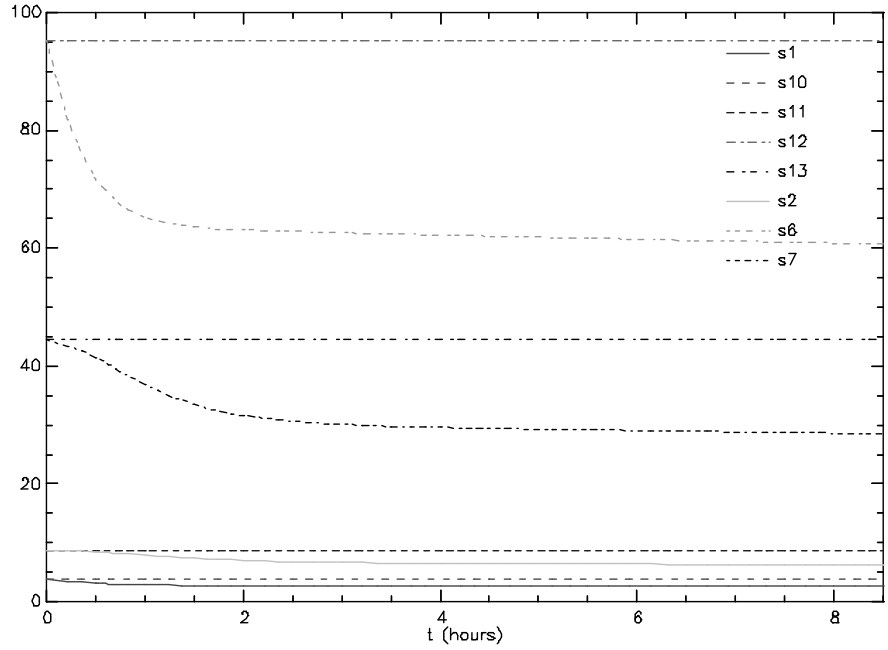

Figure B.5: 4.8(a). Pools: s1/s10 - apoB $VLDL_1$, s2/s11 - apoB $VLDL_2$, s6/s12 - TG $VLDL_1$ and s7/s13 - TG $VLDL_2$.

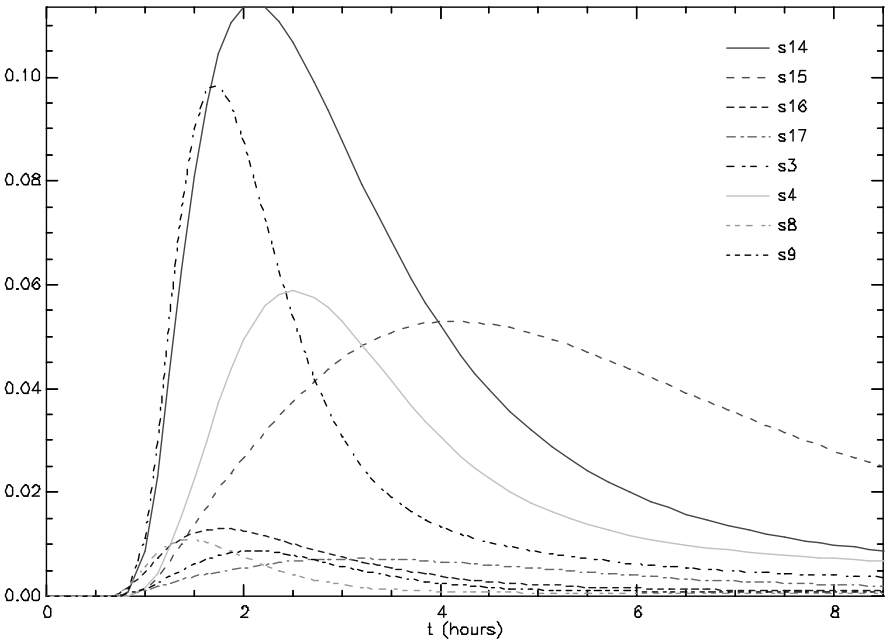

Figure B.6: 4.8(b). Enrichments: s3/s14 - apoB $VLDL_1$, s4/s15 - apoB $VLDL_2$, s8/s16 - TG $VLDL_1$ and s9/s17 - TG $VLDL_2$.

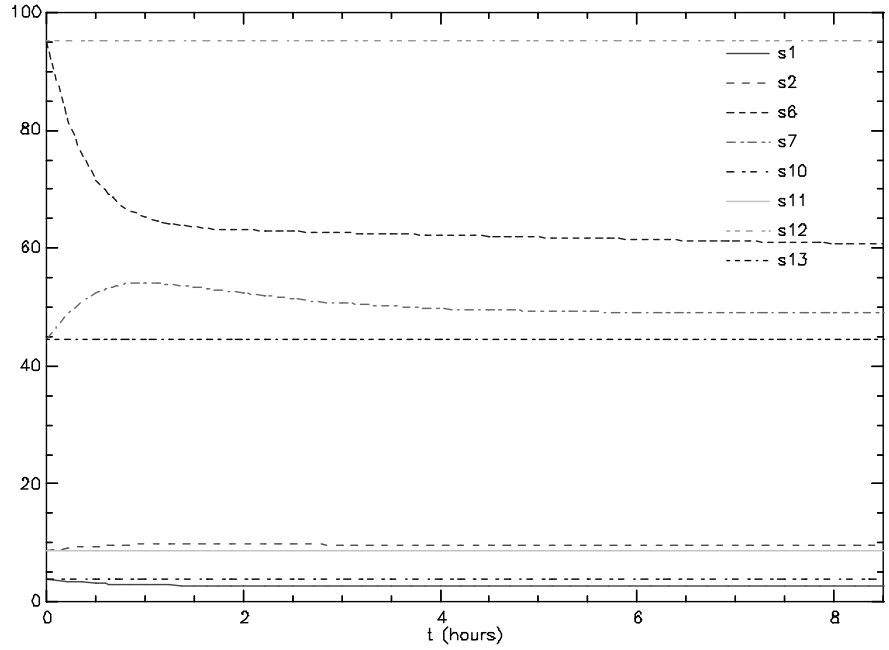

Figure B.7: 4.8(c). Pools: s1/s10 - apoB $VLDL_1$, s2/s11 - apoB $VLDL_2$, s6/s12 - TG $VLDL_1$ and s7/s13 - TG $VLDL_2$.

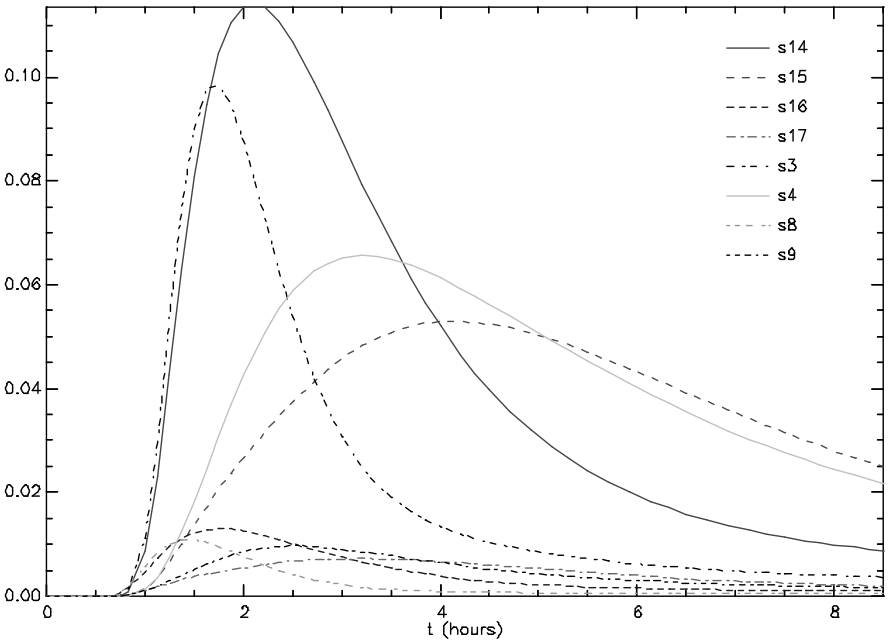

Figure B.8: 4.8(d). Enrichments: s3/s14 - apoB $VLDL_1$, s4/s15 - apoB $VLDL_2$, s8/s16 - TG $VLDL_1$ and s9/s17 - TG $VLDL_2$.

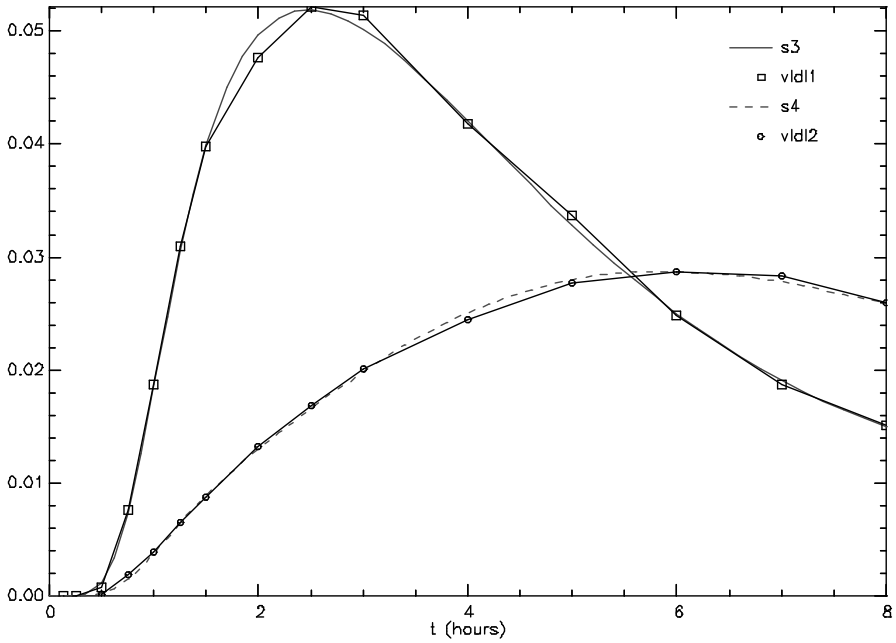

Figure B.9: 7.3(a). Leucine enrichment curves for control subject 16. □ $VLDL_1$, and ∘ $VLDL_2$ measured data.

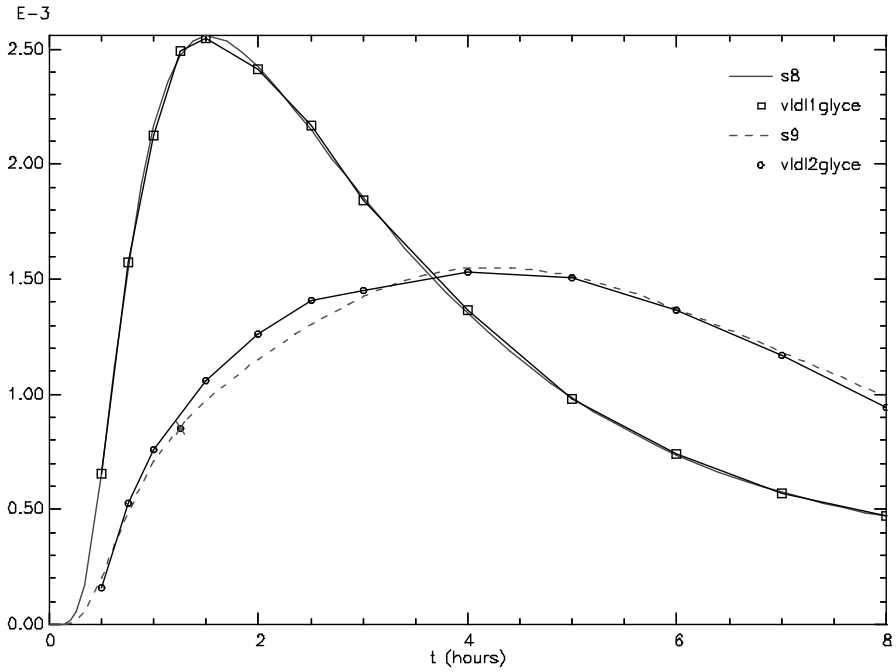

Figure B.10: 7.3(b). Glycerol enrichment curves for control subject 16. □ $VLDL_1$, and ∘ $VLDL_2$ measured data.

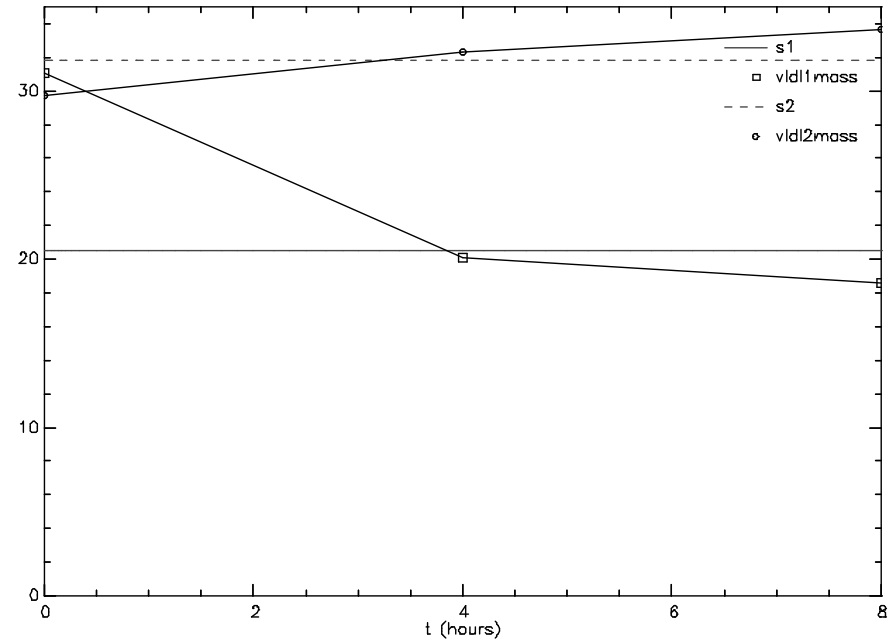

Figure B.11: 7.3(c). Leucine pool sizes for control subject 16. □ $VLDL_1$, and ∘ $VLDL_2$ measured data.

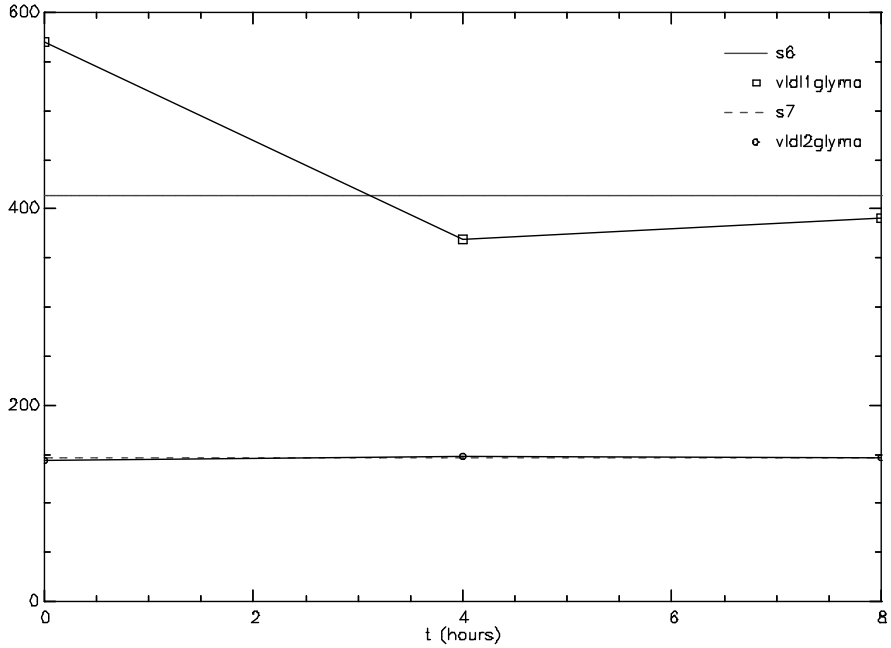

Figure B.12: 7.3(d). Glycerol pool sizes for control subject 16. □ $VLDL_1$, and ∘ $VLDL_2$ measured data.

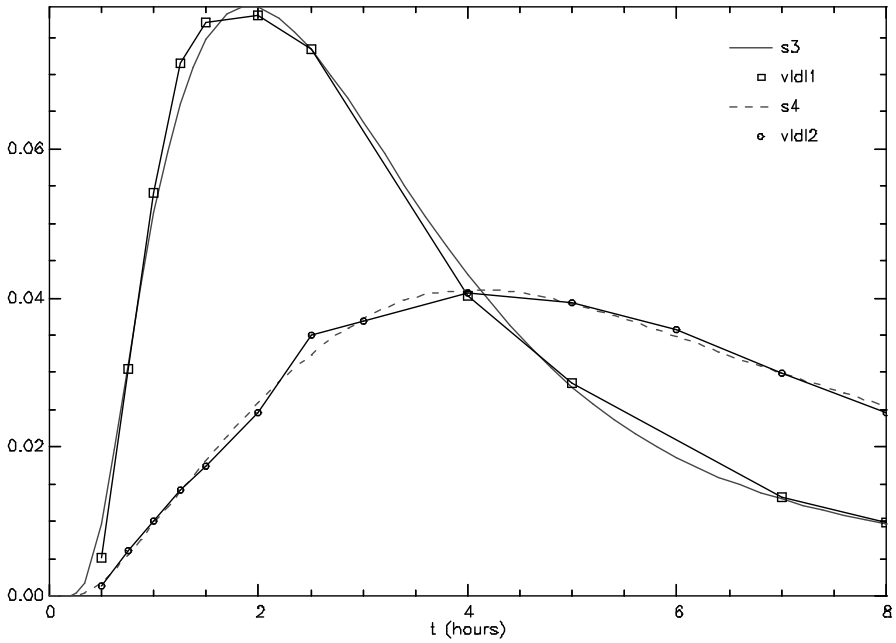

Figure B.13: 7.4(a). Leucine enrichment curves for control subject 17. □ $VLDL_1$, and ∘ $VLDL_2$ measured data.

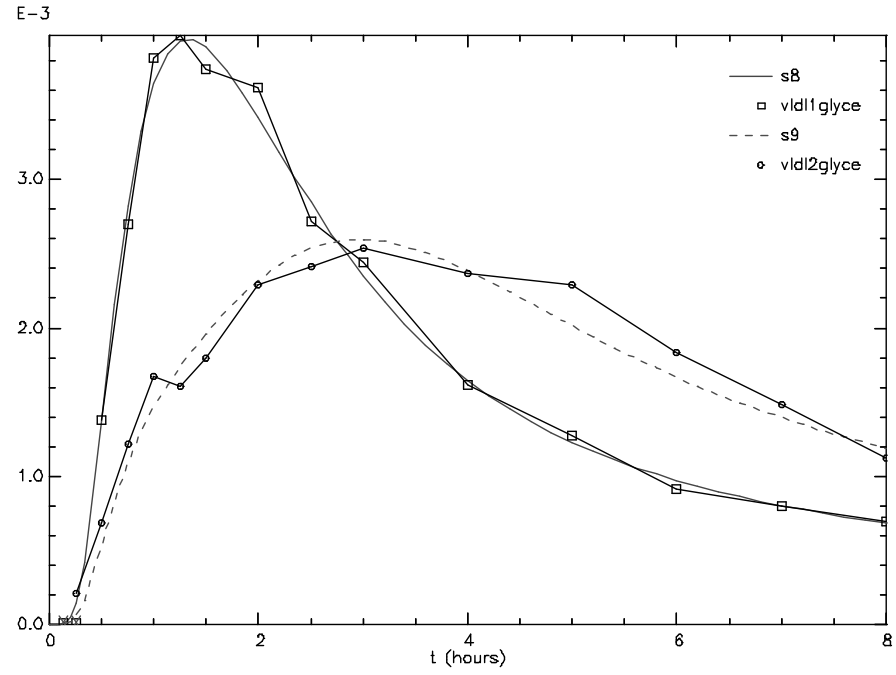

Figure B.14: 7.4(b). Glycerol enrichment curves for control subject 17. □ $VLDL_1$, and ∘ $VLDL_2$ measured data.

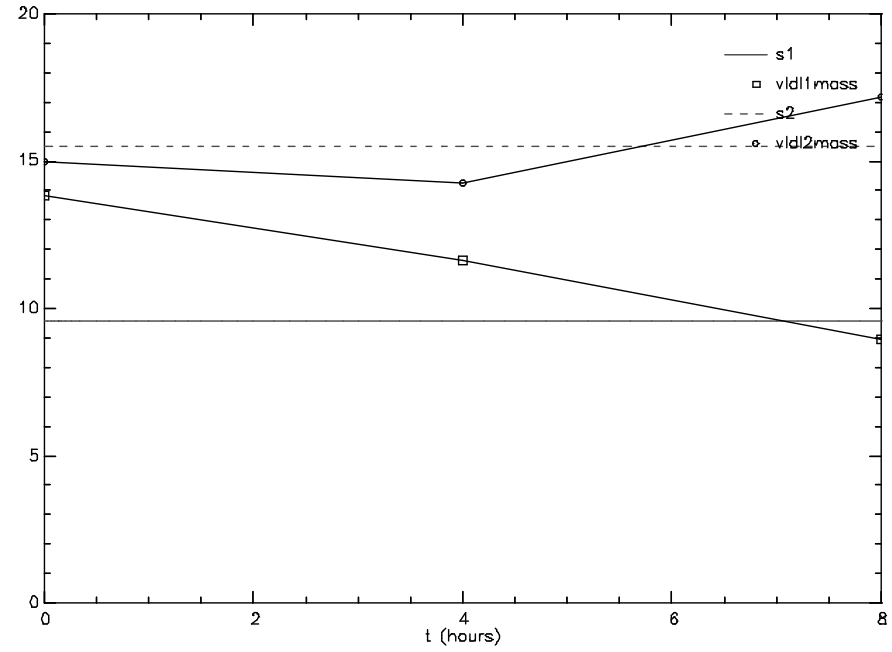

Figure B.15: 7.4(c). Leucine pool sizes for control subject 17. □ $VLDL_1$, and ∘ $VLDL_2$ measured data.

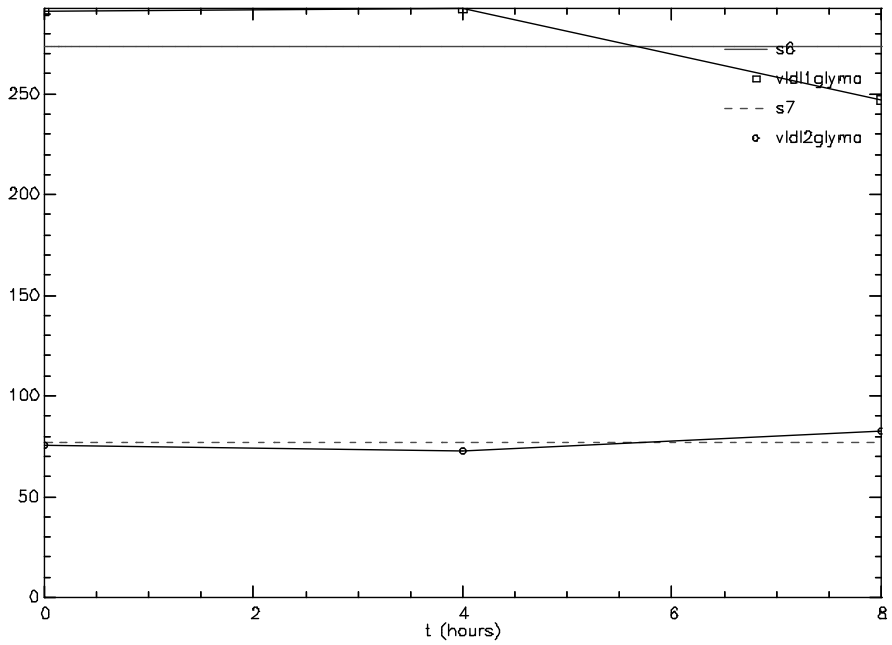

Figure B.16: 7.4(d). Glycerol pool sizes for control subject 17. □ $VLDL_1$, and ∘ $VLDL_2$ measured data.

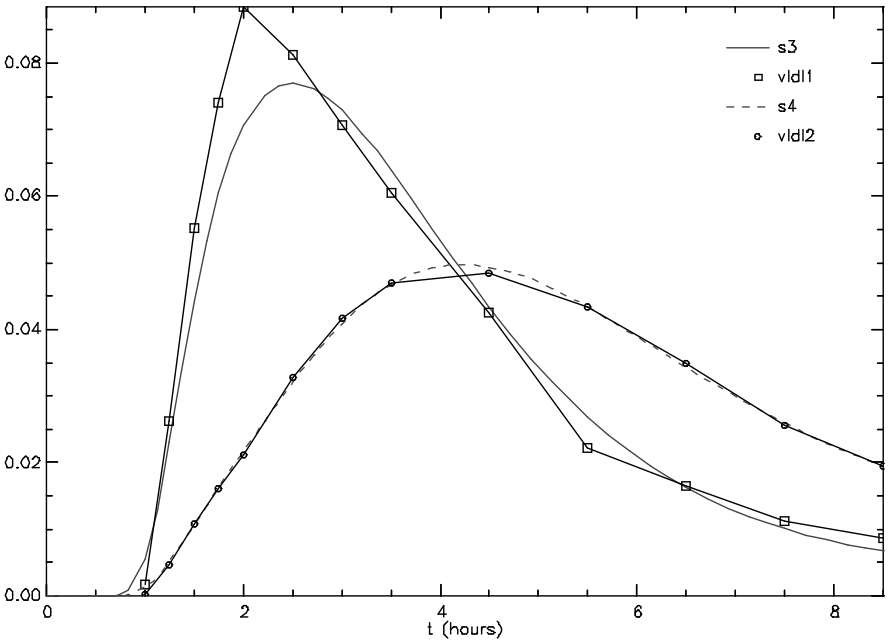

Figure B.17: 7.5(a). Leucine enrichment curves for DM2 subject 10. □ $VLDL_1$, and ∘ $VLDL_2$ measured data.

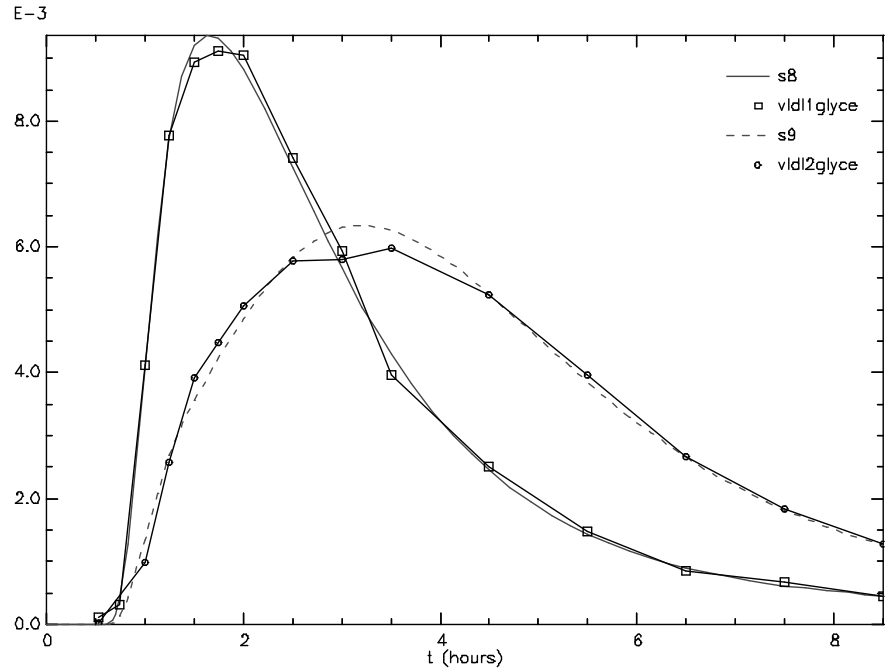

Figure B.18: 7.5(b). Glycerol enrichment curves for DM2 subject 10. □ $VLDL_1$, and ∘ $VLDL_2$ measured data.

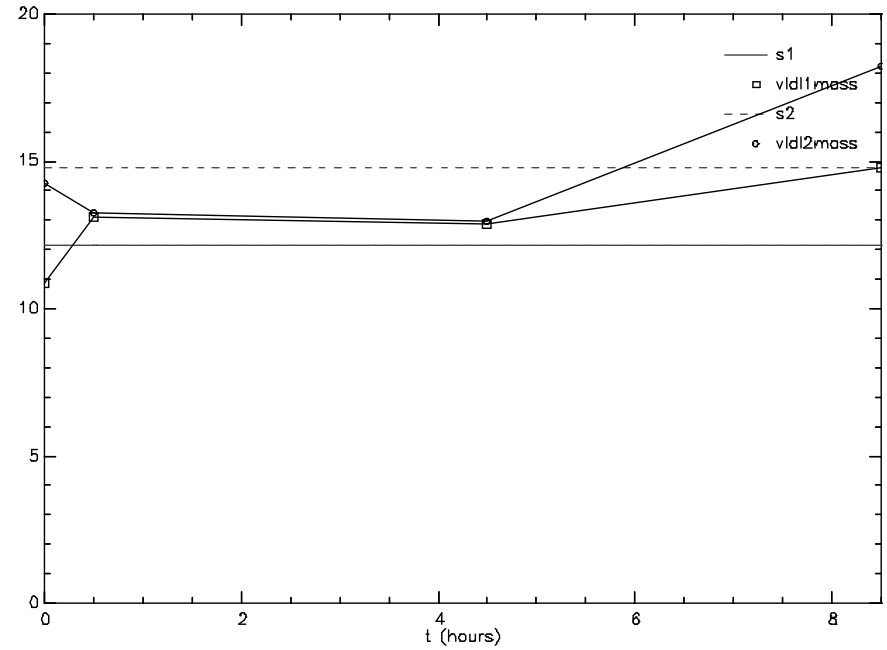

Figure B.19: 7.5(c). Leucine pool sizes for DM2 subject 10. □ $VLDL_1$, and ∘ $VLDL_2$ measured data.

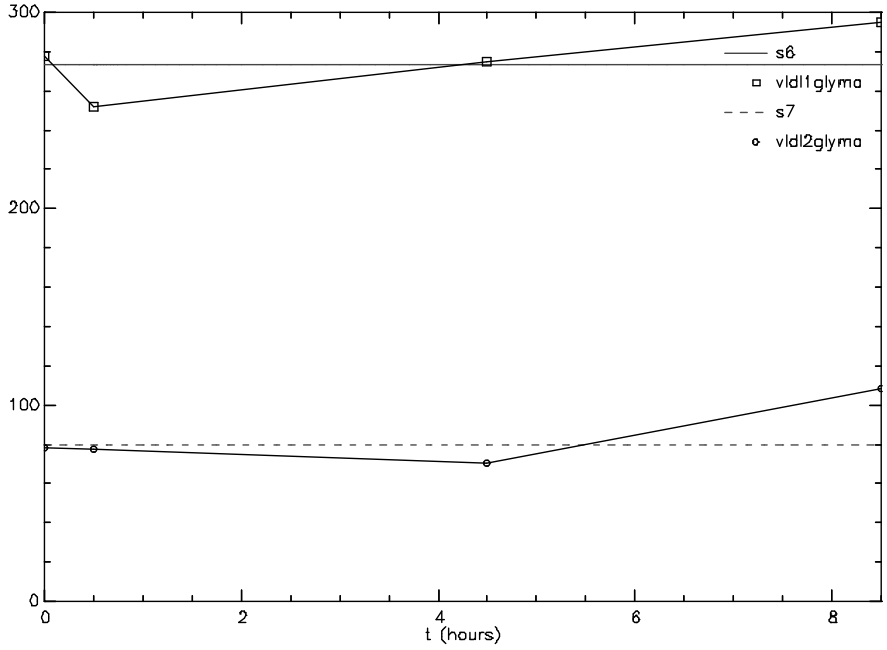

Figure B.20: 7.5(d). Glycerol pool sizes for DM2 subject 10. □ $VLDL_1$, and ∘ $VLDL_2$ measured data.

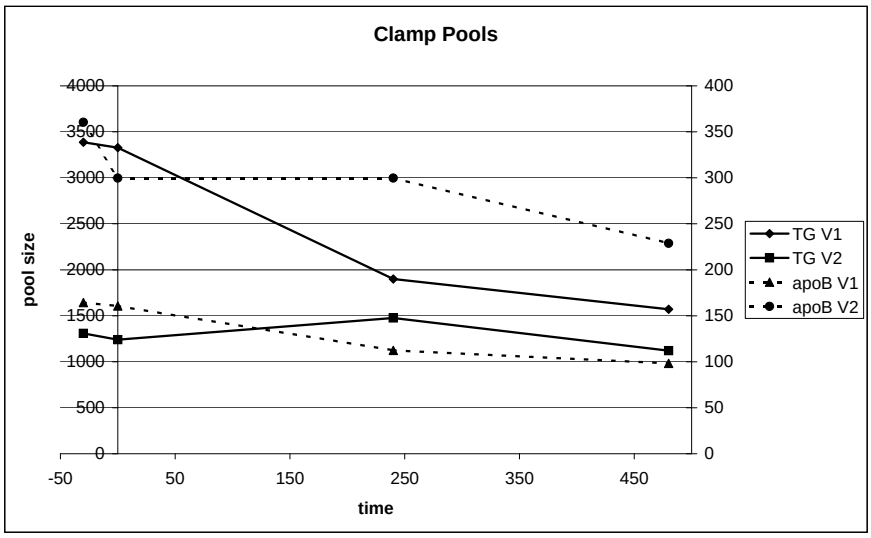

Figure B.21: 7.10(a). Here there is a fast initial drop of $VLDL_2$ pools, most pronounced for apoB. The $VLDL_1$ pools decay slowly.

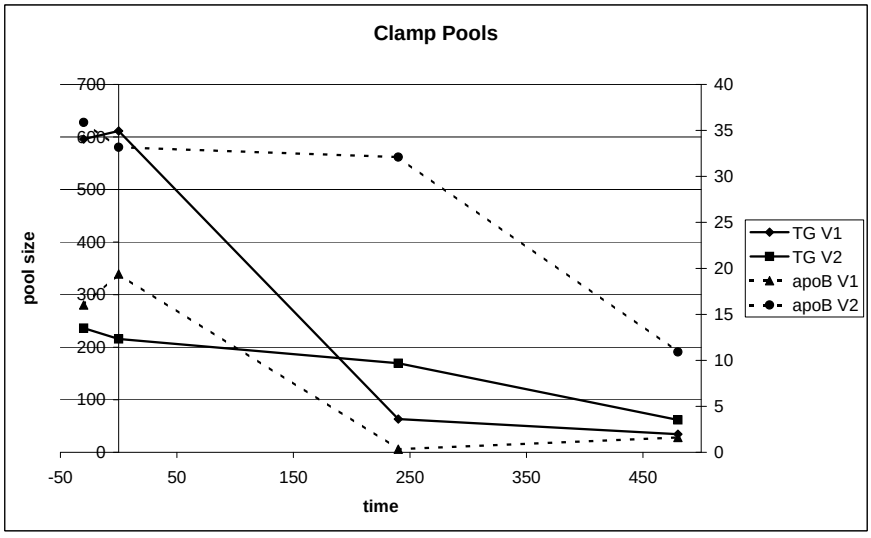

Figure B.22: 7.10(b). The pools of TG and apoB. In this particular subject the concentrations of $VLDL_1$ fell drastically, where as the falls of $VLDL_2$ were slower.

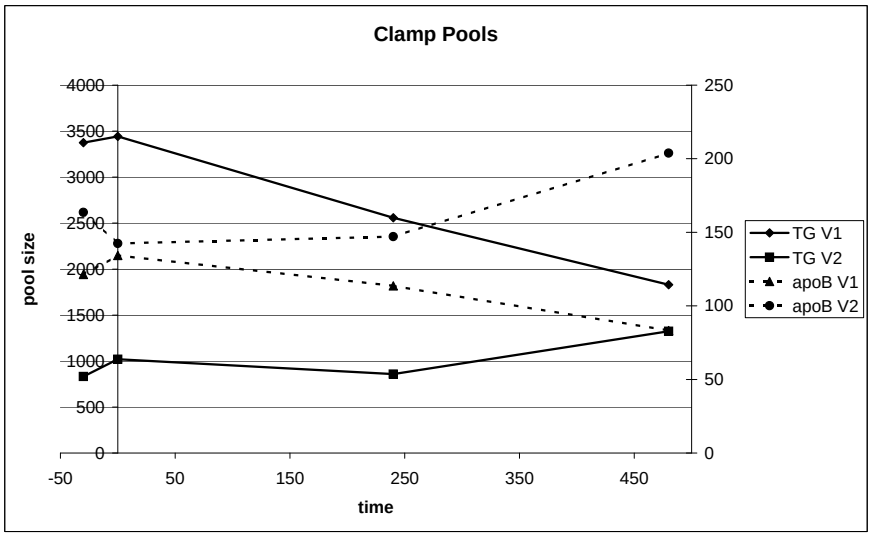

Figure B.23: 7.10(c). The TG and apoB pools. Here the $VLDL_1$ pools decrease but the $VLDL_2$ actually increase.

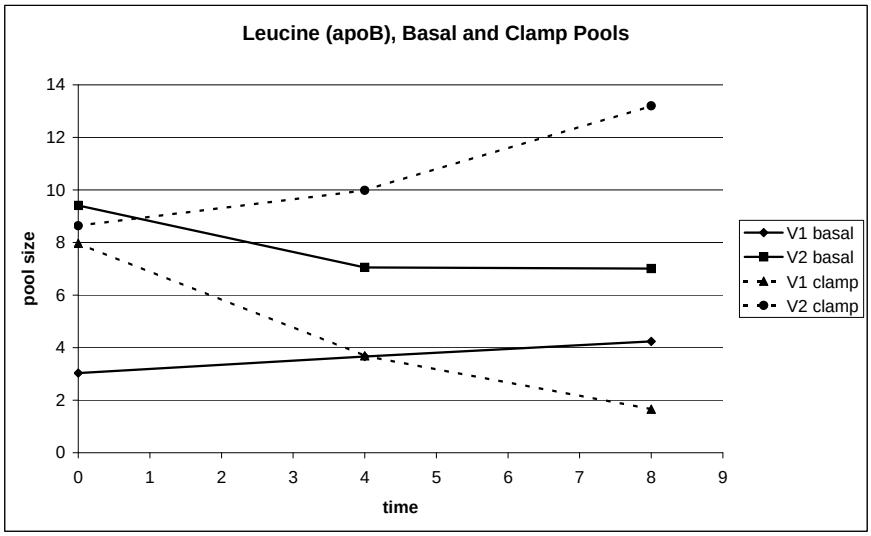

Figure B.24: 7.11(a). The leucine pools in $VLDL_1$ and $VLDL_2$ in both the clamp and basal studies. In the clamp study there is a clear drop in the $VLDL_1$ pool and an increase of the $VLDL_2$ pool.

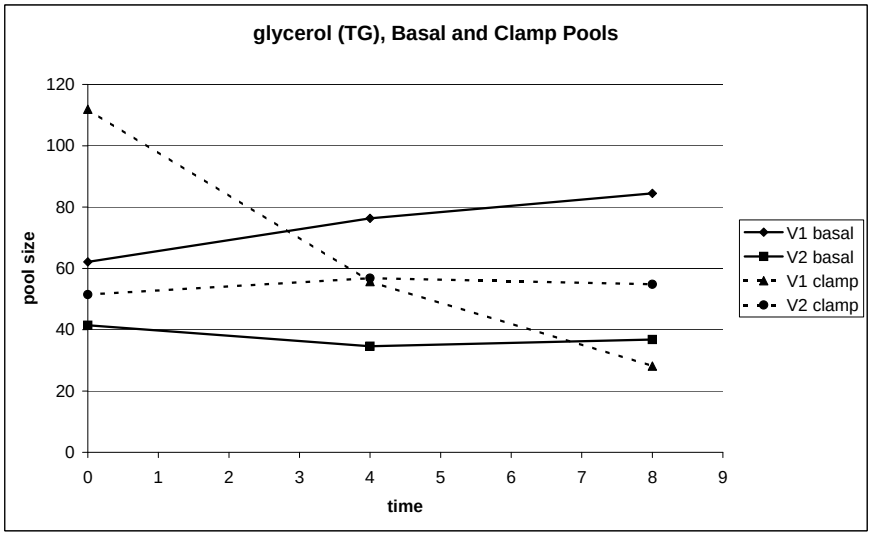

Figure B.25: 7.11(b). The basal and clamp glycerol pools for $VLDL_1$ and $VLDL_2$. As for apoB there is a clear decrease of the $VLDL_1$ pool in the clamp study.

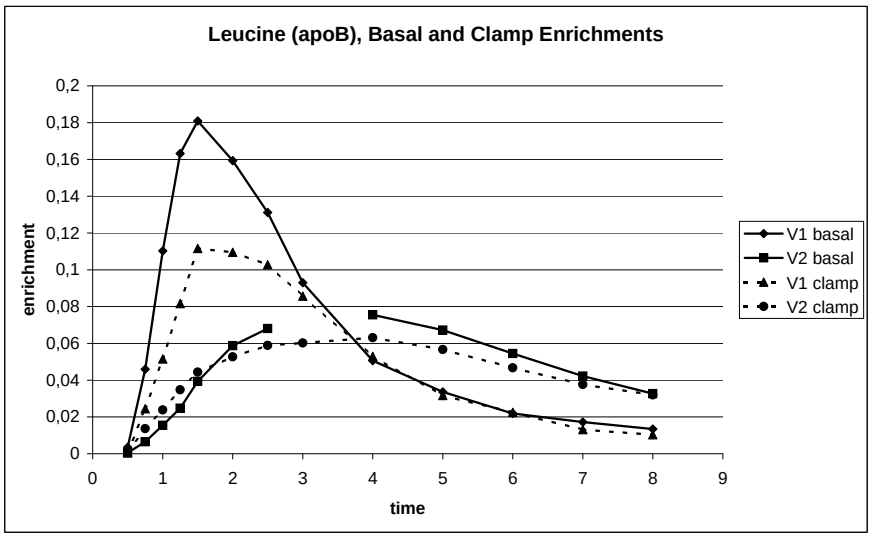

Figure B.26: 7.11(c). The apoB enrichment for the same subject. In the clamp study the maximal apoB enrichment is less than for the basal study.

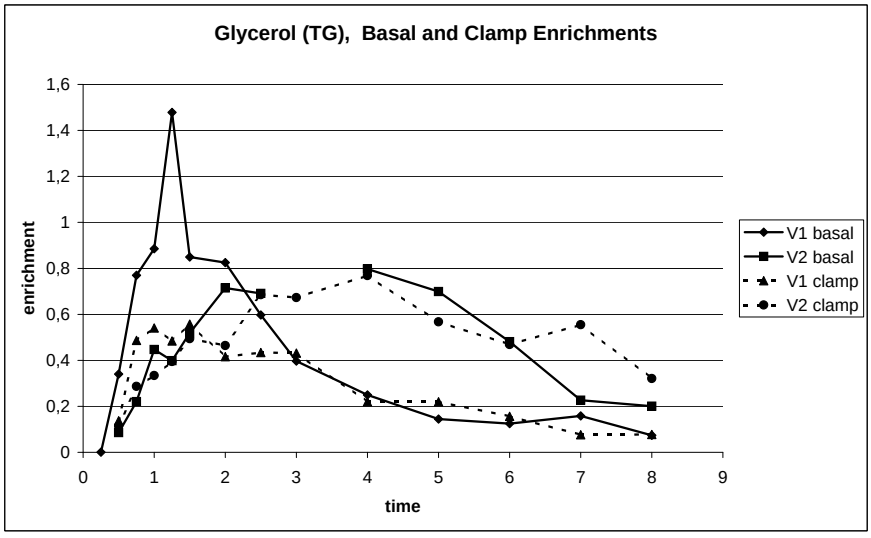

Figure B.27: 7.11(d). As for the apoB, the TG enrichment was lower in clamp study than in the basal study.

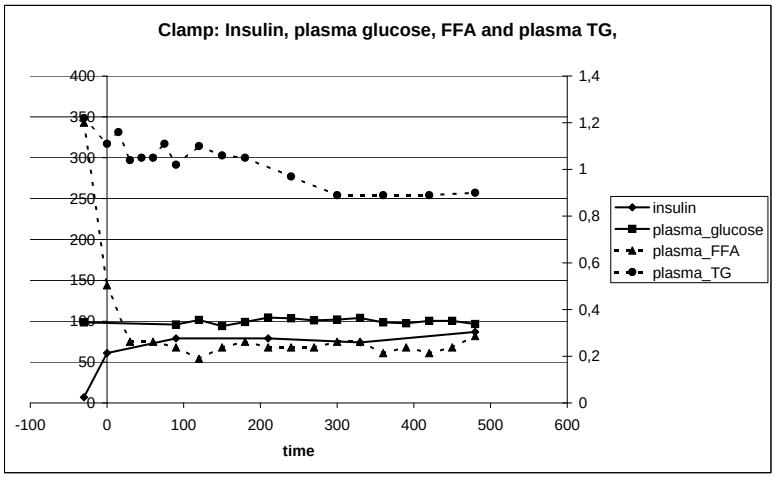

Figure B.28: 7.12(a). The concentration of FFA decreases rapidly during the first hour of the experiment. The insulin is given with an instant injection followed by a constant infusion, and the concentration is fairly constant during the experimental time. Plasma glucose levels are kept constant by giving glucose intravenously. The total plasma TG level (right axis) is decreasing.

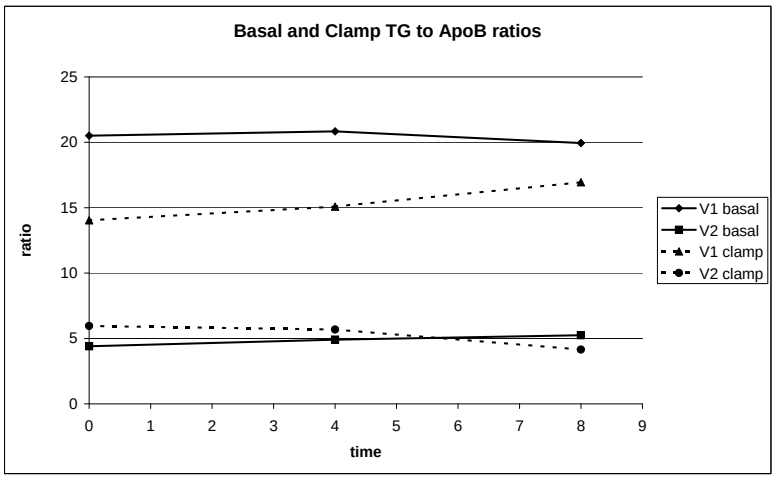

Figure B.29: 7.12(b). The TG to apoB ratios of the $VLDL_1$ and $VLDL_2$ pools in the basal and clamp studies

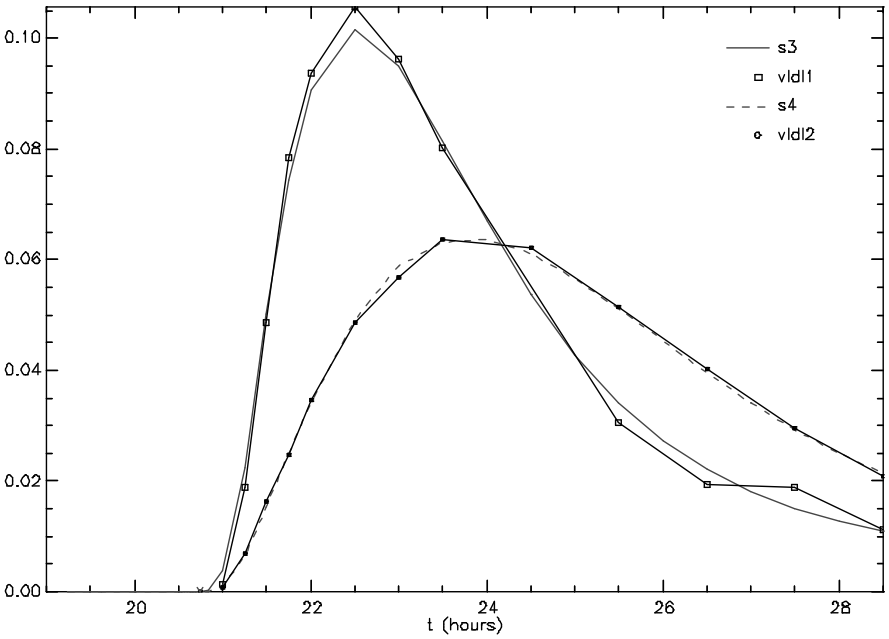

Figure B.30: 7.13(a). The fit to the apoB enrichment curve.

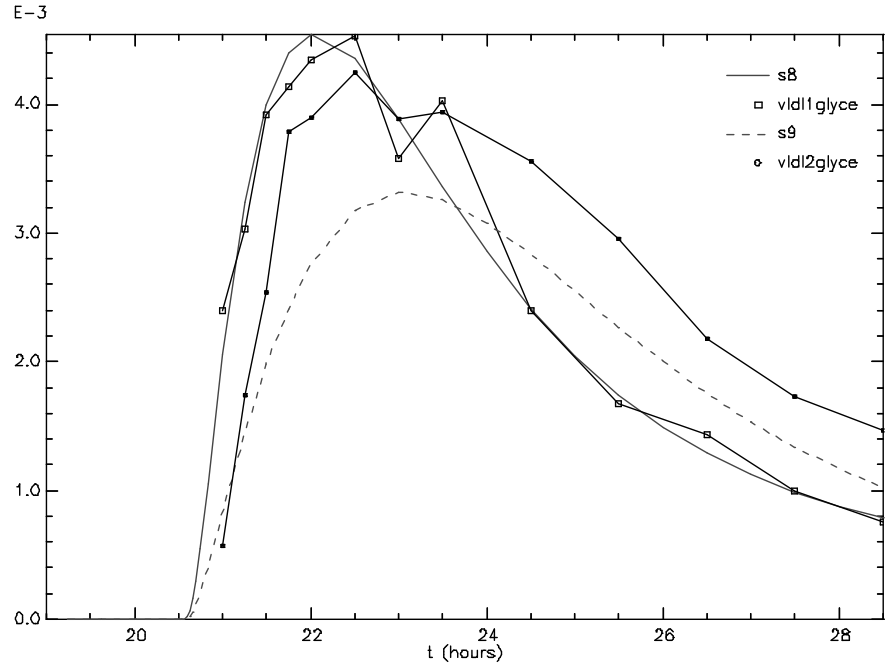

Figure B.31: 7.13(b). TG enrichment curves.

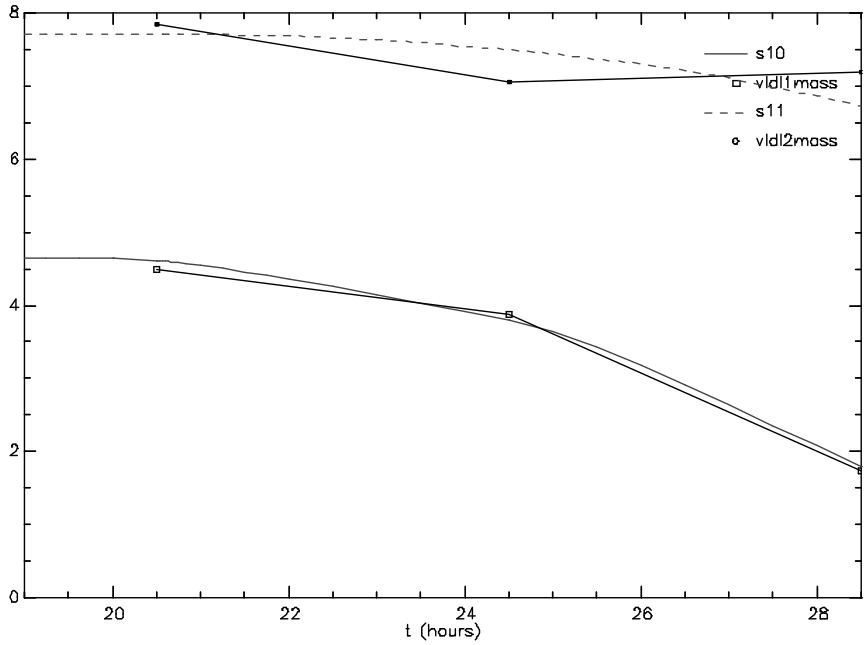

Figure B.32: 7.13(c). The fit to the decaying apoB curves.

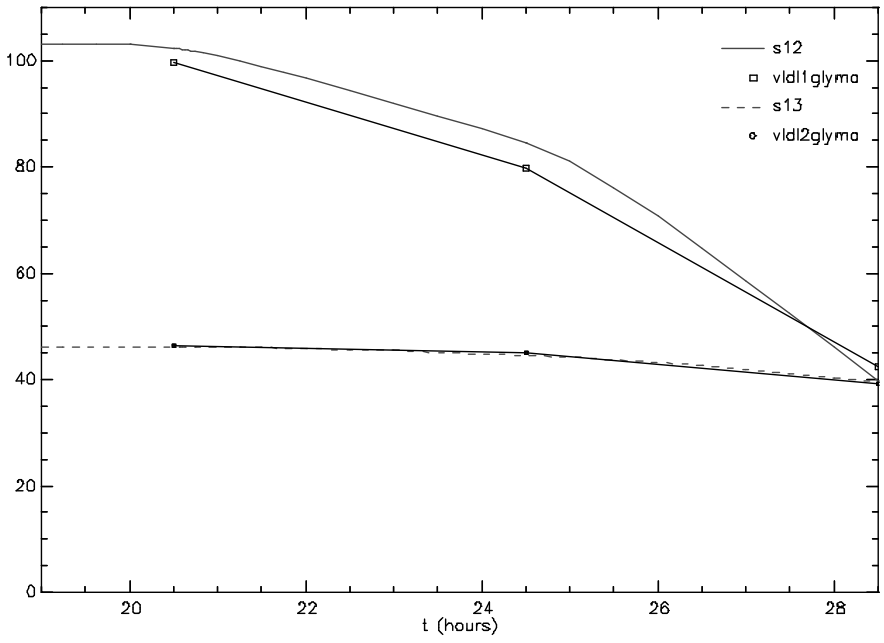

Figure B.33: 7.13(d). The fit to the decaying TG curves.

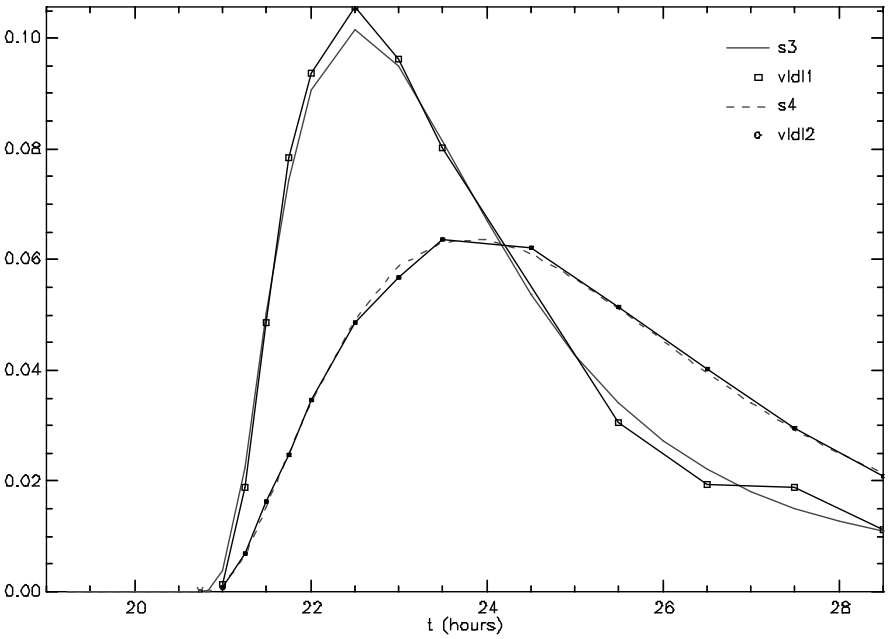

Figure B.34: 7.14(a). The fit to the apoB enrichment curve.

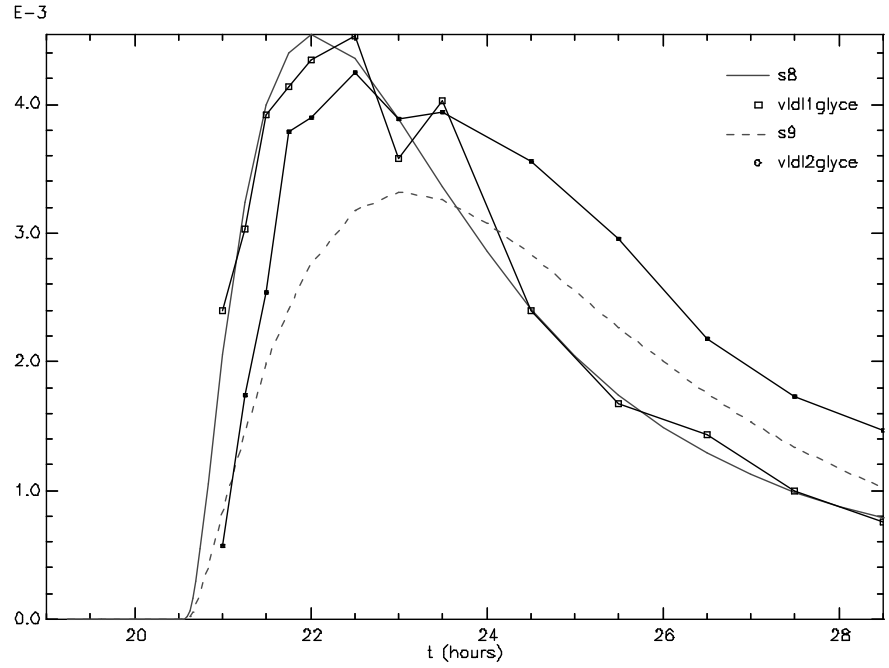

Figure B.35: 7.14(b). TG enrichment curves.

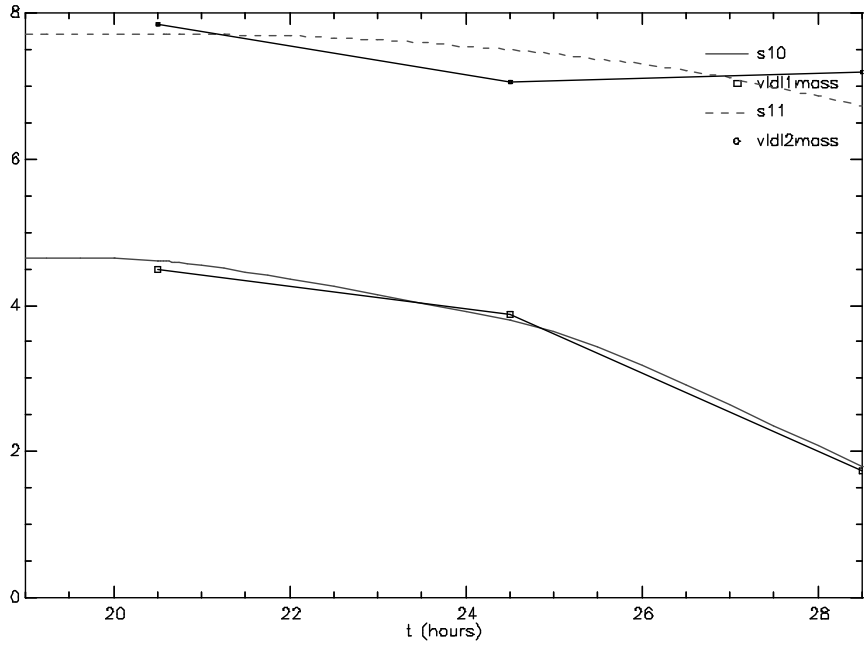

Figure B.36: 7.14(c). The fit to the decaying apoB curves.

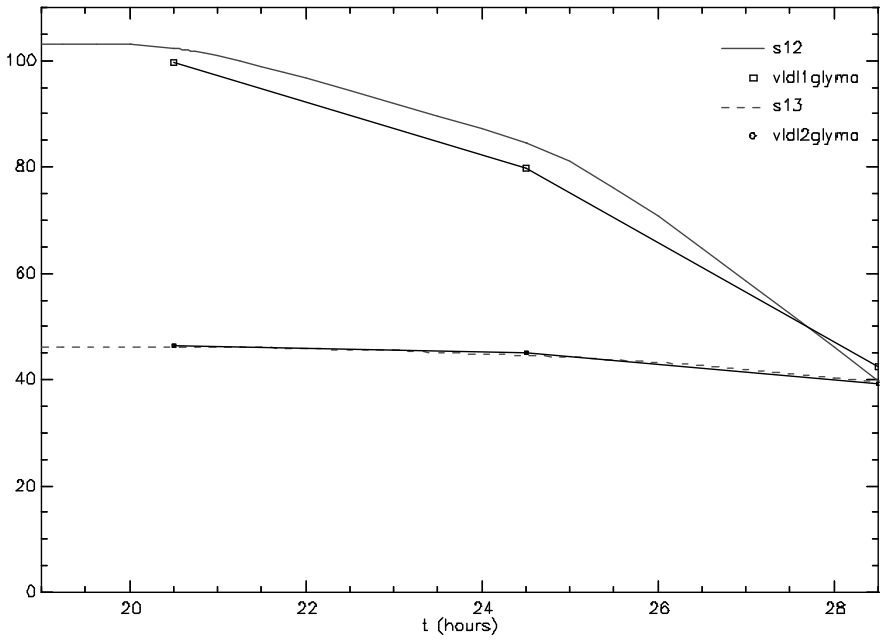

Figure B.37: 7.14(d). The fit to the decaying TG curves.

Bibliography

[1] C.A. Alexander, R.L. Hamilton and R.J. Havel *Subcellular localization of B apoprotein of plasma lipoproteins in rat liver.* Journal of Cell Biology, Volume 96, p241-263, (1976).

[2] S. Audoly, L. D'Angiò, M.P. Saccomani, and C. Cobelli *Global Identifiability of Linear Compartmental Models - A Computer Algebra Algorithm.* IEEE Transactions on biomedical engineering, Volume 45, p36-47, (1998).

[3] D.H. Anderson *Compartmental Modeling and Tracer Kinetics.* Lecture Notes in Biomathematics. Volume 50, Springer. ISBN 3-540-12303-2, (1983).

[4] R. Bellman and K.J. Åstrom *On structural indetifiability.* Mathematical Biosciences, Volume 7, p329-339, (1970).

[5] Y. Bard *Nonlinear Parameter Estimation* Academic Press, ISBN 0-12-078250-2, (1974).

[6] M. Beylot, C. Martin, B. Beaufrere, J. Riou and R. Mornex. *Determination of steady state and nonsteady-state glycerol kinetics in humans using deuterium-labeled tracer.* Journal of lipid research, Volume 28, p414-422, (1987).

[7] J. Bjorkegren, C.J. Packard, A. Hamsten, D. Bedford, M. Caslake, L. Foster, J. Shepherd, P. Stewart and F. Karpe *Accumulation of large very low density lipoprotein in plasma during intravenous infusion of a chylomicron-like triglyceride emulsion reflects competition for a common lipolytic pathway.* Journal of lipid research, Volume 37, p76-86, (1996).

[8] J. Boren, S. Rustaeus, and S.O. Olofsson *Studies on the assembly of apolipoprotein B-100- and B-48-containing very low density lipoproteins in McA-RH7777 cells.* Journal of Biological Chemistry, Volume 269, p25879-25888, (1994).

[9] C. Cobelli and J.J. Distefano III *Parameter and structural identifiability concepts and ambiguities: a critical review and analysis.* American Journal of Physiology (Regulatory Intergrative Comp. Physiology 8), Volume 239, pR7-R24, (1980).

[10] C. Cobelli, A. Lepschy and G Romanin Jacur *Identifiability Results on Some Constrained Compartmental Systems.* Mathematical Biosciences, Volume 47, p173-195, (1979).

[11] C. Cobelli, A. Lepschy and G Romanin Jacur *Identifiability Of Compartmental Systems.* Mathematical Biosciences, Volume 44, p1-18, (1979).

[12] E.J. Davidson *Connectability and Structural Controllability of Composite systems.* Automatica, Volume 13, p109-123, (1977).

[13] T. Demant, C.J. Packard, H. Demmelmair, P. Stewart, A. Bedynek, D. Bedford, D. Seidel and J. Shepherd. *Sensitive methods to study human apolipoprotein B metabolism using stable isotope-labeled amino acids.* American Journal of Physiology, Volume 270, p1022-36, (1996).

[14] N.R. Draper and H. Smith *Applied Regression Analysis.* Third Edition. Wiley, ISBN 0-471-17082-8, (1998).

[15] J. Eisenfeld *Stochastic Parameters in Compartmntal Systems.* Mathematical Biosciences, Volume 52, p261-275, (1980).

[16] G. Egusa, D.W. Brady, S.M. Grundy and B.V. Howard. *Isopropanol precipitation method for the determination of apolipoprotein B specific activity and plasma concentrations during metabolic studies of very low density lipoprotein and low density lipoprotein apolipoprotein B.* Journal of lipid research, Volume 24, p1261-1267, (1983).

[17] J. Elovson, J.E. Chetterton, G.T. Bell, V.N. Schumaker, M.A. Reuben, D.L. Puppione, J.R. Reeve and N.L. Young *Plasma very low density lipoproteins contain a single molcule of apolipoprotein B.* Journal of lipid research, Volume 29, p1461-1473, (1988).

[18] B.A. Griffin and C.J. Packard *Metabolism of VLDL and LDL subclass.* Current Opinion in Lipidology, Volume 5, p200-206, (1994).

[19] J.M. van den Hof *Structural Identifiability of Linear Compartmental Systems.* IEEE transactions on automatic control 6, Volume 43, p801-818. (1998).

[20] J.A. Jacquez and C.P. Simon *Quantitative theory of compartmental systems with lags.* Mathematical Biosciences, Volume 180, p329-362, (2002).

[21] M.L. Kashyap, B.A. Hynd and K. Robinson. *A rapid and simple method for measurement of total protein in very low density lipoproteins by the Lowry assay.* Journal of lipid research, Volume 21, p491-495, (1980).

[22] R.B. Kellogg and A.B. Stephens *Complex Eigenvalues of a Non-Negative Matrix with a Specified Graph.* Linear Algebra and its Applications, Volume 20, p179-187, (1978).

[23] Z. Kuchinskiene, and L.A. Carlson *Composition, concentration, and size of low density and subfractions of very low density lipoproteins from serum of normal men and women.* Journal of lipid research, Volume 23, p762-769, (1982).

[24] F.T. Lindgren, L.C. Jensen and F.T. Hatch *The isolation and quantitative analysis of serum lipoprotiens.* IN: Blood Lipids and Lipoproteins: Quantitation, Composition and Metabolism. Chapter 5. Edited by G.J. Nelson. Wiley Intersience, New York, (1972).

[25] W.J. Lossow, F.T. Lindgren, J.C. Murchio, G.R. Stevens, and L.C. Jensen *Particle size and protein content of six fractions of the lipoproteins isolated by gradient density centrifugation* . Journal of lipid research, Volume 10, p68-76, (1969).

[26] C.L. Malmendier, C. Delcroix, and M. Berman. *Interrelations in the oxidative metabolism of free fatty acids, glucose, and glycerol in normal and hyperlipemic patients. A compartmental model.* Journal of clinical investigation, Volume 54, p461-476, (1974).

[27] R. Malmstrom, C.J. Packard, M. Caslake, D. Bedford, P. Stewart, H. Yki-Jarvinen, J. Shepherd and M.R. Taskinen. *Defective regulation of triglyceride metabolism by insulin in the liver in NIDDM.* Diabetologia, Volume 40, p454-462, (1997).

[28] R. Malmstrom, C.J. Packard, T.D. Watson, S. Rannikko, M. Caslake, D. Bedford, P. Stewart, H. Yki-Jarvinen, J. Shepherd and M.R. Taskinen. *Metabolic basis of hypotriglyceridemic effects of insulin in normal men.* Arteriosclerosis, Thrombosis, and Vascular Biology, Volume 17, p1454-1464, (1997).

[29] R. Malmstrom, C.J. Packard, M. Caslake, D. Bedford, P. Stewart, J. Shepherd and M.R. Taskinen. *Effect of heparin-stimulated plasma lipolytic activity on VLDL APO B subclass metabolism in normal subjects.* Atherosclerosis, Volume 146, p381-390, (1999).

[30] R. Malmstrom, C.J. Packard, M. Caslake, D. Bedford, P. Stewart, H. Yki-Jarvinen, J. Shepherd and M.R. Taskinen. *Effects of insulin and acipimox on VLDL1 and VLDL2 apolipoprotein B production in normal subjects* [published erratum appears in Diabetes 1998 Sep;47(9):1532]. Diabetes 47, p 779-787, (1998).

[31] N. Mero, M. Syvanne, B. Eliasson, U. Smith and MR. Taskinen. *Postprandial elevation of ApoB-48-containing triglyceride-rich particles and retinyl esters in normolipemic males who smoke.* Arteriosclerosis, Thrombosis, and Vascular Biology, Volume 17, p 2096-2102, (1997).

[32] C.J. Packard et al. *Apolipoprotein B metabolism and the distribution of VLDL and LDL subfractions.* Journal of lipid research, Volume 41, p305-317, (2000).

[33] C.J. Packard, A. Gaw, T. Demant and J. Shepherd *Development and application of a multi-compartmental model to study very low density lipoprotein subfraction metabolism.* Journal of Lipid Research, Volume 36, p172-187, (1995).

[34] B.W. Patterson, B. Mittendorfer, N. Elias, R. Satyanarayana and S. Klein *Use of stable isotopically labeled tracers to measure very low density lipoprotein-triglyceride turnover.* Journal of Lipid Reasarch, Volume 43, p223-233, (2002).

[35] B.W. Patterson, G. Zhao, N. Elias, D.L. Hachey and S. Klein. *Validation of a new procedure to determine plasma fatty acid concentration and isotopic enrichment.* Journal of Lipid Reasarch, Volume 40, p2118-2124, (1999).

[36] F. Pont, L. Duvillard, B. Vergès and P. Gambert *Development of Compartmental Models in Stable Isotope Experiments Application to Lipid Metabolism.* Arteriosclerosis, Thrombosis, and Vascular Biology, Volume 17, p853-860, (1998).

[37] T.G. Redgrave and L.A. Carlson *Changes in plasma very low density and low density lipoprotein content, composition and size after a fatty meal in normo- and hypertriglyceridemic man.* Journal of Lipid Research, Volume 20, p217-229, (1979).

[38] J.A. Rice *Mathematical Statistics and Data Analysis* Second Edition. Wadsworth, Inc. ISBN 0-534-20934-3, (1995).

[39] M.P. Saccomani, S. Andoly, L. D'Angio, R. Saltier and C. Cobelli *Pride: a program to test a priori global identifiability of linear compartmental models.* In: Proc. SYSID '94

10th IFAC Symposium on System Identification, edited by M. Blanke and T. Söderström. Copenhagen: Danish Automation Society, Volume 3, p25-30 (1994).

[40] G.A.F. Seber and C.J. Wild *Nonlinear Regression.* Wiley, ISBN 0-471-61760-1, (1989).

[41] A. Sedoglavic *A Probabelistic Approach to Test Local Algebraic Obervability in Polynomial Time* Journal of Symbolic Calculation, Volume 33, p735-755, (2002).

[42] J. Vakkilainen, K.V. Porkka, I. Nuotio, P. Pajukanta, L. Suurinkeroinen, K. Ylitalo, J.S. Viikari, C. Ehnholm and M.R. Taskinen. *Glucose intolerance in familial combined hyperlipidaemia.* EUFAM study group. European Journal of Clinical Investigation, Volume 28, p24-32, (1998).

[43] D.E. Vance and J. Vance (editors)*Biochemistry of Lipids, Lipoproteins and Membranes.* New Comprehencive Biochemistry, Volume 31. ELSEVIER, ISBN 0-444-82364-6, (1996).

[44] R.F. Witter and V.S. Whitner. *Determination of Serum Triglycerides. Blood Lipids and Lipoproteins: Quantification, Composition and Metabolism.* In: Nelson GJ (ed.), p75-105, (1972).

[45] D. White and M. Baxter (editors).*Hormones And Metabolic Control.* Second edition, ISBN 0-340-56355-9, (1994).

[46] L.A. Zech, S.M. Grundy, D. Steinberg and M. Berman *Kinetic Model for Production and Metabolism of Very Low Density Lipoprotein Triglycerides.* Journal of Clinical Investigation. Volume 63, p1262-1273, (1979).

[47] *SAAMII user guide.* SAAM Institute, Inc., Seattle, WA, (1998).